Progress in Particle and Nuclear Physics 61 (2008) 343–393

Contents lists available at ScienceDirect

Progress in Particle and Nuclear Physics

journal homepage: www.elsevier.com/locate/ppnp

Review

Collider physics at HERA

M. Klein [a], R. Yoshida [b,*]

[a] University of Liverpool, Physics Department, L69 7ZE, Liverpool, United Kingdom
[b] Argonne National Laboratory, HEP Division, 9700 South Cass Avenue, Argonne, IL, 60439, USA

ARTICLE INFO

Keywords:
HERA
Deep inelastic scattering
Structure functions
Photoproduction
Diffraction
Heavy flavours
Searches
QCD
Electroweak physics

ABSTRACT

From 1992 to 2007, HERA, the first electron–proton collider, operated at cms energies of about 320 GeV and allowed the investigation of deep-inelastic and photoproduction processes at the highest energy scales accessed thus far. This review is an introduction to, and a summary of, the main results obtained at HERA during its operation.

Contents

* Corresponding author. Tel.: +1 630 252 7874; fax: +1 630 252 5782.
E-mail address: ryoshida@hep.anl.gov (R. Yoshida).

0146-6410/$ – see front matter © 2008 Elsevier B.V. All rights reserved.
doi:10.1016/j.ppnp.2008.05.002

1. Introduction

HERA was the culmination of 50 years of experimentation with electron, later also muon and neutrino, beams to explore the structure of the proton, first in elastic and subsequently in inelastic scattering. The idea had been simple: use the pointlike lepton as a probe to study the strong interaction phenomena of the nucleons and their internal structure. HERA emerged from a series of electron–proton accelerator studies in the 70's as the most energetic version of an *ep* collider possible. It was built in the 80's for maximum possible luminosity, and with the capability to scatter polarised electrons and positrons off protons, at a center of mass energy, $\sqrt{s}$, of about 320 GeV. The first HERA data were taken in summer 1992. It ceased operations in June 2007 after a long, successful data taking period of 16 years.

In deep inelastic lepton–nucleon scattering (DIS), the proton structure is probed by a virtual photon (γ), or weak boson (Z_0 or $W^{\pm}$), which carries a four momentum squared $Q^2 \leq s$. The momentum transferred is inversely proportional to the spatial distance inside the proton which can be resolved with the photon or the weak boson probe. High energy DIS experiments are thus microscopes with a resolution power extending much beyond the eye, optical microscopes or modern laser techniques. The basic experimental interest and challenge over decades has naturally been to enlarge Q^2 by increasing s.

The *ep* collider at the DESY laboratory in Hamburg, Germany, had its first phase of operation, "HERA I", from 1992 through 2000. In this period, the collider experiments H1 and ZEUS each recorded data corresponding to integrated luminosities of approximately 120 pb^{-1} of e^+p and 15 pb^{-1} of e^-p collisions. The energy of the electron (positron) beam was about 27.5 GeV. The energy of the proton beam was initially set to 820 GeV until it was increased to 920 GeV, in 1998, and kept at that value.

The HERA collider was then upgraded to increase the specific luminosity by a factor of about four, as well as to provide longitudinally polarised lepton beams to the collider experiments. The second data taking phase, "HERA II", began in 2003, after completion of the machine and detector upgrades and when unexpected large background problems were finally overcome. It ended in 2007. The H1 and ZEUS experiments each recorded approximately 200 pb^{-1} of e^+p and 200 pb^{-1} of e^-p data with electron (positron) energy of approximately 27.5 GeV and proton energy of 920 GeV. The lepton beams had an average polarisation of approximately $\pm 30\%$ with roughly equal samples of opposite polarities recorded.

In the last three months of HERA operation, data with lowered proton beam energies of 460 GeV and 575 GeV were taken, each experiment recording approximately 13 pb^{-1} and 7 pb^{-1}, respectively. The primary purpose of this data is the measurement of the longitudinal proton structure function F_L.

The physics at an *ep* collider, which was to follow the fixed target experiments performed in the 70's, was summarised in a well-known article by Llewellyn Smith and Wiik [1] written 30 years ago. HERA has fulfilled those early expectations but delivered much more insight. While some predictions, such as the unification of electromagnetic and weak interactions, at Q^2 values as large as the squared masses of the weak bosons, were confirmed, new, original and unforeseen, views on the structure of the proton and the dynamics of quark–gluon interactions were gained. The observations at HERA led to an enormous development in the understanding of the underlying field theory of the strong interactions, Quantum Chromodynamics (QCD). New fields of study emerged and existing fields entered a new precision phase; among these are

the physics of high parton densities, the physics of high scale photoproduction and photon structure, the chromodynamic theory of heavy quark production and of hard diffraction. The limits set at HERA in the search for new heavy particles, as predicted, for example, in supersymmetric theories, are competitive with those set at the e^+e^- collider LEP and the $p\bar{p}$ collider Tevatron. As of this writing, no compelling indications of physics beyond the Standard Model have been found at these three colliders searching in the few hundred GeV energy range. The Large Hadron Collider (LHC) is now set to expand the search to the TeV scale. The proton structure determined with precision by H1 and ZEUS at the *ep* collider HERA is of crucial importance [2] for the physics of *pp* collisions at the LHC.

The current review is an overview of, and an introduction to, the physics results as obtained during the years of operation of HERA, with emphasis on the HERA I results since much of the more recent data is still being analysed. During the years 1992–2007, H1 and ZEUS have each published more than one hundred and fifty journal publications. Given the space limitations, not all subjects can be covered in the present review. The reader is referred to the web pages of the experiments [3] and to the series of international workshops on "Deep Inelastic Scattering and QCD" [4] at which, since 1994, the physics at HERA and related results have been discussed annually, and in depth. This paper focuses on the results of ZEUS and H1 and therefore cannot do justice to the impressive amount of theoretical work, on which the interpretations of the HERA data often rely. The readers are referred to the publications of the collaborations and papers cited therein. A review on early HERA results has been given in [5]. A recent general introduction to the physics of deep inelastic scattering is [6].

The paper is organised as follows: in Section 2 HERA accelerator issues are discussed, the *ep* kinematics and the two collider detector concepts are presented. Section 3 is devoted to the basic inclusive cross section measurements and the structure functions are derived. Section 4 presents the approaches of ZEUS and H1 to extract the quark and gluon momentum distributions in the proton from QCD fits to the inclusive data. Section 5 discusses measurements of jet production and their importance to the determinations of the gluon distribution and the strong coupling constant, α_s. Section 6 is devoted to the results of the production of charm and beauty quarks and their understanding in QCD. Section 7 presents results on diffraction, including inclusive scattering, vector meson production and the new field of deeply virtual Compton scattering (DVCS). Section 8 summarises the results on tests of the electroweak theory, in neutral and in charged current *ep* interactions. Finally, in Section 9, the main results on searches for new physics at high scales are presented.

The paper closes with a short summary and outlook. As this paper is being written there is still much analysis activity devoted to the publication of new and more accurate results, mainly based on the HERA II period of operation and upgraded detectors. In some areas, work on the combination of H1 and ZEUS results has begun, which is expected to lead to the ultimate accuracy of HERA data. Some combined H1-ZEUS data, such as those of inclusive DIS cross sections, have already been presented in preliminary form; however, as there are no combined published results available yet, their presentation is deferred essentially to a later review publication.

2. Accelerator and detectors

2.1. Introduction

HERA, the "Hoch Energie Ring Anlage" at DESY, Hamburg, was the first, and so-far the only, accelerator complex in which electrons and protons were collided. In the 60's and 70's several lepton–proton experiments were performed. Among these were the pioneering SLAC electron experiments [7] and the CERN muon experiments [8,9], in which a lepton beam of energy E_l between 20 and 280 GeV was scattered off a stationary nucleon target. The maximum energy squared in the center of mass system for fixed target lepton–proton scattering is $s = 2M_pE_l$ with the proton mass M_p. The available cms energy sets the basic kinematic limits in any deep inelastic lepton–nucleon scattering (DIS) experiment.

The SLAC experiment, in 1968, resolved the proton's structure down to a distance of 10^{-15} m at which it was discovered that the proton has point-like constituents. Since the energy available to lepton beams was limited to a few hundred GeV, several proposals were put forward to build an electron–proton collider as a two-ring structure with different types of particles being stored. In such a configuration the energy s becomes equal to $4E_eE_p$ which is about $2E_p$ times larger than the fixed target energy, for a given lepton beam energy. Since the late 60's, Bjoern Wiik and colleagues had considered such machines and proposed to probe proton's structure deeper with an *ep* collider at DORIS [10], later at the e^+e^- colliders PEP [11], TRISTAN [12] and PETRA (PROPER) [13] and subsequently at the proton ring accelerator SPS at CERN (CHEEP) [14]. Another *ep* collider proposal, to use the Tevatron accelerator, was put forward by a Canadian group (CHEER) [15]. When the decision to build a large electron–positron collider, LEP, at CERN was made, DESY endorsed the HERA proposal [16], i.e. the plan to build an electron–proton collider at highest attainable energy, i.e. $s \simeq 10^5$ GeV^2 with $E_e \simeq 30$ GeV and $E_p \simeq 800$ GeV. This design was challenging since it was to use a chain of two times four pre-accelerators (see Table 1) only some of which already existed at DESY, and enormous efforts were required to ensure its reliable operation and high luminosity. The design was made for positron— as well as electron–proton collisions and to achieve a large degree of longitudinal lepton beam polarisation, using the Sokolov–Ternov effect [17] and spin-rotators around the interaction regions.

Two general purpose collider detectors with nearly 4π acceptance were proposed in 1985, H1 [18] and ZEUS [19], and were built in the 80's. They were operated over the 16 years of HERA operation. Two further experiments at HERA were built and run in the fixed target mode. The HERMES experiment [20] (1994–2007) used the polarised $e^{\pm}$ beam to study spin effects in lepton–nucleon interactions using a polarised nuclear target. The HERA B experiment [21] (1998–2003) was

Table 1
Chain of (pre)accelerators at HERA and their energies

Protons	E_p	Electrons	E_e
Source	20 keV	Source	150 keV
RFQ	750 keV	LINAC II	450 MeV
LINAC III	50 MeV	PIA	450 MeV
DESY III	8 GeV	DESY II	7 GeV
PETRA	40 GeV	PETRA	12 GeV
HERA	920 GeV	HERA	27.5 GeV

The main ring is 6223 m in circumference. High field (5 T) superconducting dipole magnets bend a proton ring of up to 1 TeV of energy. The electron ring requires high power, provided by a system of normal and superconducting 500 MHz cavities, to compensate for the synchrotron radiation losses.

designed to investigate B meson physics and nuclear effects in the interactions of the proton beam halo with a nuclear wire target. The results of the fixed target experiments are not discussed in this review.

The collider detectors H1 and ZEUS were designed primarily for deep inelastic *ep* scattering at highest momentum transfers, Q^2, and large final state energies. Thus, much attention was paid to the electromagnetic and hadron calorimeters. The H1 collaboration chose liquid argon as active material for their main calorimeter to maximize long term reliability. The ZEUS collaboration chose scintillator active media and uranium as the absorber material for the desired equalization of the calorimeter "e/π" response to electrons and hadrons. The large calorimeters were complemented by large area wire chamber systems for muon momentum and hadron shower energy tail measurements. Because the e and p beam energies were very different, the detectors were asymmetric with extended coverage of the forward (proton beam) direction. Drift chambers inside the calorimeters, both in H1 and in ZEUS, were segmented into a forward and a central part. Later, in H1 starting in 1996 and in ZEUS from 2003 onwards, silicon detectors near the beam pipe were installed for precision vertexing and tracking. Both apparatus were complemented with detector systems positioned near the beam axis in the accelerator tunnel, to measure backward photons and electrons, mainly for the determination of the interaction luminosity, and to tag leading protons and neutrons in the forward direction. Thanks to enormous efforts of several hundreds of engineers and physicists, both experiments took data for the entire time of HERA's operation at high efficiency. The only exception was a period of two years after the modification of the interaction region in 2001, which had caused unexpected problems to the *ep* operation.

2.2. Accelerator

Most of the data at HERA were taken with electron or positron energies of $E_e \simeq 27.6$ GeV and $E_p = 920$ GeV. In the first years, 1992–1997, E_p was set to 820 GeV. In the last months of operation, March–May (June) 2007, E_p was lowered to 460 (575) GeV. Typical beam currents were $I_p \simeq 100$ mA and I_e ranged from about 35 mA at injection to 10–15 mA when the beam was dumped for refilling. Initially the use of PETRA as a pre-accelerator caused some problems due to eddy-current effects in HERA proton magnets at low energies and for tight injection aperture. With 174 colliding bunches the design luminosity of 1.4×10^{31} cm^{-2} s^{-1} was reached in 1997. The accelerator performance then stabilised and could be improved to give a total delivered integrated luminosity, between 1992 and mid 2000, of close to 200 pb^{-1}to each collider experiment. In the summer 2000, HERA operation was stopped for modifications of the interaction regions devoted to a further significant enhancement of the luminosity.

For HERA, with the matched proton and electron beam sizes and head-on collisions, the luminosity is essentially given by the product of the brightness, N_p/ϵ_p, with the electron bunch current divided by the square root of the β functions in x and y. Methods considered to increase the luminosity included improvements in the injector chain which would overcome space charge effects limiting the brightness and an increase of currents with added power. Eventually, the luminosity increase was achieved by reducing the β functions at the interaction point (IP), from $\beta_{xp} = 7$ m and $\beta_{yp} = 0.5$ m to $\beta_{xp} = 2.46$ m and $\beta_{yp} = 0.28$ m. This required the separation of the e and p beams much closer to the IP than in HERA I, i.e. at 11 m instead of 24 m. Moreover, combined function (bending and focusing) magnets were introduced as close as 2 m to the H1 and ZEUS interaction points. This forced H1 and ZEUS to modify the inner detector configurations, and thus in 2000 the physics program for *ep* scattering with Q^2 between about 0.1 and 2 GeV^2 was terminated. It took some time until the effect of the superconducting magnets on the vacuum near the IR was finally understood and regular, approximately bi-monthly, warming up and cooling down cycles of these magnets were introduced which improved the vacuum.

The period 2001–2003, following the modification of the IR, was extremely demanding. Beam induced background caused the central drift chambers of H1 and ZEUS to trip at very low currents. Identification of the background sources and their suppression became of vital importance for the experiments and the luminosity upgrade to be successful. In an intense period of particularly strong collaboration between the machine and the detector experts, a series of beam based experiments and background simulations was performed over a period of more than one year [22,23].

The different components of the background, those from the e and p beams, were investigated by varying the beam currents; special runs with one type of beam only were also made. Experimentally, it turned out that the dominant contribution was due to the dynamic interplay of synchroton induced effects with the proton beam: the new beam-line components combined with the bending of the electron beam closer to the IR than in HERA I caused ions to be released,

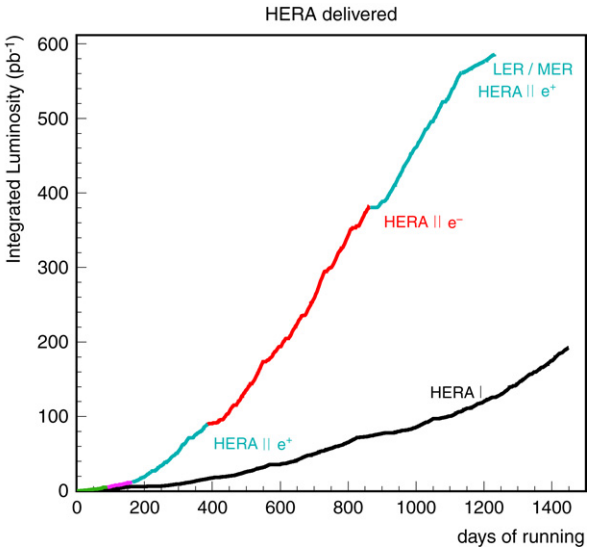

Fig. 1. Luminosity delivered by HERA to each of the collider experiments, H1 and ZEUS, as a function of the number of days of operation. HERA was operated in an initial phase (HERA I), 1992–2000, with unpolarised lepton beams, mainly with e^+. In the upgraded phase (HERA II), 2003–2007, the luminosity was increased and polarised $e^\pm$ data were taken with about equal amounts in terms of charge and polarisation states. The operation of HERA ended with two runs at 450 GeV (LER) and 575 GeV (MER) proton beam energy, in 2007.

which were scattered by the proton beam and its halo. Further problems arose due to the narrow aperture, from back-scattered synchrotron radiation and with leaks at flanges when the temperature load had risen too high due to mechanical or beam steering problems. The three successful counter measures were modifications of the beam absorber mask system, improved pumping and steady operation at slowly increasing currents to clean the surfaces using the synchrotron radiation itself. From the end of 2003 onwards, routine operation could be resumed with a specific luminosity increase as planned by a factor of about four and high positron/electron and proton currents. The annual delivered luminosity in 2006 was about 200 pb^{-1}, as much as had been delivered in the whole phase of HERA I. The machine was running very reliably and with high luminosity when its operation was ended.

Synchrotron emission leads to a build-up of transverse polarisation [17] with a characteristic time of about 30 min at HERA. Since 1994 this was used for the experimental programme of the HERMES experiment which was surrounded by spin rotators, a pair of dipole magnets flipping the spin from transverse to longitudinal orientation and back. In the first phase of HERA the collider experiments were not equipped with spin rotators. Polarisation effects, for unpolarised protons, result only from weak boson exchange at high Q^2 as the interference of Z_0-photon exchange in neutral current scattering occurs at at a size of order $10^{-4}Q^2/\mathrm{GeV}^2$. Thus, the spin rotators around H1 and ZEUS were installed only for the luminosity upgrade phase, HERA II. For HERMES, depolarising effects from the coils of H1 and ZEUS were compensated during HERA I with special magnets near the beam axis. Although the compensating magnets had to be removed when the focusing magnets were installed for the luminosity upgrade, HERA still achieved longitudinal $e^\pm$ beam polarisations with luminosity weighted means of typically 30% and maximum values of up to 40%–50%.

Eventually both H1 and ZEUS achieved total data collection efficiencies of 70%–80% and collected large $e^\pm p$ data samples corresponding to integrated luminosities of nearly 500 pb^{-1} each, as is illustrated in Fig. 1. The HERA operations ended with efficient low proton beam energy runs, in which 13 pb^{-1} at $E_p = 460$ GeV and 7 pb^{-1} at an intermediate energy of 575 GeV were collected in only three months. This would have taken about a year in the old, HERA I, configuration.

Physics at HERA would have profited from further running. Also one would have wished to accelerate deuterons at HERA in order to study the structure of the neutron in the new kinematic range, as was proposed in 2003 [24]. Nevertheless, the 16 years of data taking and analysis so far have already had a great impact on the understanding of the partonic structure of the proton and on the development of the theory of strong interaction dynamics. After the final publications, expected in a few years' time, the HERA programme will have spanned nearly three decades of exciting physics and experimentation with the participation of perhaps a thousand experts.

2.3. Deep inelastic scattering kinematics

The deep inelastic ep scattering cross section, $\mathrm{d}^2\sigma/\mathrm{d}x\mathrm{d}Q^2$, of the inclusive reaction $ep \to eX$ depends on the energy $s = 4E_eE_p$ and on two kinematic variables, usually taken to be the four-momentum transfer squared, Q^2, and Bjorken x. At HERA, x is obtained from the measurement of the inelasticity y, Q^2 and s as $x = Q^2/(sy)$. The salient feature of the HERA collider experiments is the possibility to determine the event kinematics in neutral current (NC) scattering from the electron e, or from the hadronic final state h, defined as all final state particles except the scattered lepton (and radiated

photons associated with the lepton), or using a combination of the two. This leads to a maximum exploitation of the available kinematic range and to a redundant control of the measurement which was absent in the fixed target DIS measurements. Exploiting the NC calibration for the measurement of the charged current (CC) processes, in which there is no scattered electron, is an important means to reliably reconstruct the inclusive scattering kinematics for the reaction $ep \to \nu X$. The choice of the most appropriate kinematic reconstruction method for a given phase space region is a non-unique decision based on resolution, measurement accuracy and radiative correction effects. H1 most frequently uses the "electron" and "sigma methods" while ZEUS most often uses the "PT" and "double angle methods" to reconstruct x and Q^2. These methods are introduced below.

The four-momentum transfer squared, Q^2, can be calculated from the incoming (k) and outgoing (k') electron four-momenta as follows

$$Q_e^2 = -q^2 = -(k-k')^2 = 2kk' = 2E_eE'_e(1-\cos\alpha_e) = 4E_eE'_e\cos^2\theta_e/2 \tag{1}$$

neglecting the electron mass and defining $\theta_e = \pi - \alpha_e$ to be the angle between the scattered electron direction and the proton beam axis.[1] The angle θ_e is measured with the tracking detectors, or by the determination of the impact point at the face of the calorimeters and the event-wise reconstructed position of the interaction vertex. Here E'_e is the scattered electron energy, measured by the calorimeters. The inelasticity is given by k, k' and P, the four momentum of the incoming proton, and similarly to Q_e^2, it can be calculated using the electron kinematics as

$$y_e = \frac{Pq}{Pk} = 1 - \frac{Pk'}{Pk} = 1 - \frac{E'_e}{2E_e}(1-\cos\theta_e). \tag{2}$$

Often these relations are expressed as

$$y_e = 1 - \frac{\Sigma_e}{2E_e} \qquad Q_e^2 = \frac{p_{t,e}^2}{1-y_e}, \tag{3}$$

in which Σ_e is the difference between the energy, E'_e, and the longitudinal momentum, $p_{z,e}$, of the scattered electron, and $p_{t,e}$ is its transverse momentum.

Similar relations are obtained from the hadronic final state reconstruction [25]

$$y_h = \frac{\Sigma_h}{2E_e} \qquad Q_h^2 = \frac{p_{t,h}^2}{1-y_h}, \tag{4}$$

where

$$\Sigma_h = \sum_i (E_i - p_{z,i}) \tag{5}$$

is the hadronic $E-p_z$ variable and the sum, as for the transverse momentum, extends over the calorimeter cells (and tracks in some cases) of the hadronic final state. In the reconstruction of the energy, the momentum measurements from the tracking detectors are also used and the corresponding energy deposits are removed from the sum. The hadronic energy is given by the relation

$$E_h = \frac{p_{t,h}}{\sin\theta_h}. \tag{6}$$

The angle of the hadronic system, θ_h, can be obtained from measurements of the energy and momentum components with the calorimeters as

$$\cos\theta_h = \frac{p_{t,h}^2 - \Sigma_h^2}{p_{t,h}^2 + \Sigma_h^2} \quad \text{or} \quad \tan\frac{\theta_h}{2} = \frac{\Sigma_h}{p_{t,h}}. \tag{7}$$

In the naive quark parton model (QPM), θ_h represents the angle of the struck quark.

A straightforward calculation using Eq. (1), (2) and $x_e = Q_e^2/sy_e$ relates the uncertainties on the electron energy and angle to the uncertainties on Q^2 and x as follows

$$\begin{aligned} \delta Q_e^2/Q_e^2 &= \delta E'_e/E'_e + \tan(\theta_e/2)\cdot\delta\theta_e \\ \delta x_e/x_e &= 1/y_e\cdot\delta E'_e/E'_e + [(1-y_e)/y_e\cdot\cot(\theta_e/2) + \tan(\theta_e/2)]\cdot\delta\theta_e. \end{aligned} \tag{8}$$

The uncertainty of Bjorken x_e thus appears to diverge at small y, in the presence of a possible miscalibration of the electron energy measurement or a misalignment affecting the polar angle measurement. On the contrary, the uncertainty of Q^2 has no divergent behaviour, and indeed the electron method allows Q^2 to be reconstructed optimally over the full kinematic

[1] The angles are defined between the directions of the outgoing particles and the proton beam. This somewhat unfortunate choice can lead to some confusion since Rutherford 'back-scattering' at HERA is the scattering of the electron at high Q^2 at small 'forward' angles.

range. There is also a term, $\propto \tan(\theta_e/2) \cdot \delta\theta_e$, which becomes sizable at very large angles, when the electron is scattered into the backward region, at small Q^2. This was an important motivation for building dedicated Backward Detectors, BST (H1) and BPT (ZEUS), as supplements to the original apparatus, to extend the acceptance and to reduce the influence of the resulting cross section uncertainty to a tolerable level by measuring θ_e extremely precisely at θ_e approaching 180° (see Sections 2.4 and 3.4.2).

Relations similar to Eq. (8) can be obtained for the Q^2 and x uncertainties in the hadronic final state reconstruction:

$$\begin{aligned}\delta Q_h^2/Q_h^2 &= (2-y_h)/(1-y_h)\cdot \delta E_h/E_h + [2\cot\theta_h + y_h/(1-y_h)\cdot\cot(\theta_h/2)]\cdot\delta\theta_h\\ \delta x_h/x_h &= 1/(1-y_h)\cdot\delta E_h/E_h + [-2\cot\theta_h + (1-2y_h)/(1-y_h)\cdot\cot(\theta_h/2)]\cdot\delta\theta_h.\end{aligned} \tag{9}$$

Unlike the case of electron-based reconstruction, the uncertainties, both for Q^2 and x, become large when y approaches 1. Thus the hadron reconstruction method and the electron method are complementary. It was proposed early in [26] to combine the variables Q_e^2 and y_h in the "mixed method" reconstruction of the event kinematics in order to avoid the divergent feature of x_e.

A further refinement in the kinematics reconstruction was introduced with the "sigma method" [27]. Various versions of this method exist; the basic idea relies on the exploitation of the total $E - p_z$ variable

$$E - p_z = E_e'(1-\cos\theta_e) + \sum_i \left(E_i - p_{z,i}\right) = \Sigma_e + \Sigma_h, \tag{10}$$

which for non-radiative events equals $2E_e$. Thus y_h, Eq. (4), can be redefined and one obtains

$$y_\Sigma = \frac{\Sigma_h}{E-p_z} \qquad Q_\Sigma^2 = \frac{p_{t,e}^2}{1-y_\Sigma}. \tag{11}$$

An important advantage of this construction is its reduced sensitivity to miscalibrations by using the final state energies and momenta instead of the incoming electron beam energy. The energy–momentum conservation requirement $E - p_z \simeq 2E_e$ has often been used to remove radiative events from the analysis.

A further method, the "double angle method", developed independently in [28] and [29], uses the possibility to express Q^2 and x by the electron and hadronic scattering angles which again have reduced sensitivity to energy miscalibrations

$$y_{DA} = \frac{\tan(\theta_h/2)}{\tan(\theta_e/2)+\tan(\theta_h/2)} \qquad Q_{DA}^2 = 4E_e^2\cdot\frac{\cot(\theta_e/2)}{\tan(\theta_e/2)+\tan(\theta_h/2)}. \tag{12}$$

An application of this idea is the double angle energy calibration method, in which the electron energy scale is determined from the measurements of θ_e and of θ_h, for regions of phase space in which both the electron and the hadrons are well contained in the apparatus.

H1 developed various versions of kinematic reconstruction methods. Diffractive analyses (see Section 7) often used a specific definition of the inelasticity as

$$y = y_e^2 + y_{DA}(1-y_{DA}). \tag{13}$$

A further idea has been to replace the electron beam energy in the calculation of x, similarly as it was replaced in y_Σ. This defines an extension of the Σ method which takes radiative effects at the lepton vertex completely into account giving

$$x_\Sigma = \frac{Q_\Sigma^2}{2E_p(E-p_z)y_\Sigma} = \frac{Q_\Sigma^2}{2E_p\Sigma_h}. \tag{14}$$

The hadronic final state, due to the particles lost in the beampipe as well as energy lost in the inactive material in the detector, is, in general, less well-determined than the scattered electron. In the "PT method" of reconstruction [30] used by the ZEUS collaboration, the fact that owing to the well-measured electron, $\delta_{PT} = P_{T,h}/P_{T,e}$ gives a good event-by-event estimate of the hadronic energy loss is used to improve both the resolution and uncertainties of the reconstructed y and Q^2. The PT method uses all measured variable, in a way specific to the ZEUS detector, to optimise the resolution over the entire kinematic range measured, namely,

$$\tan\frac{\theta_{PT}}{2} = \frac{\Sigma_{PT}}{P_{T,e}}, \qquad \Sigma_{PT} = 2E_e\frac{C(\theta_h, P_{T,h}, \delta_{PT})\cdot\Sigma_h}{\Sigma_e + C(\theta_h, P_{T,h}, \delta_{PT})\cdot\Sigma_h}. \tag{15}$$

The variable θ_{PT} is then substituted for θ_h in the formulae for the double angle method to determine y and Q^2. The detector-specific function C is $\Sigma_{\text{true},h}/\Sigma_h$ as a function of θ_h, $P_{T,h}$ and δ_{PT} and is determined from Monte Carlo simulations.

The double differential cross section has to be independent of how Q^2 and x are reconstructed. Many cross-checks of the results employ the underlying differences in the reconstruction algorithms and detector inputs. The measurement redundancies can also be expoited, as demonstrated in the case of the recent study of methods to average the H1 and ZEUS measurements [31], to reduce the final measurement uncertainty to, eventually, about 1%.

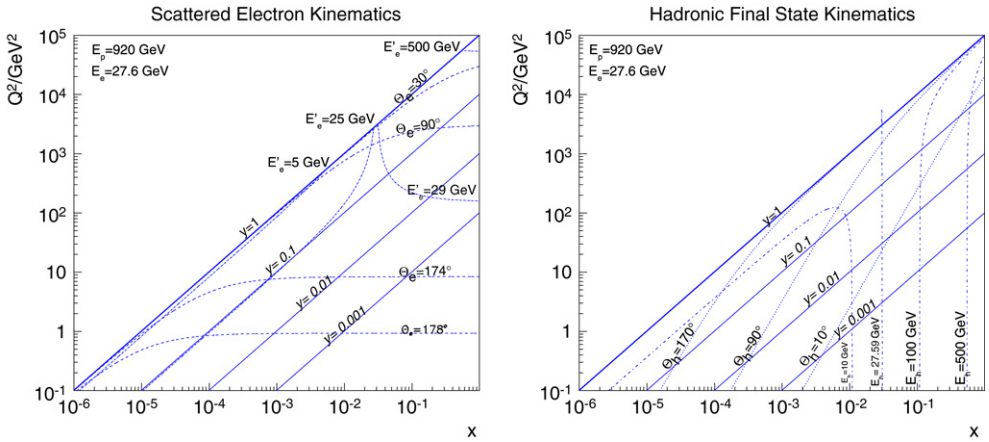

Fig. 2. Electron scattering kinematics (left) and kinematics of the hadronic final state (right). Dashed: lines of constant scattering angle, θ_e (left) and θ_h (right), in the Q^2, x plane. Dashed dotted: lines of constant energy, E'_e (left) and E_h (right). For the electron energy a large region (left), in which $E'_e \simeq E_e$ is observed, because of the relation $E'_e = Q^2/4E_e + E_e(1-y) \simeq E_e$, for small y and Q^2. The E'_e distribution thus exhibits a characteristic "kinematic peak" at E_e which is often used to cross check or calibrate the scattered electron energy scale. One also recognises in the left plot that in forward direction, at very high Q^2, the scattered electron carries very high energy of a few hundred GeV. The energy of the hadronic final state, E_h, varies rapidly with Bjorken x at intermediate x values. At high x, the hadronic final state becomes very energetic and much of the energy is emitted in forward direction. At $x = E_e/E_p = 0.03$ the iso-E_h line is independent of Q^2 and $E_h = E_e$.

2.4. Detectors

The H1 [32] and ZEUS [33] detectors are nearly 4π hermetic apparatus with a solenoidal field of 1.2 T and 1.43 T, respectively, built to investigate high energy ep interactions at HERA. Their main design features are determined by the need to measure energies and momenta up to a few hundred GeV, as is shown in the kinematic plane plots (Fig. 2).

Due to the large difference between E_p and E_e, the HERA apparatus, unlike similar devices at LEP or the Tevatron, are asymmetric. Large energy deposits, up to energies close to E_p, occur in the proton beam (forward) direction, and the particle multiplicity, due to the hard interaction and the proton remnant, is often very large. On the other hand, the hemisphere in the electron (backward) direction is less occupied, the energies deposited are below or comparable to E_e and the multiplicities are low. Such considerations have determined the final layouts of the H1 and the ZEUS detectors, as illustrated with the event displays showing an NC event in H1, Fig. 3, and a CC event in ZEUS, Fig. 4.

The main component of the H1 detector is the Liquid Argon Calorimeter (LAr). It has an inner electromagnetic part, which in the event of Fig. 3 is seen to fully contain the scattered electron energy, and an outer hadronic part, which is seen to contain the fraction of jet energy leaking out of the electromagnetic LAr. The LAr is surrounded by a superconducting coil producing a solenoidal magnetic field of 1.2 T and an instrumented iron structure acting as a shower tail catcher and a muon detector. Tracks are measured in the central tracking detector which contains three silicon detectors, the forward, central and backward trackers, FST, CST and BST. These are followed towards outer radii by the Central Inner Proportional Chamber, CIP, and the Central Jet Chamber, CJC. The CJC has two concentric parts, separated by the Central Outer-z Chamber, COZ. Tracks in forward direction are measured in the Forward Tracking Detector, FTD, a set of planar drift chamber modules of different azimuthal orientation.

The main component of the ZEUS detector is the Uranium–Scintillator calorimeter. Shown in Fig. 4 are the forward, barrel and rear components (F/B/RCAL) which are surrounded by a muon detector. The calorimeter is segmented into inner electromagnetic parts, of 5×20 cm^2 tower sizes in the barrel, followed by hadronic parts of coarser granularity, 20×20 cm^2. The space visible inside the BCAL is occupied by the coil giving a field of 1.43 T and a preshower detector. The tracking detector consists of a central cylindrical jet type drift chamber (CTD) and sets of planar drift chambers in forward (FTD) and rear (RTD) directions. During the upgrade phase, for HERA II, the FTD was modified by introducing straw tubes and inside the CTD a micro vertex detector (MVD) was added, comprising forward and central silicon strip detectors.

Besides the main parts of the H1 and ZEUS detectors, there were two instrumented areas further away from the interaction region, both in H1 and ZEUS:

- In the electron beam (backward) direction, several 'electron taggers' were placed, at 8 m, 33 m and 103 m for H1 and at 6 m, 8 m, 35 m and 44 m for ZEUS, in order to measure the scattered electron energy in a small range of θ_e close to 180°. Some of these taggers were installed for only a part of the data taking period. The electron tagger system enabled, in different acceptance regions of y_e corresponding to the different positions, inelastic ep scattering processes to be tagged at very small Q^2. The taggers thus allowed an efficient control and analyses of photoproduction processes. A process of particular interest is Bethe–Heitler scattering, $ep \rightarrow ep\gamma$, whose cross-section is known theoretically to about 0.5% accuracy and is thus suitable for the determination of the interaction luminosity. Therefore both H1 and ZEUS were also

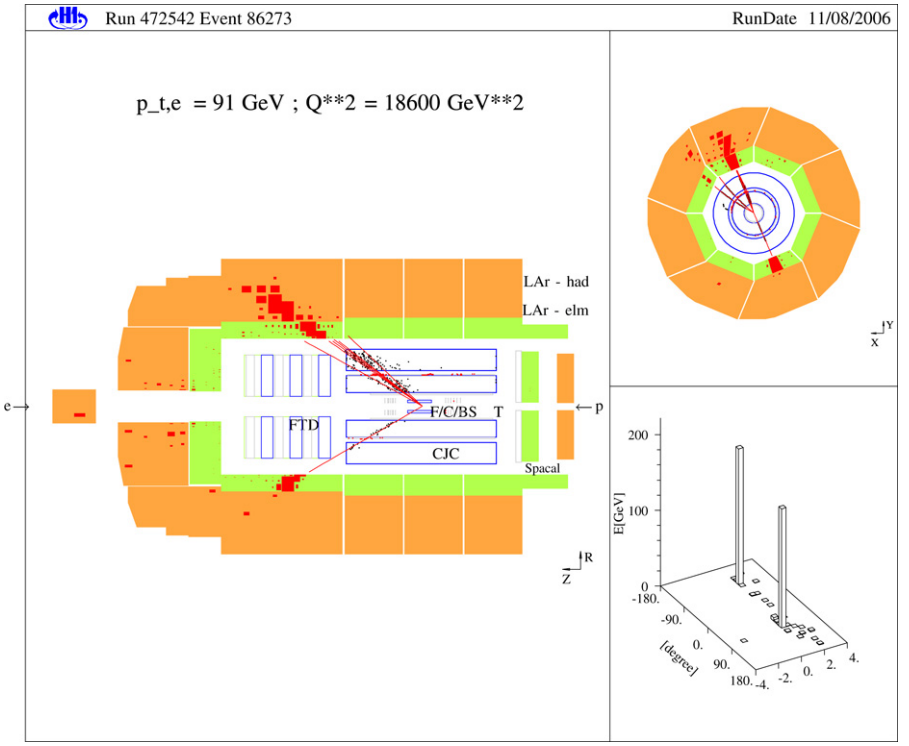

Fig. 3. Deep inelastic event from neutral current *ep* scattering as registered in the H1 apparatus in its upgraded, HERA II, configuration. The electron beam enters from the left and the proton beam from the right. On the left, an *rz* cross section shows the main components of the H1 detector as denoted, see text. The event has a transverse momentum of the scattered electron of 91 GeV and a Q^2 of 18 600 GeV^2 which correspond to $y = 0.55$ and $x = 0.33$. Thus the electron scattering angle is about $\theta_e = 30^\circ$ and $E'_e = 180$ GeV, i.e. at high Q^2 and large x the incoming electron is scattered in the forward direction and carries a rather large energy (cf. Fig. 2). The right top figure shows the event in the x, y projection exhibiting transverse momentum balance between the scattered electron and the hadronic final state as is characteristic for NC events. The lego plot visualizes the energy deposition in the LAr cells exhibiting the narrow jet structure of the hadronic final state emerging from the struck quark.

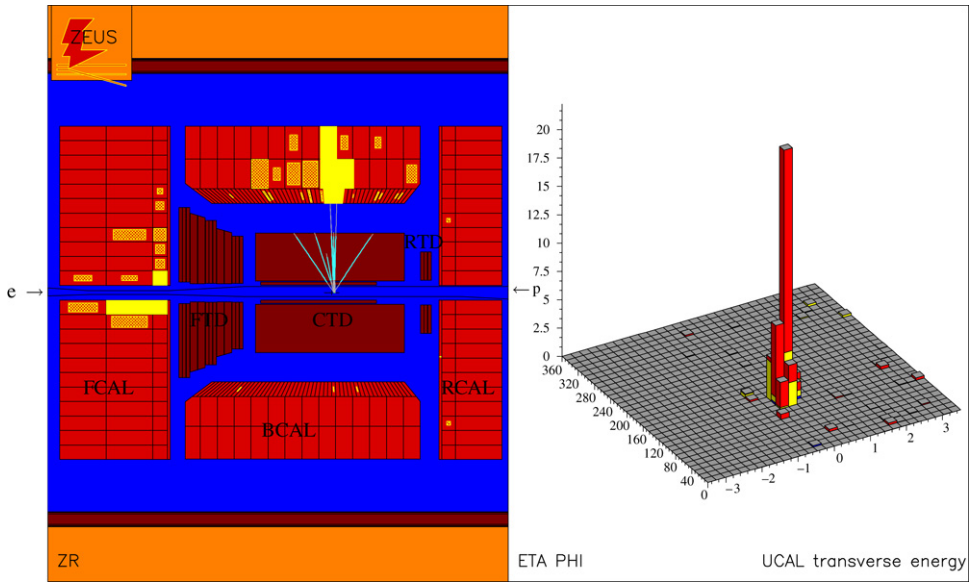

Fig. 4. Deep inelastic event from *ep* charged current scattering as registered in the ZEUS apparatus, in its HERA I configuration. The electron beam enters from the left and the proton beam from the right. On the left, an *rz* cross section shows the main components of the ZEUS detector as denoted, see text. The right figure shows the measured transverse energy in the calorimeter. The event is a typical charged current scattering event with an energetic jet, unbalanced in transverse momentum, and some energy produced from the proton remnant in forward direction. For this event one finds $\theta_h \simeq 90^\circ$ and $p_{t,h} \simeq 33$ GeV. From Eqs. (4)–(7) this corresponds to $Q^2 \simeq 2700$ GeV^2, $y \simeq 0.6$ and thus $x \simeq 0.05$, since at this time, HERA was operated with $E_p = 820$ GeV.

equipped with photon taggers positioned at $\simeq$100 m down the e beam line, at 180°. The measurement accuracy of the luminosity thus far is about 1.5% for both experiments.

- In the proton beam (forward) direction, protons and neutrons may be scattered at a small angle, via soft processes such as vacuum or pion exchange, respectively. Leading protons are a characteristic signature for diffractive processes such as hard diffraction or elastic vector meson production. Both H1 and ZEUS installed so-called forward or leading-proton spectrometers for HERA I, FPS and LPS, at about 100 m distance from the interaction point. During the upgrade, H1 kept its FPS and added another, very forward proton spectrometer, VFPS, positioned at 220 m away. ZEUS decided to remove the LPS during the upgrade phase. Similarly, H1 operated a forward neutron calorimeter (FNC) throughout the HERA lifetime while ZEUS confined the FNC operation to the first phase of HERA.

The detectors are complemented by systems of veto counters to reject beam background with time-of-flight measurements. In the forward direction, H1 had a muon detector system comprising a toroid magnet inside a system of drift chambers. Similarly ZEUS had a toroid magnet with drift tubes for muon track reconstruction and limited-streamer tubes for triggering.

The H1 and ZEUS detectors functioned very reliably although intense and challenging efforts in the operation, calibration and maintenance were required. The main components, the central drift chambers, the big calorimeters and the large area muon detectors ran over 15 years with high efficiency and without a need for replacements of the basic hardware. Parts of the readout and trigger electronics were replaced or updated. In 1997 the H1 central chamber had to be rewired when ageing effects were observed. Despite much higher backgrounds in HERA II, no ageing effects were seen in either of the H1 and ZEUS tracking chambers, apart from a small reduction of pulse-heights with time. The purity of the argon liquid in H1 was monitored and was found to worsen at a very small, tolerable rate of 0.05 ppm per year. The argon was exchanged only once, in 1995. Similarly, the scintillator material in the ZEUS Uranium calorimeter survived all the operation well.

The installation of focusing magnets near the beam pipe in the course of the luminosity upgrade, in 2001, required modifications of the H1 and ZEUS interaction regions. It also provided the only significant time period during which large detector upgrades, as mentioned above, could be made. The H1 detector upgrade program involved a large number of components; similarly ZEUS installed new hardware at various places of their apparatus. The original detector configurations are described in [32] and [33].

3. Proton structure functions

3.1. Introduction

The scattering amplitude for electron–proton scattering is a product of lepton and hadron currents times the propagator characteristic of the exchanged particle, a photon or Z_0 in neutral current scattering, a $W^{\pm}$ in charged current scattering. The inclusive scattering cross section therefore is given by the product of two tensors,

$$\frac{\mathrm{d}^2\sigma}{\mathrm{d}x\mathrm{d}Q^2} = \frac{2\pi\alpha^2}{Q^4 x}\sum_j \eta_j L_j^{\mu\nu} W_j^{\mu\nu}, \tag{16}$$

where j denotes the summation over γ, Z_0 exchange and their interference for NC, and $j = W^+$ or W^- for CC. The leptonic tensor $L_j^{\mu\nu}$ is related to the coupling of the electron with the exchanged boson and contains the electromagnetic or the weak couplings, such as the vector and axial-vector electron-Z_0 couplings, v_e and a_e, in the NC case. This leptonic part of the cross section can be calculated exactly in the standard electroweak $U_1 \times SU_2$ theory. The hadronic tensor, however, describing the interaction of the exchanged boson with the proton, can only be reduced to a sum of structure functions, $F_i(x, Q^2)$, but not be fully calculated. Conservation laws reduce the number of basic structure functions in unpolarised ep scattering to $i = 1 - 3$. In perturbative QCD the structure functions are related to parton distributions f via coefficient functions C

$$[F_{1,3}, F_2] = \sum_i \int_0^1 [1, z]\frac{\mathrm{d}z}{z} C_{1,2,3}\left(\frac{x}{z}, \frac{Q^2}{\mu_r^2}, \frac{\mu_f^2}{\mu_r^2}, \alpha_s(\mu_r^2)\right) \cdot f_i(z, \mu_f^2, \mu_r^2), \tag{17}$$

where i sums the quark q, anti-quark $\overline{q}$ and gluon g contributions and $f_i(x)$ is the probability distribution of the parton of type i to carry a fraction x of the proton's longitudinal momentum. The coefficient functions are exactly calculable but depend on the factorisation and renormalisation scales μ_f and μ_r. The parton distributions are not calculable but have to be determined by experiment. Their Q^2 dependence obeys the DGLAP evolution equations (see Section 4). A general factorisation theorem [34], however, has proven the parton distributions to be universal, i.e. to be independent of the type of hard scattering process. This makes deep inelastic lepton–nucleon scattering a most fundamental process: the parton distributions in the proton are measured best with a lepton probe and may be used to predict hard scattering cross sections at, for example, the LHC. The parton distributions are derived from measurements of the structure functions in NC and CC scattering, as is discussed below.

The following sections describe the structure function formalism, and present important NC and CC measurements. Both H1 and ZEUS have collected data samples of roughly 50–100 pb^{-1} of unpolarised e^+p data and of similar luminosity in the two charge and opposite helicity states (see Table 2).

Table 2
Integrated luminosity (L), in pb^{-1}, collected by H1 and ZEUS, for specific data selections, distinguished according to the beam charge and helicity (P) state

Exp	e^+ (0)	e^- (0)	$e^+(P)$	$e^+(-P)$	$e^-(P)$	$e^-(-P)$	Sum
H1 (P)	–	–	33	37	36	26	–
H1 (L)	100	15	95	75	46	103	432
ZEUS (P)	–	–	32	37	30	27	–
ZEUS (L)	100	15	98	76	81	105	475

The unpolarised data were taken in HERA I. The H1-ZEUS differences in polarisation and luminosity are due to somewhat different analysis criteria, data taking efficiencies and an asymmetry in rotator switches between H1 and ZEUS during the e^-p run, in the spring of 2006. While this review is being written a significant part of the polarised data, taken in the years 2004–2007, is still being analysed.

3.2. Structure functions and parton distributions

The neutral current deep inelastic ep scattering cross section, at tree level, is given by a sum of generalised structure functions according to

$$\sigma_{r,NC} = \frac{\mathrm{d}^2\sigma_{NC}}{\mathrm{d}x\mathrm{d}Q^2} \cdot \frac{Q^4 x}{2\pi\alpha^2 Y_+} = \mathbf{F_2} + \frac{Y_-}{Y_+}\mathbf{xF_3} - \frac{y^2}{Y_-}\mathbf{F_L}, \tag{18}$$

where the electromagnetic coupling, the photon propagator and a helicity factor are absorbed in the definition of a reduced cross section σ_r, and $Y_\pm = 1 \pm (1-y)^2$. The functions $\mathbf{F_2}$ and $\mathbf{xF_3}$ depend on the lepton beam charge and polarisation (P) and on the electroweak parameters, e.g. on the weak boson masses (M_Z, M_W) and the fine-structure constant α, as [35];

$$\begin{aligned}
\mathbf{F_2^\pm} &= F_2 + \kappa_Z(-v_e \mp Pa_e)\cdot F_2^{\gamma Z} + \kappa_Z^2(v_e^2 + a_e^2 \pm 2Pv_e a_e)\cdot F_2^Z \\
\mathbf{xF_3^\pm} &= \kappa_Z(\pm a_e + Pv_e)\cdot xF_3^{\gamma Z} + \kappa_Z^2(\mp 2v_e a_e - P(v_e^2 + a_e^2))\cdot xF_3^Z,
\end{aligned} \tag{19}$$

with $\kappa_Z(Q^2) = Q^2/[(Q^2 + M_Z^2)(4\sin^2\Theta\cos^2\Theta)]$ and the weak mixing angle $\sin^2\Theta = 1 - M_W^2/M_Z^2$. In the hadronic tensor decomposition [36] the structure functions are well defined quantities, independently to the parton model. In the Quark Parton Model (QPM) the longitudinal structure function is zero [37] and the two other functions are given by the sums and differences of quark (q) and anti-quark ($\bar{q}$) distributions as

$$\begin{aligned}
(F_2, F_2^{\gamma Z}, F_2^Z) &= x\sum (e_q^2,\, 2e_q v_q,\, v_q^2 + a_q^2)(q + \bar{q}) \\
(xF_3^{\gamma Z}, xF_3^Z) &= 2x\sum (e_q a_q,\, v_q a_q)(q - \bar{q}),
\end{aligned} \tag{20}$$

where the sum extends over all up and down type quarks and $e_q = e_u, e_d$ denotes the electric charge of up- or down-type quarks. The vector and axial-vector weak couplings of the fermions ($f = e, u, d$) to the Z_0 boson in the standard electroweak model are given by

$$v_f = i_f - e_f 2\sin^2\Theta \qquad a_f = i_f \tag{21}$$

where $e_f = -1, 2/3, -1/3$ and $i_f = I(f)_{3,L} = -1/2, 1/2, -1/2$ denotes the left-handed weak isospin charges, respectively. Thus the vector coupling of the electron, for example, is very small, $v_e = -1/2 + 2\sin^2\Theta \simeq 0$, since the weak mixing angle is roughly equal to 1/4. In a famous experiment [38] in polarised electron–nucleon scattering at very low Q^2, it was observed that $a_e \simeq -1/2$ which proved the absence of right-handed weak currents in the available energy range, and thus the validity of the most simple weak doublet structure, now called the standard electroweak theory [39].

Out of the eight structure functions entering in Eq. (18) four have been accessed at HERA. At low Q^2, the cross section is determined by F_2 and F_L. The longitudinal structure function F_L is measured at low x. The large gluon density in this region leads to a rather large value of F_L compared to those from the fixed target measurements which were measured at a much larger x.

At low Q^2 and low y the reduced cross section to a very good approximation is given by $\sigma_r = F_2(x, Q^2)$. Indeed the accurate knowledge of the proton structure, at low x from HERA and at large x from fixed target experiments, is mostly due to precision measurements of F_2. At $y > 0.5$, F_L makes a sizeable contribution to $\sigma_{r,NC}$. In the DGLAP approximation of perturbative QCD, to lowest order, the longitudinal structure function is given by [40]

$$F_L(x) = \frac{\alpha_s}{4\pi}x^2\int_x^1 \frac{\mathrm{d}z}{z^3}\cdot\left[\frac{16}{3}F_2(z) + 8\sum e_q^2\left(1 - \frac{x}{z}\right)zg(z)\right], \tag{22}$$

which at low x is dominated by the gluon contribution (see below). A measurement of F_L requires a variation of the beam energy since $\sigma_{r,NC}(x, Q^2; s) = F_2(x, Q^2) - y^2 F_L(x, Q^2)/Y_+$; F_L is obtained as the slope in y^2/Y_+ at fixed x and Q^2 ($y = Q^2/sx$). Two further structure functions can be accessed with cross section asymmetry measurements in which the charge and/or the polarisation of the lepton beam are varied.

Defining a reduced cross section, similar to $\sigma_{r,NC}$, for the inclusive polarised charged current $e^{\pm}p$ scattering as

$$\sigma_{r,CC} = \frac{2\pi x}{Y_+ G_F^2}\left[\frac{M_W^2 + Q^2}{M_W^2}\right]^2 \frac{\mathrm{d}^2\sigma_{CC}}{\mathrm{d}x\mathrm{d}Q^2}, \tag{23}$$

one obtains a sum of structure functions, analogous to Eq. (18), as

$$\sigma^{\pm}_{r,CC} = \frac{1 \pm P}{2}\left(W_2^{\pm} \mp \frac{Y_-}{Y_+} x W_3^{\pm} - \frac{y^2}{Y_+} W_L^{\pm}\right). \tag{24}$$

Here the Fermi constant G_F is defined [41] using the weak boson masses, in very good agreement with G_F determined from the measurement of the muon lifetime [42]. In the QPM (where $W_L^{\pm} = 0$), the structure functions represent sums and differences, that depend on the charge of the lepton beam, of quark and anti-quark distributions given by

$$W_2^+ = x(\overline{U} + D), \qquad xW_3^+ = x(D - \overline{U}), \qquad W_2^- = x(U + \overline{D}), \qquad xW_3^- = x(U - \overline{D}). \tag{25}$$

Using these equations one finds

$$\sigma^+_{r,CC} \sim x\overline{U} + (1-y)^2 xD, \tag{26}$$

$$\sigma^-_{r,CC} \sim xU + (1-y)^2 x\overline{D}. \tag{27}$$

Combined with Eq. (19), which approximately reduces to

$$\begin{aligned}\sigma^{\pm}_{r,NC} &\simeq [c_u(U + \overline{U}) + c_d(D + \overline{D})] + \kappa_Z[d_u(U - \overline{U}) + d_d(D - \overline{D})] \\ &\text{with } c_{u,d} = e^2_{u,d} + \kappa_Z(-v_e \mp P a_e)e_{u,d}v_{u,d} \quad \text{and} \quad d_{u,d} = \pm a_e a_{u,d} e_{u,d},\end{aligned} \tag{28}$$

one finds that the NC and CC cross section measurements at HERA determine the complete set U, D, $\overline{U}$ and $\overline{D}$, i.e. the sum of up-type, of down-type and of their anti-quark-type distributions. Below the b quark mass threshold, these are related to the individual quark distributions as follows

$$U = u + c \qquad \overline{U} = \overline{u} + \overline{c} \qquad D = d + s \qquad \overline{D} = \overline{d} + \overline{s}. \tag{29}$$

Assuming symmetry between sea quarks and anti-quarks, the valence quark distributions result from

$$u_v = U - \overline{U} \qquad d_v = D - \overline{D}. \tag{30}$$

Eq. (28) also shows that the vector and axial vector couplings of up and down type quarks can be determined at HERA. As will be discussed below, recent QCD fits have given quite remarkable results on joint determinations of parton distributions and of the weak neutral current coupling constants of the up and down type quarks. One notices that the underlying assumption here is that all up as all down type quarks have the same couplings, e.g. $a_u = a_c$, which holds in the Standard Model.

3.3. Measurement techniques

The inclusive neutral current scattering process is identified by the unique signature of an isolated electron cluster above some minimum energy, of a few GeV, in the LAr/Spacal (H1) or the U/Sc (ZEUS) calorimeters. In charged current scattering, a large transverse momentum, summed over all hadronic final state particles, is required (e.g. $p_T(h) > 12$ GeV). The NC and CC scattering events are required to have an interaction vertex within the nominal interaction region, ± 35 cm using the central trackers or, at the trigger level, of ± 2 ns from the nominal interaction time. Unlike H1, the time resolution of the ZEUS calorimeter is suitable for distinguishing genuine ep scattering from beam background outside the interaction region.

NC events, unlike CC events, are balanced in the transverse plane. Therefore the hadronic calorimeter can be calibrated requiring the ratio $p_T(h)/p_T(e)$ to be close to one. The calibration of the electromagnetic calorimeters is based on several types of events, in which the electron energy scale can be established, such as the QED Compton process, elastic ρ production in DIS and events within the "kinematic peak" region of phase space, in which the scattered electron has an energy very close to the initial beam energy. Also, comparisons with the tracking detector measurements and the electron energy determined with the double angle method (see Section 2.3) are used. Further adjustments to the linearity of the energy scale determination are made, for example in the case of the H1 Spacal calorimeter, with the reconstruction of the π_0 and the J/ψ mass. The calorimeters are aligned by matching the energy deposits with tracks found by the tracking system; also elastic Compton events, with characteristic back-to-back $e - \gamma$ energy deposits in the transverse plane, are exploited for this purpose.

The basic measurement technique is to compare the reconstructed event distributions with complete Monte Carlo simulation samples with much larger statistics than the data. Backgrounds are subtracted from the data; most important of these are the events due to photoproduction where the scattered electron escapes near the beam axis and an energy deposit

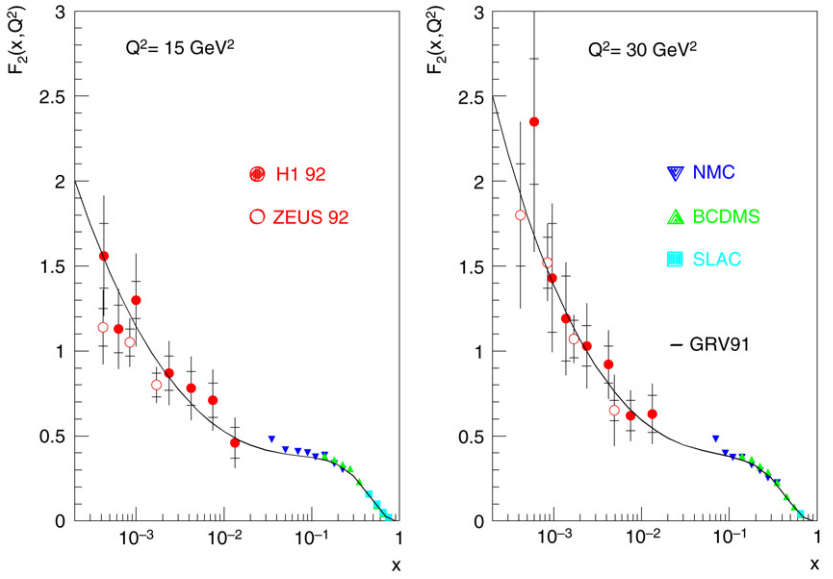

Fig. 5. The first measurements of H1 (solid points) and ZEUS (open points) of the proton structure function $F_2(x, Q^2)$ based on the data taken in 1992 shown as a function of Bjorken x. The H1 data at low (larger) x were obtained with the electron (mixed) method. The ZEUS data were obtained with the double angle method (see text). The HERA collider is equivalent to a fixed target lepton proton beam experiment of about 50 TeV lepton beam energy. The HERA experiments were thus able to extend the kinematic range of the F_2 data provided by the fixed target electron (SLAC) and muon (BCDMS, NMC) proton experiments by two orders of magnitude into the then-unknown domain of low x. The curve shows a result of the so-called dynamic parton distribution approach.

in the calorimeter is wrongly attributed to be the scattered electron. At small scattered electron energies, $E'_e \geq 2$ GeV, this background may well exceed the genuine DIS contribution. Therefore, in some analyses the calorimetric electron identification is complemented by a track associated with the calorimeter cluster. Additionally, efficiencies, such as those from the trigger condition used to select the CC or NC events, are determined from the data and are used to correct the simulation. Radiative corrections to the tree level cross section [41] in NC are much reduced by requiring the longitudinal momentum in the event to be conserved, i.e. $E - p_z \simeq 2E_e$ (see Section 2.3). The simulation is normalised to the measured luminosity, which is known to within 1%–2% at HERA using Bethe–Heitler scattering, $ep \to ep\gamma$. The cross section, binned according to detector resolution, is then determined as the ratio of the background subtracted number of DIS events in data to the simulated events, each corrected for the luminosity of the data sample and the simulation, respectively, and multiplied by the DIS cross section used in the simulation. With such techniques, refined in several aspects, both ZEUS [43] and H1 [44] have published, since 1993, about 15 papers each on the measurements of NC and CC cross sections at HERA.

3.4. Low Q^2 and x results

3.4.1. The discovery of the rise of $F_2(x, Q^2)$

The first measurements of the proton structure function $F_2(x, Q^2)$, shown in Fig. 5, were based on only 0.03 pb^{-1} of data, taken in 1992. With these first measurements the rise of F_2towards low x was discovered. This rise is in agreement with general expectations on the low x (large $\omega = 1/x$) asymptotic limit of QCD [45]; however, QCD could not predict the actual scale (Q^2) at which the limit would be applicable. The fixed target data available up to 1992 led to many extrapolations towards low x; for example, classic Regge theory [46] expected F_2 to continue to be flat at low x. The curve shown in Fig. 5 was the expectation of a model [47], in which the parton distributions were generated dynamically and evolved from a very low scale $Q^2 \simeq 0.3$ GeV ^{2} towards higher Q^2. In this approach a rise towards low x was indeed expected.

With increasing luminosity and improving understanding of such measurements, the accuracy increased from about 20% in the first data to 2% for the most recent measurements. The data of H1 and ZEUS have been rather consistent and mostly in good agreement for the various NC and CC cross section data. The best published measurements, thus far, of the reduced cross section at low Q^2 ($<$200 GeV^2) are displayed in Fig. 6. The left plot demonstrates the rise of the cross section from the rise of F_2 towards low x in all bins of Q^2. In the intermediate Q^2 range the cross section, $\sigma_r = F_2 - y^2 F_L/Y_+$, is observed to flatten or even turning over under the influence of the F_L term at high y. Dedicated measurements and analyses are being performed to extract F_L as is discussed below.

Another dramatic observation on the behaviour of $F_2(x, Q^2)$ was its strong dependence at fixed x on Q^2, (see Fig. 6 right). Thus the very first observations of scaling, the independence of $F_2(x, Q^2)$ on Q^2, has been confirmed only for $x \simeq 0.1$ where

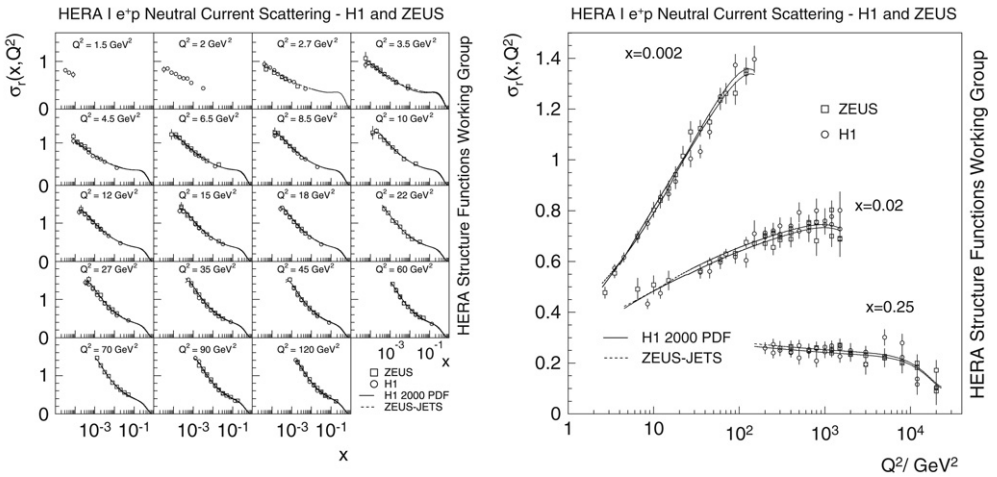

Fig. 6. Deep inelastic neutral current e^+p scattering cross section measurements, from the HERA I data taking period, as a function of x in different Q^2 intervals (left) and for three selected x bins as a function of Q^2 (right). Open points: H1, open squares: ZEUS. The error bars show the total uncertainty. The curves are NLO QCD fits as performed by H1 and ZEUS to their own data. The flattening of the curves for the two lower x values at large Q^2 is due to the effect of F_L (right plot). At $x = 0.25$ the data and the curves decrease visibly for Q^2 above a few 1000 GeV^2. This effect results from the γZ interference which reduces the cross section in positron–proton scattering at high Q^2, cf. Eq. (19), $\propto a_e x F_3^{\gamma Z}$ with $a_e = -1/2$.

it was first discovered at SLAC.[2] The H1 and ZEUS measurements illustrate the important differences between the scaling violations at high x, where F_2 decreases as a function of Q^2 due to gluon bremsstrahlung, and at low x, where F_2 increases as a function of Q^2 mainly due to $q\bar{q}$ pair production from photon–gluon fusion. The strong rise with Q^2 at low x is a major discovery of HERA.

3.4.2. Remarks on low x physics

Confrontation of the measurements with the DGLAP evolution equations (see Section 4) leads to the result that at low x the quark contribution to the $\ln Q^2$ derivatives is nearly negligible. This has two consequences: the measurement as presented in Fig. 6 (right) can be interpreted as the observation of a very large gluon distribution $xg(x, Q^2)$ at low x which at fixed Q^2 rises with x. Furthermore, neglecting the quark part (see [49]), one can infer from the second DGLAP equation that $xg(x, Q^2) \propto \exp\sqrt{c\ \ln T\ \ln(1/x)}$ with $T = \alpha_s(Q^2)/\alpha_s(Q_0^2)$ [50] and get a valid estimate of F_2 and its behaviour in Q^2 and x. Indeed one is thus able to obtain that $F_2(x, Q^2)$rises towards low x as $x^{-\lambda}$ with $\lambda \propto \sqrt{\ln T/\ln(1/x)}$. The rise is thus expected to be stronger as Q^2 increases as indeed is observed (see Fig. 6 left). A numerical study of this behaviour was performed in [51]. Much deeper theoretical evaluations can be found in [52]. Apart from the numerical success of this and further studies (see for example [53]) one finds that the proton structure at low x differs qualitatively from the large x limit: while the latter is given by the valence quark behaviour, the low x region is dominated by the dynamics of the QCD vacuum, the gluons.

Studies quoted above, and QCD fits discussed below, appear to validate the application of DGLAP equations over most of the HERA kinematic range. However, questions remain; because x is as small as 10^{-5} for $Q^2 > 1\,\text{GeV}^2$, there are expectations that terms neglected in DGLAP evolution, those proportional to $\ln(1/x)$, should become sizable and important [54]. Also, as Q^2 becomes small, the applicability of perturbative QCD becomes suspect and impossible when α_s approaches 1.

The rise of F_2 towards low x has been examined quantitatively [55,56] (see Fig. 7). For $x < 0.01$, where the valence quarks have a negligible role, the rise at fixed Q^2 may be expressed as $F_2 = Cx^{-\lambda}$. It has been measured that for $Q^2 > 3.5$ GeV^2, i.e. in the DIS region, the parameter C is approximately constant and $\lambda = 0.048 \cdot (\ln Q^2/\Lambda^2)$ with $\Lambda = 0.29$ GeV. At lower Q^2, the rise becomes weaker and C dependent on Q^2. This may be interpreted as a change from the partonic behaviour, at larger Q^2, to a hadronic behaviour [57] at lower Q^2, the transition taking place near $Q^2 \sim 1\,\text{GeV}^2$ corresponding to a resolution distance of about 0.3 fm. The so-called BPT data [58] below 1 GeV^2 which were obtained by ZEUS with a dedicated detector placed near to the beampipe, together with the precision measurements based on the central apparatus of H1 and ZEUS, play a crucial role in this observation.

The transition region is often studied in terms of the "colour dipole model" (CDM), which will also be discussed in connection with diffractive DIS in Section 7. The CDM is able to provide predictions, using a phenomenological ansatz for

[2] For rather accidental reasons the energy and angular range of the SLAC ep spectrometer was such that the measurements correspond to $x \simeq 0.1$. Therefore the first observations of inelastic DIS [7] occurred in a region where the behaviour of F_2 could rather directly be related to the quark interpretation of the proton structure. Departures from this behaviour, which were expected in field theory, were first observed at Fermilab [48], and with more accurate data, they could be shown subsequently to be logarithmic in Q^2. This was a major success in the process of establishing Quantum Chromodynamics as the appropriate field theory for quark–gluon dynamics.

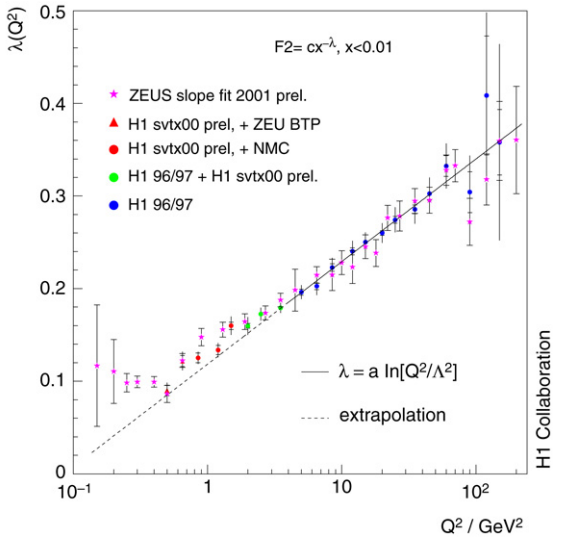

Fig. 7. Rise of F_2 versus x as a function of Q^2, see text. Note that with Q^2 also x varies, roughly as $x \sim Q^2/0.1$ s. The figure is from [59].

a hard scattering cross section, for a variety of cases, as for the structure functions F_2, F_L but as well for the diffractive and heavy quark structure functions, which are introduced below. The strict relations between these predictions lead to crucial tests of the validity of this approach [60], results of which can still be expected at HERA. The CDM model fundamentally does not distinguish between the partonic or hadronic behaviour of the proton and thus is applicable for large as well as very small values of Q^2 in DIS. It is to be also noted that the transverse size of the dipole is $2/\sqrt{Q^2}$; thus by varying the momentum transfer, one is able to probe the transverse extension of the proton. Most notably at HERA, the transverse size of gluons was measured for the first time [61].

The HERA physics of low x has important relations to other fields. The knowledge of the rising parton densities is of importance for investigations of the quark–gluon plasma phase in nucleus–nucleus collisions, as are studied at RHIC [62] and at the forthcoming LHC, as well as for cosmic super-high-energy neutrino physics [63]. Furthermore there is a wide range of forward scattering at the LHC, in which low x values are involved and it is, so far, not clear whether one may use the DGLAP equations, evolved to the LHC range, in order to understand large rapidity particle production characteristics. It is possible that modifications from the large contribution of $\ln(1/x)$ terms in this domain are needed for a full description.

3.4.3. The longitudinal structure function

There is a strong interest in F_L since the longitudinal structure function is a measure of the gluon distribution which is independent and complementary to the derivative $\partial F_2(x, Q^2)/\partial \ln Q^2$. A measurement of $F_L(x, Q^2)$ represents a crucial test of QCD to high orders as had long been studied experimentally [64] and theoretically [65]. The importance of this test at HERA rests also on the observation that the determinations of the gluon density at low x and low Q^2 (< 10 GeV^2) are not constrained well because of the lack of range and the uncertainties of the measurements of $\partial F_2(x, Q^2)/\partial \ln Q^2$.

At lowest x, corresponding to large y, the reduced cross section departs from F_2 because of F_L. This had been seen for the first time at HERA in [66]. A subsequent accurate measurement of the cross section up to high values of y is shown in Fig. 8. This measurement is particularly difficult because at high $y \simeq 1 - E'_e/E_e$, the scattered electron energy is rather small; $E'_e = 2.7$ GeV for $y = 0.9$. At such low energies the DIS electron signal is mimicked by hadronic energy depositions in photoproduction processes which poses severe difficulties in extracting the genuine DIS contribution.

The measurements of the high y cross section have been used by H1 to determine the longitudinal structure function at low x. This is enabled by the large kinematic coverage of HERA: the range in y extends over two orders of magnitude, thus at lower y (<0.35) one is able to determine F_2 which then may be extrapolated to the high y region. At larger Q^2, in the DIS region, as is illustrated in Fig. 8, one may use the NLO QCD fit to predict F_2 in the region where only σ_r is actually measured and subtract the F_2 part from the cross section. At lower Q^2 pQCD cannot be trusted and different means have been developed by H1 [67,68] to simultaneously determine F_L with F_2. The published H1 data on F_L are shown in Fig. 8, further results were presented subsequently in [68]. The principal problem of such determinations is of course their unavoidable dependence on the knowledge of F_2.

During the last 4 months of its operation, HERA was operated at reduced proton beam energies. Data samples of 13 pb^{-1} at 460 GeV and of 7 pb^{-1} at 565 GeV were collected by both ZEUS and H1. This data will allow a model-independent separation of the contributions of F_2 and F_L. Since the luminosity behaves as $L \propto E_p^2$, a reduction to half the energy requires 4 times longer running. A more precise measurement for statistical reasons will thus be restricted to the lower Q^2 region. As this paper is being written, both the ZEUS and H1 Collaborations are analysing the low energy run data and results are much

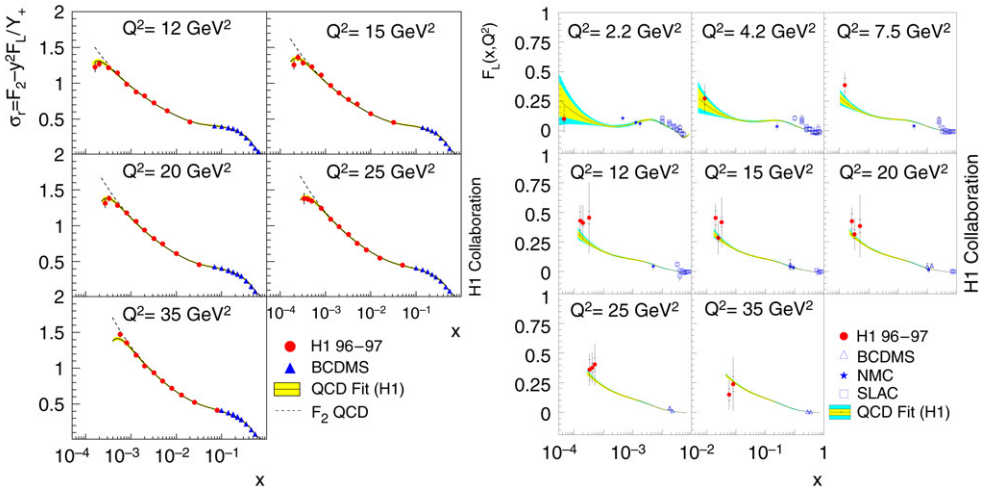

Fig. 8. Left: Measured reduced cross section as a function of x in the mid Q^2 region. The data at lowest x are seen to depart from the extrapolated behaviour of F_2. This departure, for each bin, occurs at about $y \simeq 0.5$ and is attributed to the effect of the longitudinal structure function F_L which at low x is large. The curves are the NLO QCD fit result on σ_r for $F_L = 0$ (dashed) and for F_L (solid) obtained in the fit. Right: The longitudinal structure function $F_L(x, Q^2)$ for different Q^2 bins as obtained by H1 at low x, and by charged lepton–proton scattering experiments at large x (see [67]). The curves are from the H1 α_s NLO QCD fit, described below, and its uncertainties.

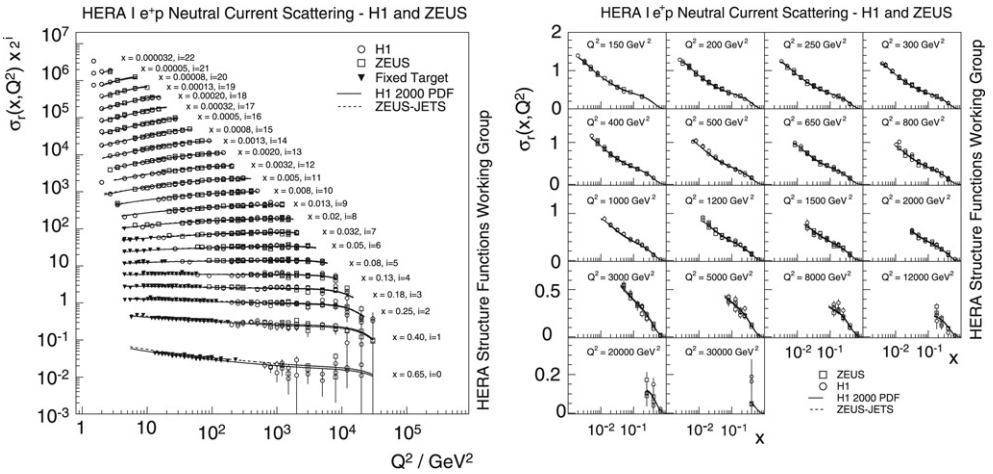

Fig. 9. Deep inelastic neutral current e^+p scattering cross section data from the HERA I data taking period. Left: NC reduced cross section data versus Q^2 for different x. The measurements are consistent with earlier DIS fixed target measurements but considerably extend the kinematic range in Q^2 and x. Right: NC cross section data versus x in different intervals of Q^2. The curves are NLO QCD fits as performed by H1 and ZEUS to their own data (see Sections 4 and 5.4).

anticipated. These will complement and perhaps validate previous attempts by the H1 Collaboration to extract F_L as were summarised briefly above. An attempt will also be devoted to the extraction of the diffractive longitudinal structure function, F_L^D, which is of particular theoretical interest and about which nothing is known experimentally so far [69].

3.5. High Q^2 results

The large cms energy of HERA has permitted the extension of the measurements of DIS lepton–proton scattering cross sections, as compared to previous fixed target experiments by about two orders of magnitude towards high momentum transfers squared, Q^2. This can be seen in Fig. 9 (left) which presents the cross section measurements as obtained previously in fixed target experiments and those from H1 and ZEUS as a function of Q^2 for the full range of Bjorken x covered. One observes scaling to hold for the complete Q^2 range at $x \simeq 0.1$. At larger x, negative scaling violations, due to quark bremsstrahlung, continue to exist up to high Q^2. One also observes in this range the tendency of the cross section to decrease stronger at highest Q^2 which marks the onset of the effects of the γZ interference contribution which for e^+p scattering is destructive, (see Eq. (19)). Fig. 9 (right) shows the H1 and ZEUS data

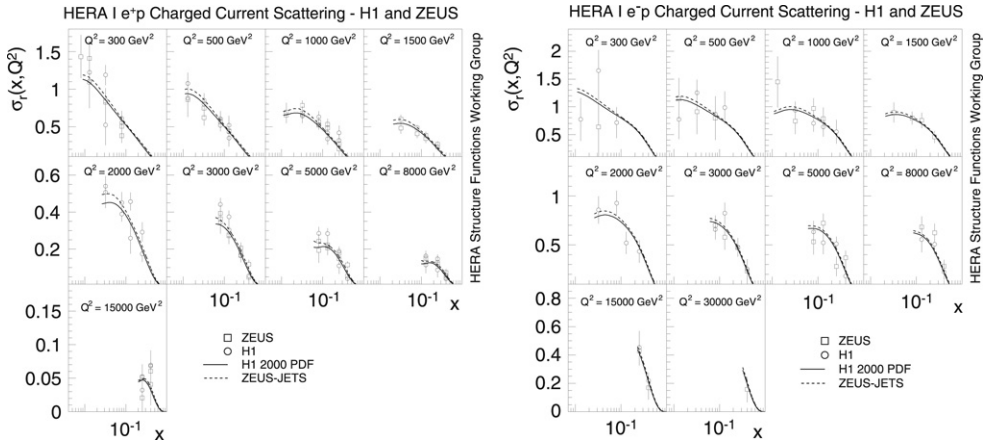

Fig. 10. Deep inelastic charged current $e^{\pm}p$ scattering cross section for Q^2 between 300 and 30 000 GeV^2, measured by H1 and ZEUS using data taken in HERA I. The errors shown are the total errors, which are dominated by the statistical uncertainty. The curves are NLO QCD fits as performed by H1 and ZEUS to their own data (see Sections 4 and 5.4).

in the high Q^2 region as a function of x. The data agree rather well and are described by NLO QCD fits. HERA has thus established perturbative QCD to be valid up to Q^2 values beyond 10^4 GeV^2 which was one of the questions posed initially [1] when one envisaged a high energy ep collider to be built.

Unlike fixed target experiments, which required separate electron/muon— and neutrino–nucleon scattering apparatus, neutral and charged current data could be taken simultaneously at HERA because at larger $Q^2 \geq 100$ GeV^2 the weak interaction process $ep \rightarrow \nu X$ becomes measurable. Fig. 10 shows the published results from ZEUS and H1 on $e^{\pm}p$ CC scattering. These data are of unique nature: they further support QCD, allow flavour contributions to proton's structure to be disentangled Eq. (25) and, as is discussed below, they demonstrate clearly that the electromagnetic and the weak interactions become of similar strength for $Q^2 \simeq M^2_{W,Z}$.

The data presented here belong to the initial (HERA I) period of data taking. The luminosity increase and the polarisation in HERA II have much enhanced the importance of the high Q^2 NC and CC data, which will be published in the future. Yet, the data from the HERA I period have already had a major impact on the determinations of the quark and the gluon distributions in the proton, and also on the determination of the strong coupling constant as is discussed in the following.

4. QCD fits

4.1. Introduction

In perturbative QCD the quark and gluon distributions $D(x, Q_0^2) = q, g$, determined at an initial value Q_0^2, can be evolved further in Q^2 using a system of coupled integro-differential equations (DGLAP equations)

$$\frac{\mathrm{d}q_i(x, Q^2)}{\mathrm{d}\ln Q^2} = \frac{\alpha_s(Q^2)}{2\pi} \int_x^1 \frac{\mathrm{d}z}{z} \left[\sum_j q_j(z, Q^2) P_{ij}\left(\frac{x}{z}\right) + g(z, Q^2) P_{ig}\left(\frac{x}{z}\right) \right] \tag{31}$$

$$\frac{\mathrm{d}g(x, Q^2)}{\mathrm{d}\ln Q^2} = \frac{\alpha_s(Q^2)}{2\pi} \int_x^1 \frac{\mathrm{d}z}{z} \left[\sum_j q_j(z, Q^2) P_{gj}\left(\frac{x}{z}\right) + g(z, Q^2) P_{gg}\left(\frac{x}{z}\right) \right], \tag{32}$$

which was introduced independently by Dokshitzer [70], Gribov and Lipatov [71] and by Altarelli and Parisi [72]. The splitting functions $P_{\alpha\beta}(x/z)$ in leading order represent the probability for a parton β with a momentum fraction z of the proton to emit a parton α with momentum fraction x of the parent parton. From χ^2 comparisons of these QCD predictions with data, the quark and gluon momentum distributions and the strong coupling constant $\alpha_s(M_Z^2)$can be determined. The equations can be applied in 3rd order (NNLO) perturbation theory due to a major progress, achieved recently, in pQCD calculations [73]. Most of the parton distribution analyses, as those presented subsequently, are still done in NLO. The next order will be important to match the still increasing accuracy of further DIS measurements from H1 and ZEUS. In the upcoming NNLO analyses, the dependences of the fit results, such as that for $\alpha_s(M_Z^2)$, on the chosen scales μ are expected to be reduced significantly.

The HERA data are at sufficiently high Q^2 at large x such that higher twists, power corrections $\propto Q^{-2}$ can be neglected. They extend to such low values of x, however, that issues as to whether the evolution equations need to be modified to include $\ln 1/x$ terms have been under investigation for many years [74]. Besides attempts to replace the DGLAP equations by different equations [54,75], corresponding to modified rules of multi-gluon emission at low x, the effects have also been investigated of their modification with a resummation of small x logarithms [52]. These studies, so far, have not lead to

definite conclusions. For the resolution of these questions, an increase in energy beyond HERA, as is considered with the LHeC [76], is very desirable in order to reach even lower x and to perform such investigations in a region of large enough Q^2 where $\alpha_s$is small.

The following sections present a brief overview on the most important pQCD analyses performed so far by ZEUS and H1 to examine the partonic content of the proton.

4.2. Determinations of parton distributions

The quark and gluon distributions in the proton define the various structure functions and their x, Q^2 dependence as given in Eqs. (17), (31) and (32). The principal method of extracting a complete set of quark distributions, $q(x, Q^2)$, and the gluon distribution, $xg(x, Q^2)$, requires a parameterisation of their x dependence at some initial value of $Q^2 = Q_0^2$, of a few GeV^2, as input to the DGLAP evolution equations and to the factorisation equation Eq. (17) leading to the structure functions. This procedure defines a pQCD prediction of the cross-sections at all Q^2 and x, which can be confronted in a χ^2 minimisation procedure to the data under study. Two DGLAP evolution programs QCDNUM [77] and QCDFIT [78], which were independently developed, are used most often in the HERA QCD analyses. They have been cross-checked against each other and against a Mellin transformation code at both the HERA Physics Workshop in 1995 and subsequently at the HERA–LHC Workshop in 2005.

The ZEUS and the H1 Collaborations so far focused mainly on analyses of their own data, as are described subsequently. There have been different attempts for global determinations of the parton distributions, such as those by the MRST [79] group, by the CTEQ [80] group and by Alekhine [81], in which much wider sets of data, in particular those from lepton–nucleon fixed target experiments and the Drell–Yan measurements, are considered. Unlike the fixed-target data, the HERA data constitute a complete set of NC and CC cross sections over a very wide range in x and Q^2. The additional constraint obtained from having both e^+p and e^-p data allows the extraction of sets of parton distributions that approach the accuracy of global determinations. There are specific regions for which HERA data do not have sufficient accuracy; examples are the high x behaviour of the u/d valence quark ratio, which is better derived from lp and lD data, and the $\bar{u} - \bar{d}$ difference, which is clearly observed at medium $x \simeq 0.01$ [82] in Drell Yan data but was only barely discernable in the initial H1 data [83]. This could have been accessed at low x with electron–deuteron data at HERA.

An important consideration in doing pQCD pdf fits is the treatment of systematic errors. In the H1 fits, the correlated systematic uncertainties are treated as fit parameters; this means the optimum value of systematic shifts of the cross-sections are determined through the fit. After the initial fit, the model assumptions (the shape of the pdf parameterisation, for example) in the fit are varied to determine the "model uncertainties" which are separate from the systematic uncertainties of the data. In the ZEUS fits, on the other hand, the initial fit that determines central values of the parameters is made with the systematic offsets set to zero. Then an "envelope" of n systematics errors is determined by repeating the fits $2n$ times after off-setting the cross-sections to the $+1$ standard deviation and -1 standard deviation values allowed by the systematic uncertainties and then adding the changes in quadrature.[3] The model uncertainties are then found by repeating the central fit with the variation on model assumptions. The uncertainties of the H1 pdf results are dominated by the model uncertainties, whereas the systematic uncertainties dominate the ZEUS data. It is remarkable that the uncertainties of H1 and ZEUS fits are, in the end, about the same [84].

A further challenge for the QCD pdf determinations consists in the treatment of the heavy flavours. At HERA, the charm and beauty contributions to the cross section are significant (see below) and the data are in Q^2 regions which include the c and b thresholds. A quark which is heavy, compared to the QCD parameter $\Lambda \sim 0.3$ GeV, becomes light at very high Q^2 compared to $M_{c,b}^2$. Correspondingly there exist various theoretical prescriptions on the treatment of c and b, as light quarks, as variable in their appearance or as heavy quarks, from γg fusion (see [85] for reviews). Fits have been presented with different heavy flavour treatments or versions of the variable flavour scheme (VFNS). ZEUS (Section 4.2.1), has specifically used the VFNS scheme of [86]. H1 has presented a fit to data at lower Q^2 using the fixed flavour scheme, in the determination of α_s (Section 4.3), or assumed the heavy quarks to be light in the analysis, described in Section 4.2.2, which focused on their high Q^2 data. These and further differences lead to somewhat different results. Work is in progress, both by the global fit groups and by ZEUS and H1, to further pin down such differences and arrive at fits, desirably at NNLO, based on the most plausible assumptions as well as on new and possibly combined data sets.

The following sections describe briefly the different fits of ZEUS and H1 in the determination of the parton distributions. In Section 5, the influence of di-jet data is illustrated on the determination of the parton distributions, in particular on xg at medium x. Important insight to the behaviour of the gluon distribution at low x is expected from the forthcoming direct measurement of the longitudinal structure function.

4.2.1. The ZEUS approach

The ZEUS Collaboration performed, in recent years, three major NLO QCD analyses, a ZEUS-S (standard) fit [87], which includes the fixed-target DIS data in the fit, a ZEUS-O (ZEUS data only) fit [88] and a fit to the inclusive data together with

[3] In practice this is done through a matrix inversion procedure [78].

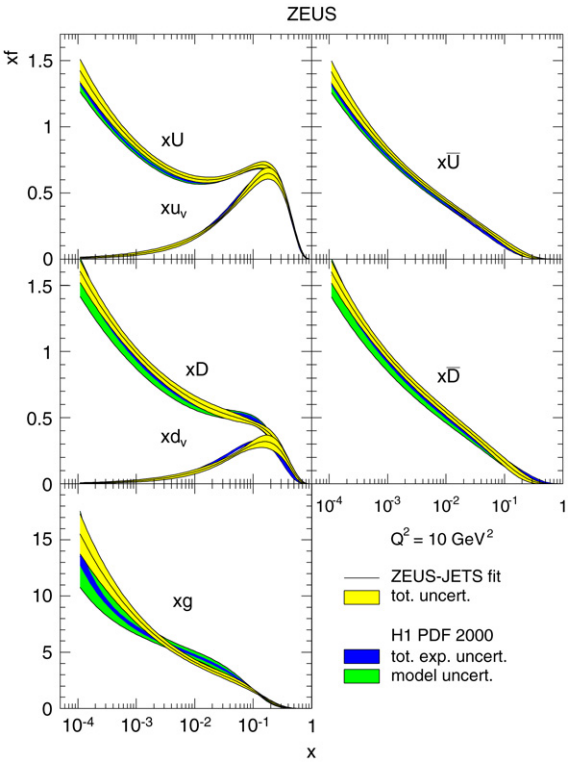

Fig. 11. Quark and gluon distributions determined by the ZEUS-Jets and the H1PDF2000 fits vs. x at $Q^2 = 10\ \mathrm{GeV}^2$. Shown are the total error bands which include the experimental and the model uncertainties (not separated for ZEUS). One notices the gluon dominance at low x at which xg is about 10 times larger than xU, for example.

di-jet data in DIS and photoproduction, ZEUS-Jets fit. The ZEUS-O fit exhibited the power of the HERA data in coming quite close in accuracy and detail to the ZEUS-S fit. Here only the ZEUS-O fit is briefly presented. The effect of adding jet cross section information, (the ZEUS-jets fit) in particular on the gluon determination, is described in the next Section.

The main idea of the ZEUS-O pdf parameterisation, following a QCD fit tradition, is to decompose the quark contributions into sea quarks and valence quarks. Four quark distribution combinations were used:

$$S = 2(\bar{d} + \bar{u} + \bar{s} + \bar{c}), \quad \Delta = \bar{d} - \bar{u}, \quad d_v = d - \bar{d}, \quad u_v = u - \bar{u}. \tag{33}$$

These distributions (times x) and xg are parameterised as four-parameter polynomials of the type

$$xf(x) = p_1 x_2^p (1-x)^{p_3}(1 + p_5 x). \tag{34}$$

The strange sea was coupled to the light sea, $x\bar{s} = 0.1xS$, and the charm contribution was dynamically generated [88]. The most detailed information in the HERA data is on the sea, xS, for which all 4 parameters were determined, using in addition the momentum sum rule, which fixes the integral over $xg + xS + xu_v + xd_v$ to be one. There is a weak constraint coming from the charged current data, on the difference between $\bar{u}$ and $\bar{d}$. Such a difference has been established in the muon-nucleon data as a violation of the Gottfried sum-rule and rather accurately measured in Drell–Yan scattering [82]. For $x\Delta$ a choice was taken to let only the normalisation parameter p_1 float and set $p_2 = 0.5$, $p_3 = p_3(S) + 2$ and $p_5 = 0$. Both valence quark distributions were used fixing $p_2 = 0.5$ and requiring the integral over u_v to be 2 and over d_v to be 1 (quark counting rule). Finally $p_5 = 0$ was used for xg which constrains the high x gluon to be positive. Results from these fits are discussed in detail in [88]. Subsequently fits were performed with additional information on jets. This lead generally to a consistent set of pdf's, both with the purely inclusive ZEUS-O fit, and with the H1 fit which is briefly described in the following.

A comparison of the ZEUS and H1 pdf's is presented in Fig. 11. The agreement can be called indeed remarkable for it uses different data, different flavour decompositions, different parameterisations, different χ^2 definitions and independent programs imposing differing heavy flavour treatments. More detailed inspection reveals that there are differences to be understood, as on the behaviour of xg at low x and Q^2.

4.2.2. The H1 approach

The NLO QCD analysis (H1PDF2000 fit) [89] of the H1 Collaboration of the CC and NC cross sections exploits Eqs. (26) and (28) which suggest a decomposition of the various structure functions into the four basic combinations of up (U, $\bar{U}$) and

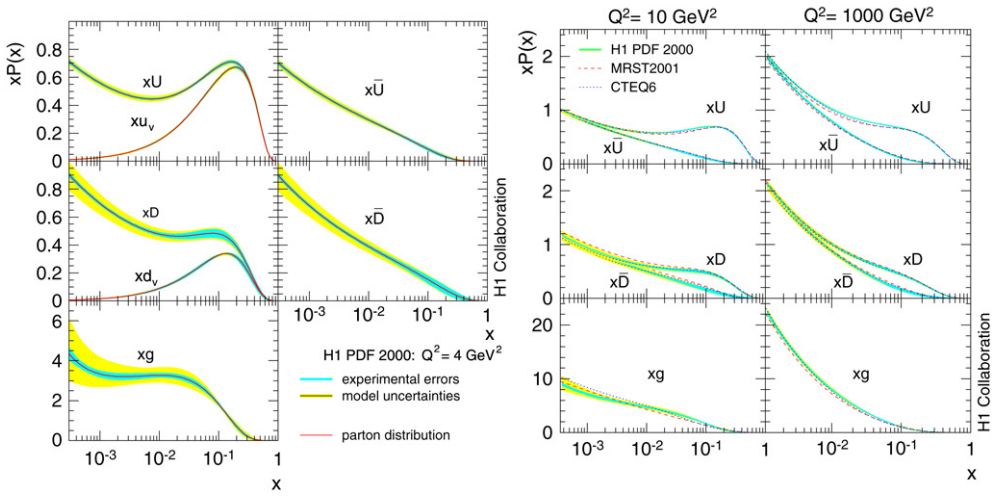

Fig. 12. Determination of the sum of up, anti-up, down and anti-down quark distributions and of the gluon distribution in the proton based on the H1 neutral and charged current cross section data. Left: the parton distributions with their experimental and model uncertainties as determined by H1 at the starting scale $Q_0^2 = 4\ \mathrm{GeV}^2$; Right: for Q^2 of 10 and 1000 GeV^2, the H1 fit is compared with results from MRST and CTEQ.

down (D, $\overline{D}$) quarks and antiquarks Eq. (29). The data used as input are the fixed-target BCDMS data as well as the H1 data. The fit was developed in conjunction with the publication of the HERA I high Q^2 data. It was thus decided to use the simplest heavy flavour treatment and consider all quarks to be light. As illustrated in Fig. 12, the four effective quark distributions and the gluon distribution xg are rather accurately determined. The accuracy achieved so far, at $Q^2 = Q_0^2$, for $x = 0.01$, 0.4 and 0.65, is 1%, 3%, 7% for the sum of up quark distributions and 2%, 10%, 30% for the sum of down quark distributions, respectively. It is to be noted that in this particular fit the gluon distribution comes out to be rather steeply rising towards lowest x at $Q_0^2 = 4\ \mathrm{GeV}^2$, $\propto x^{-0.9}$, a behaviour which in most other analyses is not confirmed. While this low x peculiarity had been noted, the fit was still accepted because of a large uncertainty of xg in this region. Also, in the higher Q^2 region for which this analysis was optimised, the fit is in good agreement both with previous H1 results [67] and with the results obtained in global fits by the MRST [90] and CTEQ [91] collaborations (Fig. 12).

The larger x domain is dominated by the valence quarks. In this analysis, these are extracted from the differences $u_v = U - \overline{U}$ and $d_v = D - \overline{D}$. Note that this implies the assumption that sea and anti-quarks are equal which is contradicted by some non-perturbative QCD models.

In the H1 fit the parton distributions at the initial scale $Q_0^2 = 4\ \mathrm{GeV}^2$ are parameterised as $xP = A_P x^{B_P}(1-x)^{C_P} \cdot f_P(x)$. The function f_P is a polynomial in x which is determined by requiring "χ^2 saturation" of the fits, i.e. starting from $f_P = 1$ additional terms $D_P x$, $E_P x^2$ etc. are added and only considered if they cause a significant improvement in χ^2, half integer powers were considered in [92]. The result for fitting the H1 data has been as follows: $f_g = (1+D_g x), f_U = (1+D_U x+F_U x^3)$, $f_D = (1+D_D x)$ and $f_{\overline{U}} = f_{\overline{D}} = 1$. The parton distributions at low x are thus parameterised as $xP \to A_P x^{B_P}$. The strange (charm) anti-quark distribution is coupled to the total amount of down (up) anti-quarks as $\bar{s} = f_c \overline{D}$ ($\bar{c} = f_c \overline{U}$). In the absence of more detailed information, two assumptions have been made on the behaviour of the quark and anti-quark distributions at low x. It has been assumed that quark and anti-quark distributions are equal and, moreover, that the sea is flavour symmetric. This implies that the slopes B of all four quark distributions are set equal, $B_U = B_D = B_{\overline{U}} = B_{\overline{D}}$. Moreover, the normalisations of up and down quarks are the same, i.e. $A_{\overline{U}}(1-f_c) = A_{\overline{D}}(1-f_s)$, which ensures that $\overline{d}/\overline{u} \to 1$ as x tends to zero. If the normalisation and slope conditions are relaxed, the uncertainties of the pdf's at lower x becomes large [83]. Some constraints can be inferred from fixed target deuteron DIS data and will also be derived from $W^{\pm}$ asymmetry data at the LHC. A high energy collider eD experiment would deliver the ultimate answer as to how the sea at low x is composed.

4.3. Measurements of α_s in inclusive DIS

The scaling violations at large Bjorken x are due to gluon bremsstrahlung. In the valence quark approximation the DGLAP equation for F_2 takes a non-singlet form, i.e. there is no contribution from the gluon to the scaling violations which are solely regulated with α_s. At low x, on the contrary, the dominant process is boson–gluon fusion and the scaling violations are governed by the product of α_s and xg. The HERA data, unlike previous fixed target data at lower energy, therefore have the potential of resolving the correlation between α_s and the gluon distribution for they span such a large range in x and Q^2. This has been exploited by ZEUS and H1 to determine both the strong coupling constant and xg from the inclusive DIS data using NLO perturbative QCD.

The ZEUS Collaboration has used its standard (S) fit and parameterisations as described above. In addition to the ZEUS data, a number of fixed target experiment data was used in addition (see [88]), in order to have better accuracy for the

Table 3
Dependence of $\alpha_s(M_Z^2)$in the H1 fit on the renormalisation and factorisation scales m_f and m_r, respectively, expressed as the difference of $\alpha_s(M_Z^2)$obtained for scales different from one and the central value of $\alpha_s(M_Z^2) = 0.1150$

	$m_r = 0.25$	$m_r = 1$	$m_r = 4$
$m_f = 0.25$	−0.0038	−0.0001	+0.0043
$m_f = 1$	−0.0055	–	+0.0047
$m_f = 4$	–	+0.0005	+0.0063

The combination $m_f = 4$ and $m_r = 0.25$ is abandoned since the splitting function term $\propto \ln(m_r/m_f)^2$ becomes negative at low Q^2 which causes a huge increase of χ^2.

high x region and constraints on the up-down quark asymmetry at medium x. The heavy quarks were treated in a variable flavour scheme. Standard cuts were made on the input data with $Q^2 > 3$ GeV^2 and $W^2 > 20$ GeV^2 in order to be in the DIS region and avoid higher twist contributions, from low Q^2 and large x, respectively. The input scale at which the pdfs are parameterised was chosen to be $Q_0^2 = 7$ GeV^2. The result obtained is

$$\alpha_s(M_Z^2) = 0.1166 \pm 0.0049(\text{exp}) \pm 0.0018\ (\text{model}) \tag{35}$$

where the experimental error comprises three uncertainties, 0.0008 from uncorrelated error sources, 0.0032 from correlated error sources and 0.0036 from normalisation uncertainties. The model uncertainties stem from variations of the fit parameters, Q^2_{min}, x_{min} and W^2_{min}, and of variations of quark and gluon distribution function parameterisations. The result changes by 0.001 if the heavy flavours are treated in the fixed flavour scheme. Special care was devoted to the effect of higher twists as the fit included fixed target data at rather small Q^2 but large x. With an x dependent parameterisation of power corrections $\propto Q^{-2}$, it was observed that $\alpha_s(M_Z^2)$may be lowered by 0.0032.

The H1 Collaboration developed a dedicated procedure [67] for the determination of α_s which differed in several respects from their pdf fit described above. The input data were restricted to H1 and BCDMS lepton–proton scattering data when it was found that the NMC data, extending to low Q^2 of a few GeV^2 introduced a significant dependence of the $\alpha_s(M_Z^2)$result on Q^2_{min} (see also [93]). Since this requires the movement of the minimum Q^2 for the fixed target data up to about 10 GeV^2, the accuracy of the BCDMS data is so overwhelming that no further fixed target data has to be included, apart from consistency checks [67]. The analysis also excluded the low y data of BCDMS from the analysis for systematic reasons. The second feature of the H1 fit was the attempt to reduce the number of quark distributions to be fitted from the usual three to two. This was possible as the fit was essentially on F_2 only, which can be written as a sum over singlet and non-singlet contributions as

$$F_2 = \frac{2}{9} \cdot x\Sigma + \frac{1}{3} \cdot x\Delta = \frac{1}{3} \cdot xV + \frac{11}{9} \cdot xA. \tag{36}$$

The V, A functions are given as

$$V = \frac{3}{4}[3(U + \overline{U}) - 2(D + \overline{D})] = \frac{9}{4}u_v - \frac{3}{2}d_v + \frac{9}{2}\overline{u} - 3(\overline{d} + \overline{s}) \tag{37}$$

$$A = \frac{1}{4}[2(D + \overline{D}) - (U + \overline{U})] = -\frac{1}{4}u_v + \frac{1}{2}d_v - \frac{1}{2}\overline{u} + (\overline{d} + \overline{s}) \tag{38}$$

for 3 flavours as heavy flavours were generated according to boson–gluon fusion. In the simplified approximation, $u_v = 2d_v$ and $\overline{u} = \overline{d} = 2\overline{s}$, one finds that V and A are valence and sea quark dominated functions, respectively, as in this approximation $V = 3u_v/2$ and $A = \overline{u}$. Despite the reduction in the pdf space, the fit could impose the usual momentum and quark counting rules and also a non-zero $\overline{u} - \overline{d}$ difference. The result obtained is

$$\alpha_s(M_Z^2) = 0.1150 \pm 0.0017(\text{exp})^{+0.0009}_{-0.0005}\ (\text{model}). \tag{39}$$

The first error represents the experimental uncertainty of the data sets. The second error includes all uncertainties associated with the construction of the QCD model for the measured cross section. A number to be noted may be that a 100 MeV uncertainty on the value of the charm mass results in an $\alpha_s(M_Z^2)$uncertainty of 0.0005.

The experimental results of ZEUS and H1 are consistent, and with more accurate and the combined data sets a further improved measurement will be reached. A rather large theoretical uncertainty of the NLO analysis, however, results from the choices of the renormalisation scale $\mu_r^2 = m_r \cdot Q^2$, and of the factorisation scale $\mu_f^2 = m_f \cdot Q^2$ which leads to scale dependent parton distributions. In the $\overline{MS}$ renormalisation scheme both scales are set equal to Q^2, i.e. $m_r = m_f = 1$. The effect of both scales on $\alpha_s$was estimated by both ZEUS and H1 through variations of the scale factors m_r and m_f.

The ZEUS Collaboration [94] has varied $m_{r,f}$ by factors between 0.5 and 2. This caused shifts in $\alpha_s(M_Z^2)$of $\simeq \pm 0.004$. Variations between 0.25 and 4, as are often common, resulted in unacceptable χ^2 variation effects and were thus not considered. Similar results were obtained by H1 [67] as are summarized in Table 3.

The numerical size of the effects depends on the data and Q^2_{min}, the H1 and ZEUS observations are thus found to be consistent. In agreement with previous studies [93] it was observed that the renormalisation scale causes a much larger uncertainty on $\alpha_s(M_Z^2)$than the factorisation scale. Depending on which set of m_r and m_f is chosen, the obtained χ^2 typically

differs by a number much larger than 1. This suggests that the assumed variations of the scales are too large. It has to be stressed again that while there is an arbitrariness in the scale choices, which is inherent to the renormalisation group equation, the actual prescription of variations by typically 1/4 to 4 times the scale is *ad hoc* and needs to be revisited. The scale dependence gets diminished in NNLO [73], yet future determinations of $\alpha_s(M_Z^2)$from HERA data and possibly from new colliders [95] will push the experimental accuracy to a per cent or per mille, respectively. In order to take advantage of such small experimental uncertainties, a new understanding of theoretical uncertainties – particularly that of the scale uncertainties – will be necessary.

5. Jet measurements

5.1. Theoretical considerations

According to the QCD improved parton model, a DIS differential cross section, $\mathrm{d}\sigma$ can be written as,

$$\mathrm{d}\sigma_{ep} = \sum_{a=q,\bar{q},g} \int \mathrm{d}x f_a(x, \mu_F^2; \alpha_s) \cdot \mathrm{d}\hat{\sigma}_a(xP, \alpha_s, \mu_R, \mu_F). \tag{40}$$

This has the form of a convolution of a partonic, or hard, cross-section $\mathrm{d}\hat{\sigma}$ with the proton PDF f_a. It should be noted that both $\mathrm{d}\hat{\sigma}$ and f_a depend on α_s which depends on μ_R.

In order to produce theoretical predictions in practice, semi-analytical programmes such as DISENT [96] MEPJET [97] or DISASTER [98] are used. The partonic cross-section, $d\hat{\sigma}$, above a specified scale μ_R, is calculated to NLO in α_s by these programs. The PDF of the proton, f_a, is normally taken from the results of global fits such as the MRST [99] or CTEQ [100] sets of PDFs. These global sets do not include the HERA jet data in their fits. These PDF fits are made using a fixed value of α_s, but PDFs are, in principle, a function of α_s, as indicated in Eq. (40).

In order to produce jet cross-sections from the partonic cross-sections produced by DISENT and DISASTER, a jet algorithm[4], the inclusive k_T algorithm [103,104] in case of HERA jet analyses, are run on the final partons to produce the "parton-level" jet predictions to NLO. The actual measurements, however, are not made at the parton-level, so additional corrections are necessary.

Monte Carlo (MC) programs currently available for DIS event generation, such as LEPTO [105] or ARIADNE [106,107], only contain the LO matrix elements. They are, however, supplemented by ad-hoc additions of NLO processes as well as a simulation of higher order processes through the Parton–Shower model. In addition, the partons are "hadronised" using the LUND [108] model. Thus, after running the jet algorithm on the events produced by MC programs, both "parton-level" and "hadron-level" MC predictions can be obtained.

In order to obtain the "hadron-level" prediction to order α_s^2, a multiplicative "hadronisation correction" is applied to the parton-level prediction. In most cases the hadronisation correction is the ratio of hadron-level to parton-level MC predictions. While there is no rigorous justification for this procedure, it is a reasonable one if (a) the parton distributions in the MC are close to those of the fixed order calculation, (b) the MC reproduces the experimental measurements reasonably well and (c) the hadronisation correction is small (5%–10%). Normally at least two MC programs are compared and used to evaluate a systematic uncertainty due to this procedure.

It is convenient to symbolically write the above procedure to obtain the jet cross sections in DIS as:

$$\mathrm{d}\sigma_{ep}^{\mathrm{jet}} = \sum_{a=q,\bar{q},g} \int \mathrm{d}x f_a(x, \mu_F^2; \alpha_s) \cdot \mathrm{d}\hat{\sigma}_a^{\mathrm{jet}}(xP, \alpha_s(\mu_R), \mu_R, \mu_F) \cdot (1 + \delta_{\mathrm{had}}), \tag{41}$$

where $d\hat{\sigma}_a^{\mathrm{jet}}$ is now the "jet", rather than the partonic, hard cross-section and δ_{had} is the hadronisation correction.

In the case of photoproduction, where $Q^2 \approx 0$ (i.e. an almost real photon collides with the proton), the photon PDF, as well as the proton PDF is factorized. Thus, the photoproduction (γp) jet cross-section can be written as:

$$\mathrm{d}\sigma_{\gamma p}^{\mathrm{jet}} = \sum_{a=q,\bar{q},g} \sum_{b=q,\bar{q},g} \int\int \mathrm{d}x_p f_a(x_p, \mu_F^2; \alpha_s) \cdot \mathrm{d}x_\gamma f_b(x_\gamma, \mu_F^2; \alpha_s) \cdot \mathrm{d}\hat{\sigma}_a^{\mathrm{jet}}(x_p, x_\gamma, \alpha_s(\mu_R), \mu_R, \mu_F) \cdot (1 + \delta_{\mathrm{had}}), \tag{42}$$

where f_b is the PDF of the photon, x_γ is the Bjorken x of a parton of the photon, and the convolution extends over partons a in the proton and b in the photon.

At LO (i.e. to zero-th order in α_s), the photoproduction process can be thought of as being in two pieces; the "direct" process in which the photon couples directly to the proton ($x_\gamma = 1$), and the "resolved processes" where a parton from the photon interacts with the proton ($x_\gamma < 1$). While this distinction does not have a strict meaning at higher orders, it is convenient to distinguish these two processes defined by means of a cut on x_γ, usually at 0.75 or 0.8 by convention. The

[4] Jet algorithms produce a small number of "jets" from a larger number of final state objects. The four-momenta of jets should correspond closely to those of hard partons. Discussions of theory and application of jet algorithms at collider experiments may be found in [101,102].

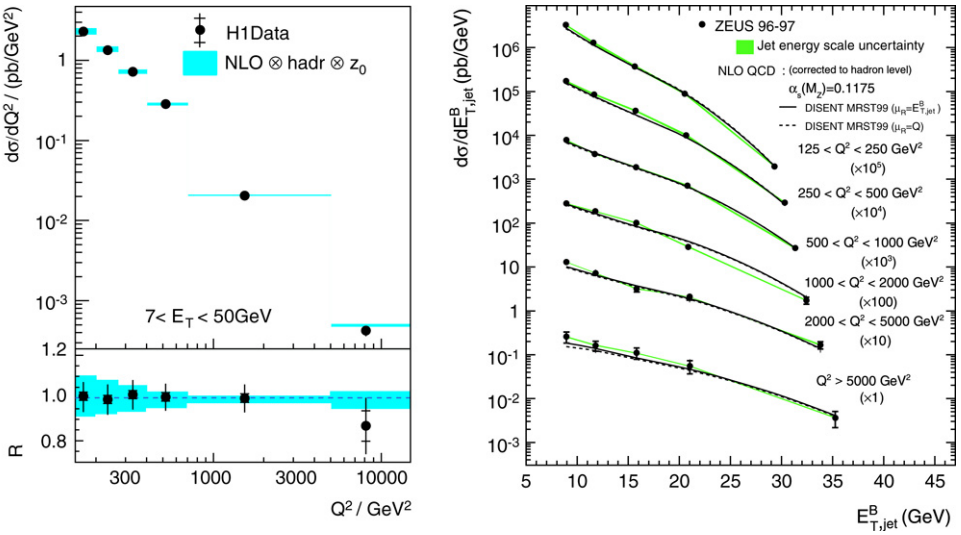

Fig. 13. Measurement of jet cross-sections at HERA. The filled dots are the data. The inner error bars represent the statistical uncertainty. The outer error bars show the statistical and systematic uncertainties in quadrature. The NLO QCD calculation, corrected for hadronisation effects (and Z^0 exchange when the calculations do not take electroweak effects into account) is shown. (Left-top) The differential cross-section $d\sigma/dQ^2$ for the inclusive jet production. (Left-bottom) the ratio between the measured $d\sigma/dQ^2$ and the NLO QCD calculation. The shaded band displays the total theoretical uncertainty. (Right) The differential cross-section $d\sigma/dE^B_{T,\text{jet}}$ in bins of Q^2, where $E^B_{T,\text{jet}}$ is the transverse energy of the measured jet in the Breit frame [117].

"direct" process loosely corresponds to the case where $f_b = 1$, and is not very sensitive to the hadronic nature of the photon through its PDFs.

The NLO theoretical prediction for photoproduction is obtained in much the same way as in the case for DIS. The NLO analytical programme often used is that of Frixione and Ridolfi [109]. The most usual LO MC programs are PYTHIA [110] and HERWIG [111].

Jet production in the region of transition between photoproduction and DIS has also been extensively studied at HERA. The reader is referred to the following HERA results for further information on this subject [112].

5.2. Jet cross-section measurements

The experimental jet measurements are made at the "detector-level". This means that the energy deposits in the calorimeters and tracks found in tracking detectors are subjected to the jet algorithms to determine the jets and their four momenta. The jet algorithm used is the same as that used in the theoretical predictions described in the previous section, i.e. the inclusive k_T algorithm.

A Monte Carlo simulation is used to correct the measured detector-level jet cross-sections to the hadron-level cross-sections, which can be compared to the theoretical predictions. Events generated by MC generators such as LEPTO or ARIADNE for DIS, and PYTHIA and HERWIG for photoproduction, are processed through detector simulations based on GEANT [114] to give a sample of fully simulated events. The correction factors are calculated using the difference between the detector - and hadron-level event rates of the fully simulated event samples. The event selection and kinematic cuts are devised in such a way to keep these corrections relatively small. Typically the corrections are $<30\%$.

Fig. 13 shows the measurement of inclusive jet cross-section in DIS [115,116], in this case as a function of Q^2 and E_T. The uncertainties of the measurement, except at the highest Q^2, where statistical errors are large, are dominated by the jet energy scale uncertainties. The energy uncertainties are 1%–2% at HERA experiments which translates to 5%–10% uncertainties in the cross-sections.

The measured cross-section in Fig. 13 (right), for example, is compared to the predictions of NLO QCD, in this case based on the DISENT programme. The inputs to the calculation are α_s for the partonic cross-section, chosen to be 0.1175, the factorisation and renormalisation scales (set to be either Q or E_T^{jet}) and the proton PDF, chosen to be the version of MRST99 [118] extracted with α_s set to 0.1175. The hadronisation correction was determined using ARIADNE and LEPTO MC programmes. The comparisons to the theory are generally satisfactory, and the residual difference can be attributed to the input parameters of theory, namely α_s and the PDF of the proton.

Very similar considerations apply to the study of photoproduced jets at HERA. One difference is that the PDF of the photon is an additional input to the theoretical prediction as discussed above. Fig. 14 shows the comparison of the theory and data [119] for photoproduced dijets for the "direct" and "resolved" samples. Many calculations of jet photoproduction at NLO exist, all of which have been compared to each other and agree to within 5%–10%. The calculations shown here are due to Frixione and Ridolfi [109]. The photon PDF used in this case is GRV-HO [120,121].

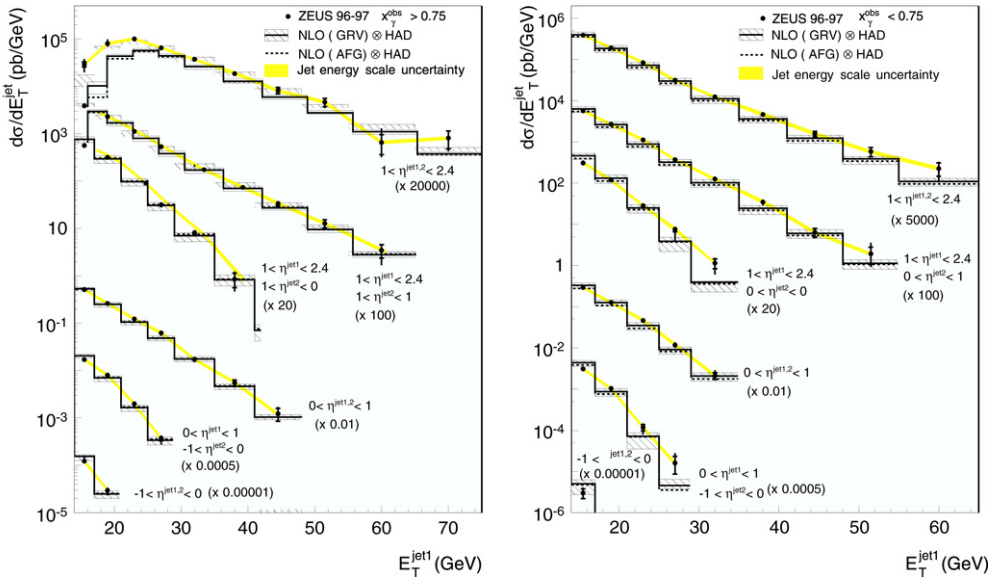

Fig. 14. The measured photoproduction dijet cross-sections differential in $E_{T,\mathrm{jet1}}$, the transverse energy of the highest energy jet, is shown separately for $x_\gamma > 0.75$ (left) and $x_\gamma < 0.75$ (right). The NLO prediction corrected for hadronisation effects is shown calculated using the GRV-HO and CTEQ5M1 PDFs for the photon and the proton, respectively. The hatched band represents the theoretical uncertainties. The prediction using an alternative photon PDF, AFG-HO [113], is also shown.

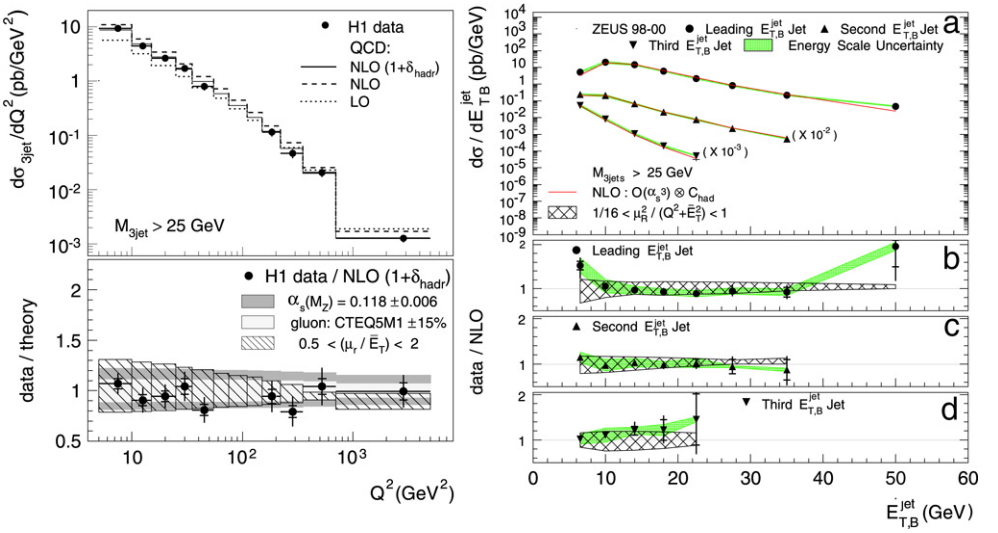

Fig. 15. Left: The inclusive trijet cross-section measured as a function of Q^2. The prediction of pQCD in leading order (dotted line) and in NLO (solid line) and without hadronisation corrections (dashed line) are compared to the data. Also shown is the ratio of the measurement and the theoretical prediction. Right: (a) The inclusive trijet cross-sections as a function of $E_{T,B}^{jet}$ with the jets ordered in $E_{T,B}^{jet}$. The cross sections of the second and third jet were scaled by factors shown in the figure for readability. The NLO prediction uses CTEQ6 PDFs of the protons. The other details are the same as in Fig. 13. (b) (c) and (d) are ratios of the measurements to the NLO predictions.

The DIS inclusive and photoproduction dijet measurements discussed in some detail above are two of the most basic jet measurements at HERA. The follow-up measurements to these can be found in [122,116,123,124]. An example of a more complex measurement is that of multijet in DIS which is shown in Fig. 15 [125,126]. The NLO calculations describe the data satisfactorily. There exist many more detailed measurements which are listed here [127–129] for reference.

In addition to the measurements of cross-sections, there are tests of pQCD that can be performed at HERA using jet measurements. An example is the angular distribution of photoproduced dijets. Fig. 16 shows a measurement by the H1 Collaboration [122] of the photoproduction dijet cross-section differential in cosine of the angle of dijets, $|\cos\theta^*|$, in their

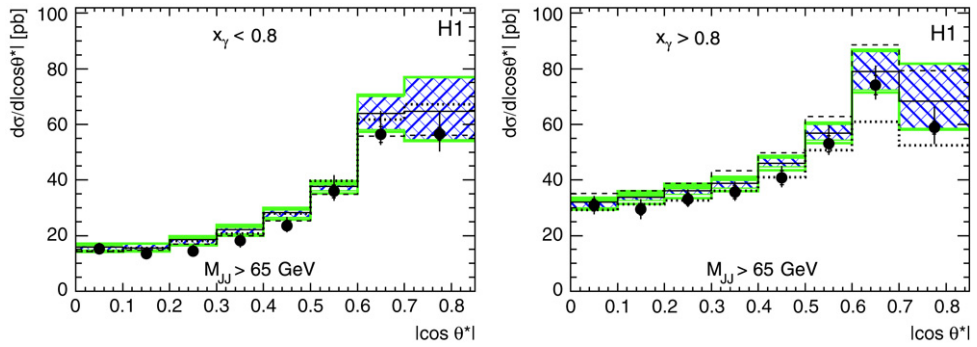

Fig. 16. Photoproduction dijet cross-section as a function of $|cos\theta^*|$ for events with the dijet mass greater than 65 GeV. The QCD NLO calculations with (solid line) and without (dashed line) hadronisation corrections, δ_{had} and for the PYTHIA Monte Carlo (dotted ine) scaled by a factor 1.2 are shown. The inner (hatched) band is the scale uncertainty the outer (shaded) band is the total uncertainty. The cross-section are shown for the two regions of x_γ enhancing the resolved (left) and direct (right) photon contribution.

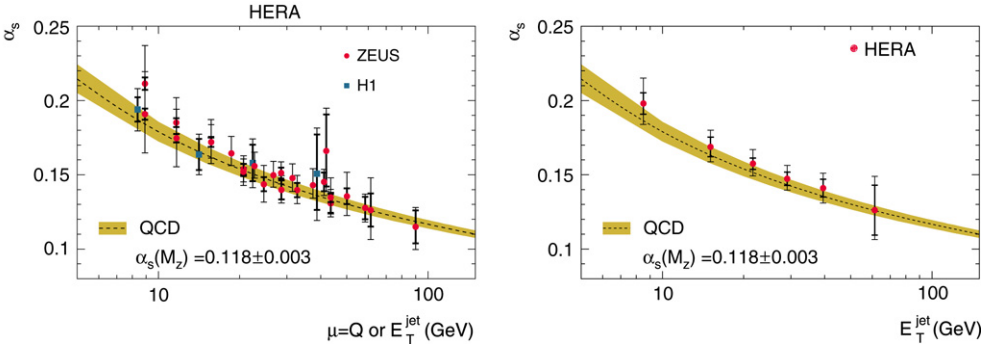

Fig. 17. Left: A compilation of $\alpha_s(E_{T,\text{jet}}, Q^2)$ measurements at HERA determined from the QCD fit of the measured $d\sigma/d(E_{T,\text{jet}}, Q^2)$ as a function of $E_{t,\text{jet}}$ or Q^2. The band shows the current world average (excluding HERA data). Right: The combined HERA measurements from [130]. The dashed line and the band shows the result of a global analysis (not using the HERA data) from [131].

centre-of-mass, with respect to the beams. The difference of steepness of the $|\cos\theta^*|$ dependence between the cross-sections from resolved and direct samples is predicted by the dominance of gluon exchange in the resolved process and is related to the spin of gluons and quarks.

5.3. Tests of pQCD and determination of α_s

The strong coupling constant α_s is extracted by a fit of the theoretical predictions to the data with α_s as a parameter of the fit. At HERA, the dependence of PDFs on α_s may be handled consistently by a use of sets of PDFs determined at different α_s such as the MRST99 set. The best fit is found by simultaneously varying α_s in the hard cross-section as well as the PDFs. The PDFs determined at discrete values of α_s are used to interpolate to the intermediate values. In this way, α_s is obtained in a consistent manner taking the correlations into account.

The extraction of α_s can be done in bins of E_T (or Q^2) to show its running as a function of the renormalisation scale. This is shown in Fig. 17 (left) for a variety of jet measurements at HERA [129]. In all measurements of α_s from jets at HERA, theoretical uncertainties dominate the systematic error, the largest of these are due to unknown higher order contributions, evaluated by a variation of the renormalisation scale, μ_R.

A compilation of the α_s values has been made; a combined HERA α_s has been derived [130] and is shown in Fig. 17 (right). The overall experimental uncertainty of the combined measurement is 1%, the theoretical uncertainty, which is dominated by the scale uncertainty of the NLO theory, is about 5%. As was noted in the inclusive case, there is no firm procedure which would define the theoretical uncertainty which remains ad-hoc to a large extent. This combined HERA measurement has been used in a determination of the world average of the strong coupling constant [132] of 0.1189 ± 0.0010. Recently, a determination of the strong coupling constant was made using a simultaneous fit of the HERA data from [116,127] to give a value of 0.1198 ± 0.0019 (exp) ± 0.0026 (th) [133]. In this analysis only data at large scales were used. This halved the theoretical error but enlarged the experimental one. Whether theoretical uncertainties can be settled in a more satisfactory way remains to be seen.

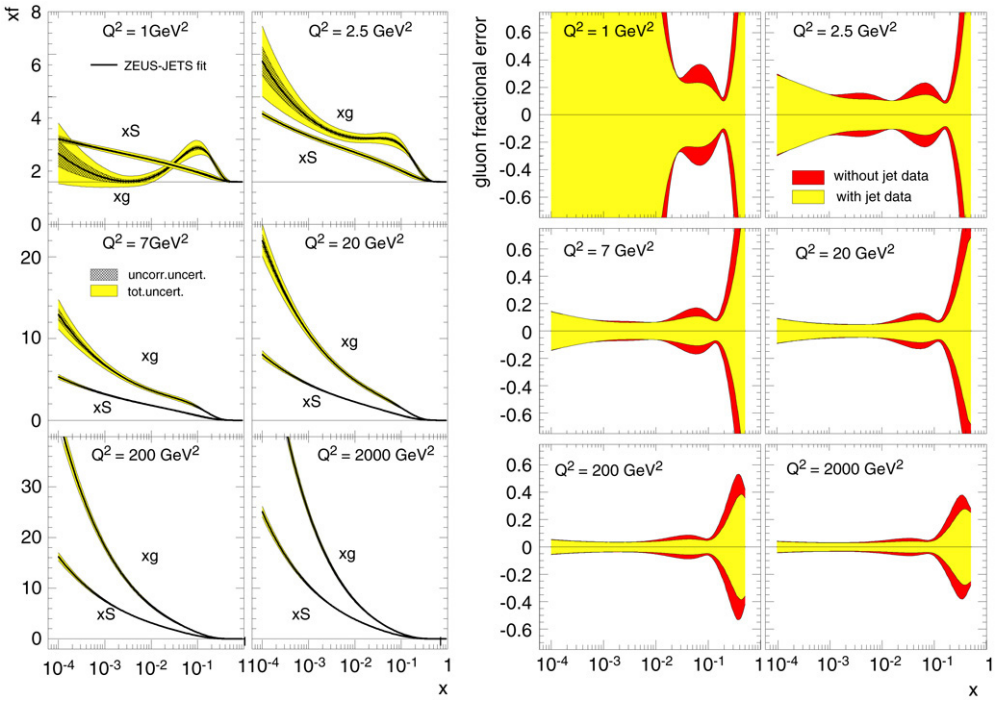

Fig. 18. Left: The gluon and sea PDFs extracted from the ZEUS-JETS fit. The inner cross-hatched error band shows the statistical and uncorrelated systematic uncertainty, the grey error bands show the total uncertainty including experimental uncorrelated and correlated systematic uncertainties, normalisation and model uncertainty. Right: The total experimental uncertainty on the gluon PDF for the ZEUS-JETS fit (central error bands) compared to the total experimental uncertainty on the gluon PDF for a fit not including the jet data (outer error bands). The uncertainties are shown as fractional differences from the central values of the fits for various values of Q^2.

5.4. Simultaneous determination of PDF and α_s using jet data

An examination of Eqs. (40) and (41) shows that the jet cross-sections at HERA are sensitive to both proton PDFs and α_s. In the previous section, the dependence on proton PDFs was treated as a systematic uncertainty in determining α_s from the jet data. One may also think of determining the PDFs from jet data using α_s determined elsewhere. Indeed, the simultaneous determination of proton PDF and α_s in a combined NLO QCD fit of DIS inclusive and jet cross-sections (and possibly other data) is the most consistent approach.

The inclusion of HERA jet data, or indeed any jet data in an NLO QCD fit, such as the one described in Section 4, is not conceptually difficult; the problem is technical. While the DGLAP equation can be rapidly evaluated in a programme such as QCDNUM [77], the NLO jet cross-section calculations are time consuming enough to make using them in an iterative fitting procedure impractical. Only recently have technical difficulties been overcome, making this procedure possible.

In [134], the hard jet cross-section, $d\hat{\sigma}^{\text{jet}}$ in Eq. (41) is pre-calculated on a grid of four dimensions, x, the proton momentum fraction, α_s, μ_R, the renormalisation scale and μ_F, the factorisation scale. By an appropriate choice of the grid points at which the pre-calculations are carried out, an accuracy of better than 0.5% with respect to a full calculation can be achieved using interpolations for all relevant cross-sections. In this way, the full NLO jet calculations can be incorporated into a NLO QCD fit on the same rigorous footing as the DGLAP equations for inclusive cross-sections.

The results of the fit using the ZEUS DIS inclusive cross-sections as well as both DIS inclusive jet cross-sections and the direct photoproduction dijet cross-section are shown in Fig. 18. In this instance, the fit is made with the value of α_s fixed to the world average value. There is a significant improvement to the PDF uncertainties, particularly at values of x above 10^{-2}, which is expected since jet production is dominated by gluon–photon fusion process in this range of x at HERA.

The next step is to simultaneously fit α_s as well as the PDFs. In a QCD fit using only the structure function data from HERA, α_s is so far weakly constrained as is shown in Fig. 19. The same figure shows the strong constraint on α_s jet data add to the fit. The uncertainties of the PDFs also remain stable and relatively small for the simultaneous fit as shown in the same figure. The extracted value of $\alpha_s(M_Z) = 0.1183 \pm 0.0028(\text{exp}) \pm 0.0008(\text{model})$, with an additional uncertainty of ± 0.005 due to unknown higher order effects to the NLO theoretical calculations, is very close to the value used in the fixed-α_s fit, and thus does not change the central values of the PDFs significantly. The level of the precision of this determination of α_s is as good as any existing single measurement; it is also, so far, the only accurate one that is derived from HERA data only, with minimal assumptions in the PDF fit parameterisation that derive from outside data. The other jet measurements use PDF fit parameterisations derived using world data.

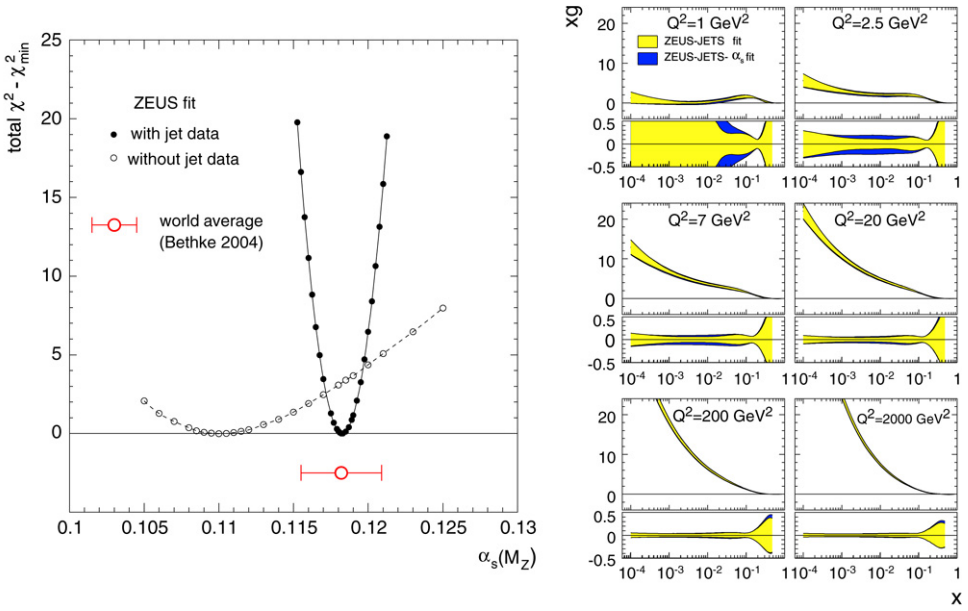

Fig. 19. Left: The χ^2 profile as a function of $\alpha_s(M_Z)$ for the fit to ZEUS data with (black dots) and without (clear dots) including the jet data. The ordinate is given in terms of the difference between the total χ^2 and the minimum χ^2 for each fit. Right: The gluon distributions extracted from the simultaneous fit to ZEUS DIS and jet data. The uncertainties on these distribution are shown beneath each distribution as fractional differences from the central value. The outer error band shows the total uncertainty and the inner band the uncertainty in case α_s is fixed in the fit.

5.5. Summary and outlook of jet measurements at HERA

The jet cross-section measurements at HERA have achieved about 5% precision, with the main contribution coming from the understanding of the jet-energy scale at the level of 1%–2%. With this precision, a meaningful comparison can be made to the QCD NLO predictions of jet predictions. Indeed, in most cases, the precision of the experimental measurements are such that the theoretical part dominates the uncertainties.

Based on the good description of the data, QCD parameters can be extracted. The strong coupling constant α_s is determined to about 1% experimental uncertainty (5% theoretical uncertainty) from the current measurements. The jet measurements help to constrain the gluon PDF when combined in a simultaneous fit with the DIS inclusive cross-sections. The current measurements constrain the gluon to about $\pm$10% at x around 0.05 and Q^2 around 200 GeV^2, based so far on the ZEUS jet data only.

All of the results discussed here come from the HERA I data taking phase which comprises about 120 pb^{-1} per experiment. While many of the jet measurements are now limited by the theoretical uncertainties, there are areas, such as the measurements at the highest E_T, which will benefit from the 800 pb^{-1} of which is available from the HERA II data taking period. The projections are that this data should be able to improve the uncertainty of the gluon PDF in the x range of 0.1 to 0.05 by about a factor of two [135].

6. Heavy flavours

6.1. Introduction

Processes involving heavy quarks, Q, with mass, $M_Q \gg \Lambda_{QCD}$, are, in principle, amenable to pQCD calculations. At HERA, the production of charm and beauty particles are measured and compared to theoretical predictions. While M_Q is one QCD scale, there are two other relevant scales in heavy quark production processes at HERA. These are the virtuality, Q^2, of the exchanged photon, and the transverse energy, E_T, of the final state particles or jets. The relative size of these three scales is important in choosing what kind of calculation is appropriate for comparison to which data. For example, in the limit, $Q^2 \gg M_Q^2$, an approximation where $M_Q = 0$ may be appropriate. On the other hand, since there are no quantitative predictions of what "much greater than" may mean, the study of heavy quark production, as is often the case with QCD, is an iterative one where the appropriate theory is arrived at gradually as better and better data are compared to the theory.

6.2. Theoretical calculations of heavy quark production

In the conventional co-linear approximation, heavy quark production in DIS cross-section can be written generically as

$$\mathrm{d}\sigma = \sum_a \int \mathrm{d}x f_a(x, \mu_F^2; \alpha_s) \cdot \mathrm{d}\hat{\sigma}_{HQ}(xP, \alpha_s(\mu_R), \mu_R, \mu_F, M_Q). \tag{43}$$

If the renormalisation scale, μ_R, usually taken to be the virtuality Q^2, is $\gg M_Q^2$, then the heavy quark should be treated as a massless quark on the same footing as the other quarks in the PDF in the framework of $\ln \mu_R^2$ resummation (DGLAP approximation). In this case, f_a is the PDF of the heavy quark, and the cross section $d\hat{\sigma}$ is the photon- (photoproduction) or electron- (DIS) quark cross-section for a massless quark. This type of calculation is called "massless".

If the scale, $Q^2 \approx M_Q^2$, then it is appropriate to treat the heavy quark separately as a massive quark. In this case, the sum over a in the above equation will be for all partons *except* the heavy quark. The cross-section $d\hat{\sigma}$, will be for a production of a massive quark from an electron colliding with a (massless) parton at a fixed order in α_s. This type of calculation is called "massive".

There are three types of treatments of heavy quark production in DIS based on co-linear factorisation.

- Zero-Mass Variable Flavour Number Scheme (ZM-VFNS), is a purely "massless" treatment where the heavy quarks are treated as massless quarks which become "active" in the proton PDF at the production thresholds of a $Q\bar{Q}$ pair. This is the oldest and still the most common theoretical treatment. As discussed above, this is, in principle, incorrect near the production thresholds.
- Fixed Flavour Number Scheme (FFNS) is a purely massive treatment. This is, in principle, incorrect at high Q^2. The most common treatment uses the analytic programme HVQDIS [136].
- Matching Schemes. Sometimes these are called Massive Variable Flavour Number Scheme (Massive-VFNS) or Generalised Mass Variable Flavour Number Scheme (GMVFNS). There are several predictions which match the massless and massive schemes at an intermediate value of Q^2. Examples of these are Roberts–Thorne (RT) [137,138], ACOT [139], Kniehl et al. [140] and ResBos-HQ [141].

The cross-sections, calculated to order α_s^2, are available in all three schemes. Some of the predictions, such as those of HVQDIS and ResBos-HQ, are of semi-analytical type similar to those discussed in Chapter 4 for jet production. In these cases, a detailed prediction for comparison to the data of measurements of production of hadrons containing heavy quarks is possible. Such predictions are made using a fragmentation function [142–144] that give the probability of producing a particular hadron given an initial heavy quark. Also, a cross-section of jets associated with heavy quark production can be predicted in the same way as for ordinary jet production discussed in Section 5. Many predictions give only the x and Q^2 dependence of the charm cross-section, and thus can only be compared after some, more or less large, extrapolation of the data (see also the end of this Section).

The theoretical treatment of the photoproduction of heavy flavours is similar to that of DIS but complicated by the second "hadron", the real photon. In this case the photon–proton cross-section can be represented as;

$$\mathrm{d}\sigma = \sum_{a,b} \int\int \mathrm{d}x_p \mathrm{d}x_\gamma f_a(x_p, \mu_F^2; \alpha_s) \cdot f_b(x_\gamma, \mu_F^2; \alpha_s) \cdot \mathrm{d}\hat{\sigma}_{HQ}(xP, \alpha_s(\mu_R), \mu_R, \mu_F, M_Q), \tag{44}$$

where f_b is the PDF of the photon. In practice, the measurements use jets associated with heavy quark production to determine the kinematics—in particular the Bjorken variable of the photon, x_γ.

As in the case of DIS, predictions in FFNS, ZM-VFNS and Massive-VFNS exist for the photoproduction case. The renormalisation scale μ_R is usually chosen to be some combination of the quark mass M_Q and the transverse momentum of the produced heavy quarks, P_T^Q.

The predictions discussed above are all based on co-linear factorisation. A different approach is to use k_t factorisation and the CCFM equations [145], which, unlike the DGLAP equations, resum terms proportional to $\ln 1/x$ as well as to $\ln \mu_R^2$. The actual predictions in this approach are made by the Monte Carlo programme CASCADE [146] that uses the off-shell photon–gluon fusion process convoluted with the gluon distribution unintegrated in k_t, obtained via a fit to HERA F_2 data [147]. These predictions are currently available only at order α_s. Like the predictions of HVQDIS, the CASCADE programme is capable of providing predictions at the parton level, and is therefore easily comparable to measurements.

The reader is referred to [148] for a more complete discussion of the theory of heavy quark production than is possible here.

6.3. D^* cross sections in DIS

While many different kinds of charmed hadrons have been measured at HERA, the measurements of the D^* mesons have, by far, the highest statistical significance. This is due to the well-known ease of reconstructing the D^* meson, using tracking detectors alone, by exploiting the "slow" pion from the decay, $D^* \to D + \pi_s$.

Fig. 20 shows a recent measurement of the D^* cross-sections in DIS [149]. The theoretical predictions, which all describe the data reasonably well are of the FFNS type, HVQDIS, as well as the CCFM based CASCADE and a massive VFNS calculation.

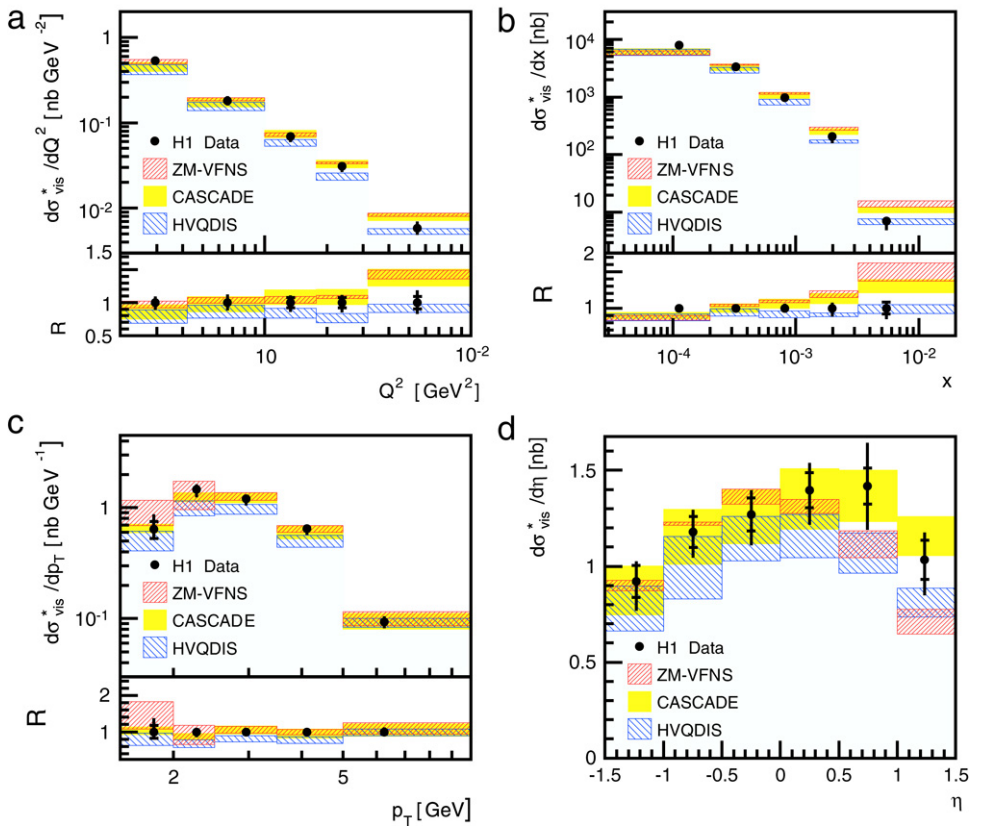

Fig. 20. Differential $D^* ep$ cross-sections as a function of (a) Q^2, (b) x, (c) $p_T(D^*)$ and (d) $\eta(D^*)$ compared to calculation of HVQDIS CASCADE and a Massive-VFNS calculation from Kniehl et al. [150]. The inner error bars indicate the statistical uncertainty, while the outer show the statistical and systematic uncertainties in quadrature. Figures (a), (b) and (c) also present the ratios $R = \sigma_{\text{theory}}/\sigma_{\text{data}}$, taking into account their theoretical uncertainties. See [149] for details.

The predictions use a range of proton structure functions and charm quark masses. It is interesting to note that the description of FFNS appears to be somewhat better than the others even at rather high Q^2 values near a hundred GeV^2 despite the fact that FFNS should be, in principle, incorrect when $Q^2 \gg M_Q^2$. Indeed this good description is known to hold up to several hundred GeV^2 [151].

6.4. Derivation of the charm structure function $F_2^{c\bar{c}}$

The measured charm hadron cross-section can be extrapolated to the full charm cross-section differential only in x and Q^2. This, in turn, can be interpreted as the charm part of the cross-section, described essentially by the structure function $F_2^{c\bar{c}}$. Thus,

$$\frac{\mathrm{d}\sigma^{cc}}{\mathrm{d}x\mathrm{d}Q^2} = \frac{2\pi\alpha^2}{xQ^4}\{[1+(1-y)^2]F_2^{c\bar{c}}(x,Q^2) - y^2F_L^{c\bar{c}}(x,Q^2)\}. \tag{45}$$

Since the D^* cross-section is measured in a kinematic range limited in P_T and η, a method of extrapolation is needed. A most straightforward way to determine this is, for the D^* cross-section $\sigma_i(ep \to D^*X)$ in the ith bin of x and Q^2:

$$F_{2,\text{meas}}^{c\bar{c}}(x_i,Q_i^2) = \frac{\sigma_{i,\text{meas}}(ep\to D^*X)}{\sigma_{i,\text{theo}}(ep\to D^*X)}F_{2,\text{theo}}^{c\bar{c}}(x_i,Q_i^2), \tag{46}$$

where x_i and Q_i^2 are chosen to be within the measured bin. The uncertainties in this extrapolation are determined by varying the parameters of the theoretical models being used. While these uncertainties, at 10%–20%, are usually smaller than the uncertainties already present in the D^* cross-section measurement, it is worth keeping in mind that the extrapolation factors range from about 1.5 up to nearly 5. Thus reliance on the correctness of the theoretical prediction of the cross-section in η and P_T is relatively large. This is overcome with impact parameter based measurements as are discussed below.

Fig. 21 shows a compilation of the measurements of $F_2^{c\bar{c}}$ based on measurements of D^* mesons [151,152]. The measurements are compared to a prediction of a PDF obtained from a fit using a VFNS scheme. It should be noted that

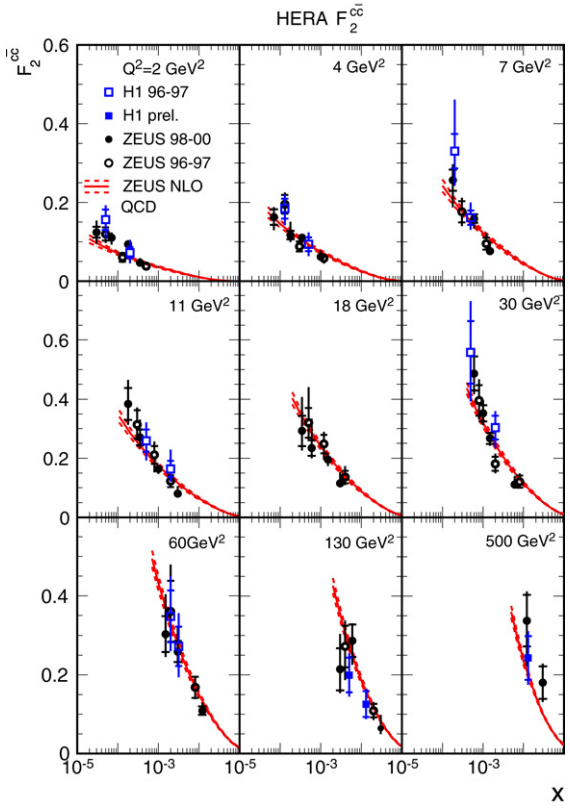

Fig. 21. The measured $F_2^{c\bar{c}}$ in bins of Q^2 as a function of x. The data are shown with statistical uncertainties (inner bars) and statistical and systematic uncertainties added in quadrature (outer bars). The lower and upper curves show the fit uncertainty propagated from the experimental uncertainties of the fitted data.

the comparison of theory to data in the form of $F_2^{c\bar{c}}$ derived from the D^* measurements do not contain more information than the comparison of the differential cross-sections in the measured kinematic range to the theory of the kind shown in Fig. 20.

6.5. D^* production in photoproduction

A recent measurement [153] of charmed meson production in photoproduction is shown in Fig. 22. The theoretical predictions of the massive scheme (FMNR [154]) have a tendency to have too shallow a slope in p_T of the D^* and be below the data at forward η of the D^*. The predictions of the variable flavour number scheme (GMVFNS) [155], while describing the data, have a very large uncertainty associated with effects of missing higher orders.

In photoproduction, one factorizes the photon structure as well as the proton structure in order to apply pQCD. Therefore, in order to compare the predictions to the data in more detail than above, it is necessary to measure, in addition to the total γp cms energy, W, and the kinematics of the charmed hadron, quantities that can determine the kinematics of the partons in the photon. This can be achieved by measuring the jets produced in the events with charm hadrons. The jet finding is done in the same way as is described in the previous section. The jets found may contain the charmed hadron produced in the event.

Fig. 23 shows a measurement of dijet photoproduction associated with a D^* [156]. The cross-section is plotted differentially in x_γ, the Bjorken variable of the photon. The theoretical prediction, a massive calculation, tends to fall below the data in the region of low x_γ indicating that the description in the resolved region is not adequate. Fig. 24 shows the same data now plotted separately for high x_γ (direct component) and low x_γ (resolved component) in terms of $\Delta\phi_{ij}$, the azimuthal separation of the two jets. It is seen that the theory tends to fall below the data away from $\Delta\phi_{jj} = \pi$ (i.e. back-to-back jets) particularly in the resolved region. Since $\Delta\phi_{jj}$ is equal to π to LO in α_s, NLO is the order at which the first non-trivial prediction is given. A failure to describe this distribution may be an indication of a need for higher order terms in the calculation.

The comparison of the data on photoproduction of charm with the present theoretical predictions indicate some inadequacies of the theory. The indications, both from relatively large renormalisation uncertainties and from examination

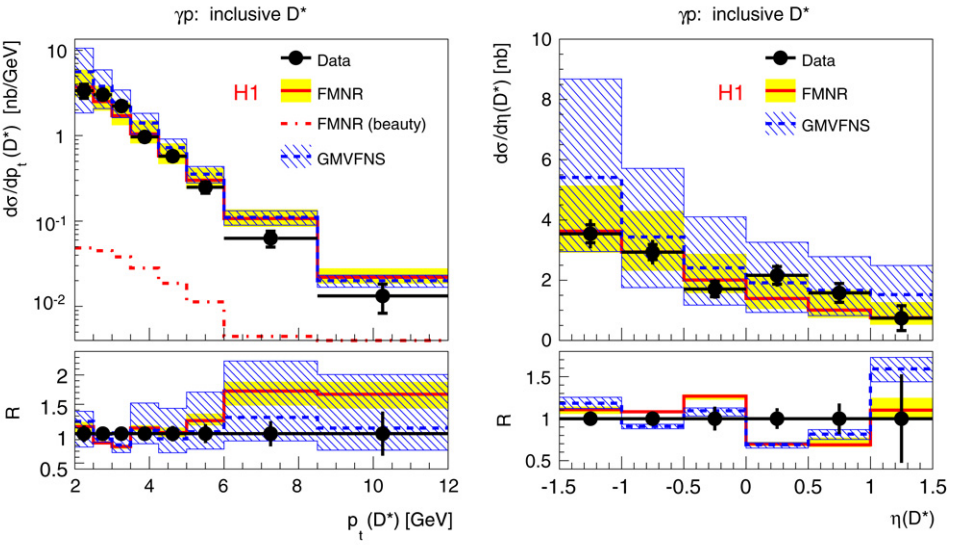

Fig. 22. Inclusive D^* cross-sections as a function of $p_T(D^*)$ and $\eta(D^*)$ compared to the QCD NLO calculations of FMNR and GMVFNS. For FMNR the beauty contribution is shown separately for $p_T(D^*)$. The ratio of the measurement and the prediction, R, is also shown.

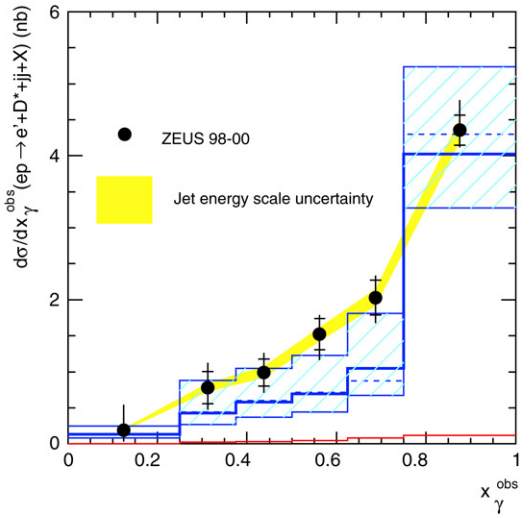

Fig. 23. Charm dijet cross-section $d\sigma/dx_\gamma^{obs}$ compared to QCD predictions in the massive scheme, with (solid line) and without (dotted line) hadronisation corrections applied. The theoretical uncertainties (hatched band) come from the change in scales simultaneously with the change in charm mass.

of differential distributions, are that the theory still requires the inclusion of higher order terms in order to give a good description of the available data.

6.6. Photoproduction of beauty particles

The measurements of beauty photoproduction are based on the semi-leptonic decay of the B-hadron. Because of the large mass of the b-quark, the leptons from the decay tend to be produced with large transverse momentum with respect to the momentum of the rest of the associated jet. In this case, the signal is extracted from the distribution of momenta of the leptons relative to that of the jets. Alternatively, a D^* may be explicitly reconstructed with a decay lepton and their momentum separations. In the latter case, which exploits the specific decay chain $B \to D^*\mu\nu$, further constraints, such as charge of the D^* and the μ, and the mass of the pair, can be used in the selection.

Fig. 25 is a compilation of all currently available measurements [157–162] of b-photoproduction, measured via its decay, converted to a b-quark cross-section differential in the transverse momentum of the b-quark. It can be seen that while the massive calculation gives a prediction which is somewhat lower than the measurements, particularly at lower ranges of p_T^b,

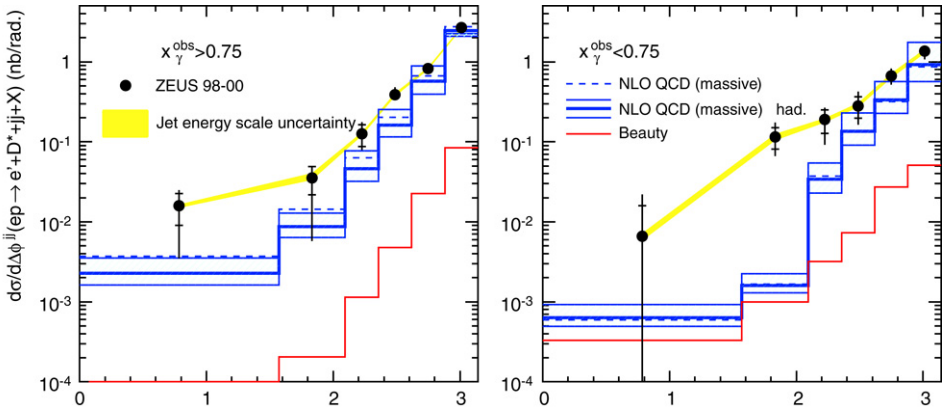

Fig. 24. Cross-section $d\sigma/d\Delta\phi^{ij}$ separated into resolved enriched ($x_\gamma^{obs} < 0.75$) and direct enriched ($x_\gamma^{obs} > 0.75$) region. The theoretical uncertainties come from the change in scales simultaneously with the change in charm mass. The beauty component is also shown (lower histogram).

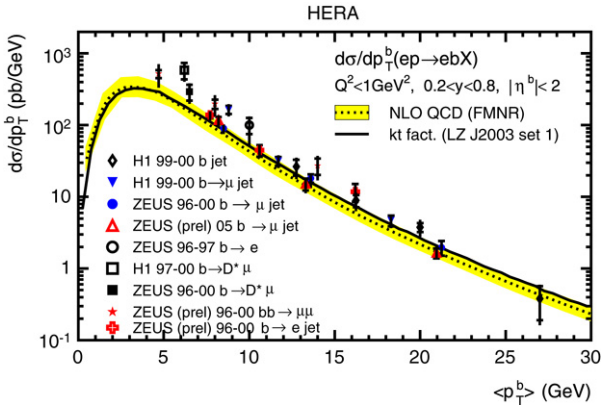

Fig. 25. A summary of all available HERA data on beauty photoproduction plotted as the cross-section $d\sigma/dp_T^b$ and compared to NLO QCD in the massive scheme and a k_T factorisation calculation.

the general description is good. It can also be seen that the k_t factorisation calculations from [163] is very similar to that of FMNR.

6.7. *Measurements of heavy quark production using vertex separation*

Qualitatively different measurements of heavy quark production at HERA than discussed above are achieved by the use of the precision tracking made possible by the use of silicon vertex detectors. These devices have been installed as upgrades to the HERA detectors. The H1 vertex detector [164] was installed in 1996–7 and the ZEUS one [165] in 2001.

The spatial impact parameter resolution of the silicon detectors, in the order of tens of microns, makes possible the use of the long lifetimes of c and b flavoured hadrons for selection of these events without explicit reconstruction of the hadrons. The events containing heavy quarks are distinguished from those containing only light quarks by reconstructing the displacement of tracks from the primary vertex. The major advantages of this method compared to that of reconstructing particular c or b hadrons are that (a) there are little or no uncertainties associated with properties of particular hadrons, such as its fragmentation function or decay branching ratios, and (b) the severe limitation in the measurable kinematic range in p_T and η due to the use of central tracking chambers for the reconstruction of hadrons is removed since the acceptance for the silicon detectors is close to 100%. The latter point is very important when extracting the total c and b cross-sections (and therefore $F_2^{c\bar{c}}$ and $F_2^{b\bar{b}}$) since the extrapolation factors from previous analyses can be as large as 4 or 5 and, thus rely heavily on the correctness of the models.

The first such type of measurements of the heavy quark structure functions [166,167] was performed by H1 and is shown in Fig. 26 together with previous H1 and ZEUS measurements of $F_2^{c\bar{c}}$ that rely on the reconstruction of D^* mesons. It is notable that the $F_2^{c\bar{c}}$ measurements from D^* reconstruction agree well with the newer results, which is an indication of the reliability of the extrapolations used in the older results. While there is an earlier measurement of $\sigma(b\bar{b})$ in DIS based on the relative transverse momenta of muons [168] this is the first measurement at HERA of $F_2^{b\bar{b}}$ in a relatively wide kinematic range.

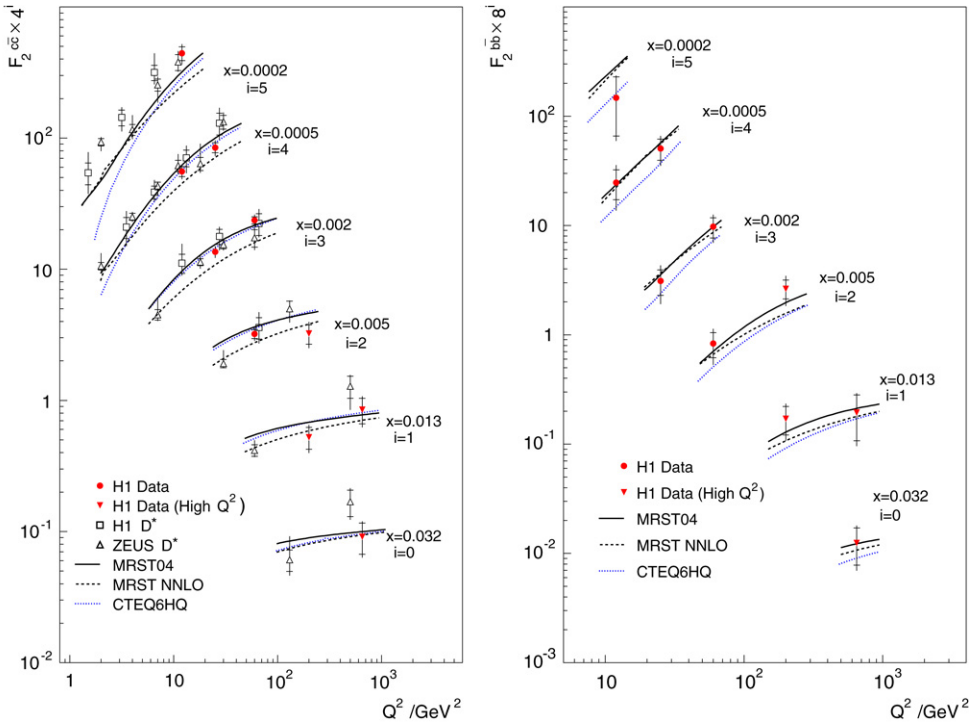

Fig. 26. The measured heavy quark structure functions $F_2^{c\bar{c}}$ and $F_2^{b\bar{b}}$ shown as a function of Q^2 for various x bins. The solid points are the measurements utilising the silicon vertex detector of H1. The open points on $F_2^{c\bar{c}}$ are older measurements made using the reconstruction of D^* mesons.

Both $F_2^{c\bar{c}}$ and $F_2^{b\bar{b}}$ rise steeply as a function of Q^2 at fixed x, especially at small x, reflecting the large gluon density there. The predictions of NLO QCD in the Massive VFN schemes describe the data well, except at the lowest x for $F_2^{c\bar{c}}$ where the predictions tend to undershoot the data.

6.8. Summary of heavy quark production at HERA

In the deep inelastic scattering regime, the heavy quark production at HERA is generally well described by NLO QCD. Massive scheme calculations combined with a conventional fragmentation function, fitted to data from e^+e^- colliders, work well in describing c-meson production. Both the massive VFN and purely massive schemes describe the c and b production within the current uncertainties. Within their uncertainties, k_t factorization calculations are also able to reproduce the data.

In photoproduction, the descriptions by NLO QCD fall short in some regions. The predictions tend to undershoot the data in the region of lower transverse momenta and forward rapidity. Investigations show that the discrepancy is largely in the resolved photoproduction regime and there are indications that missing higher orders is the cause.

The data covered here are all based on about 120 pb^{-1} each for H1 and ZEUS in the HERA I data taking period. There is about 400 pb^{-1} of data for each experiment which is yet to be analysed and published from the HERA II period. For ZEUS, the HERA II data set is taken with their newly installed microvertex detector.

Due to space limitations, a large part of heavy quark studies at HERA could not be covered. These topics include studies of productions of c-hadrons other than the D^* and the study of fragmentation functions [169], the study of the transition region between DIS and photoproduction [170] as well as the study of the photoproduction region using the H1 central silicon tracker [171].

7. Diffraction

7.1. Inclusive diffraction

Diffraction as a hard deep inelastic scattering process was discovered at HERA when ZEUS [172] and H1 [173] observed an unexpected excess of DIS events characterised by the absence of activity in the forward direction which is usually occupied by hadrons emitted from the final state (Fig. 27). In conventional QCD the hadronic final state is produced in the radiation from colour charges exchanged in the interaction. The observation of an excess of large rapidity gap (LRG) events, as the absence of hadronic activity at small angles is named, was readily understood as being due to a virtual photon–proton interaction without colour exchange. The basic process is sketched in Fig. 28. An exchange of a colour singlet with vacuum

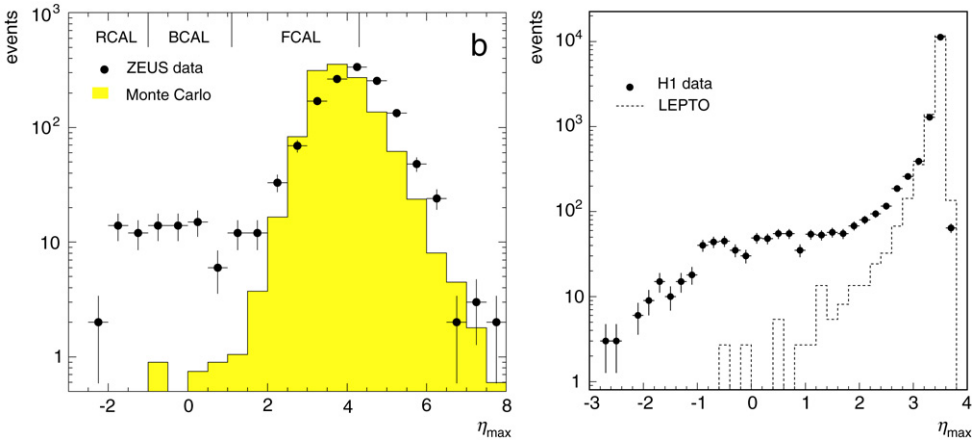

Fig. 27. The first observations of hard diffraction by ZEUS (left) and H1 (right). Left: Distribution in DIS events of η_{max}, the maximum pseudorapidity of a cluster of energy larger than 400 MeV, in the ZEUS calorimeters, the range of which is indicated at the top. There is a clear excess seen at small η_{max} of events in the data over a conventional DIS Monte Carlo simulation. Right: Similar observation in the H1 DIS η_{max} distribution, $E_{min} = 400$ MeV.

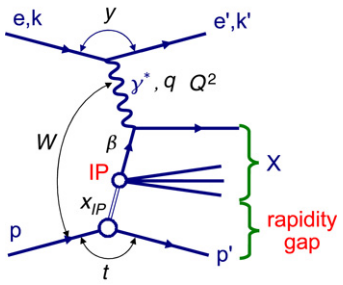

Fig. 28. Schematic diagram of hard diffractive deep inelastic scattering. The scattered proton mostly stays intact but also may dissociate into a system of small mass M_Y. The diffractive exchange carries a fraction x_{IP} of proton's momentum. A parton of momentum fraction $\beta = x_{IP}/x$ interacts with the virtual photon which in DIS has a large virtual mass squared, Q^2. The salient feature of these events is the absence of forward particle production, near the proton beam pipe, which is measured as a gap in polar angle, or equivalently rapidity, from the proton beam axis to the more centrally produced particles which stems from the struck parton in the diffractive exchange. Despite the violence of the interaction diffraction comprises about 10% (3%) of the total cross-section at Q^2 of 10 (1000) GeV^2.

quantum numbers is historically called Pomeron exchange. The early discovery of hard diffraction in DIS at HERA gave rise to the development of the chromodynamic theory of diffraction, based largely on the proof of collinear factorisation [174] of DDIS cross sections at fixed x_{IP} and t. Here x_{IP} is the fraction of proton momentum the diffractive exchange carries and t is the 4-momentum transfer at the proton vertex. This allowed diffractive parton densities to be introduced with the constraint that the proton does not fragment during the violent ep collision. In fact the calculus of diffractive structure functions can be introduced quite analogously to the inclusive case [175].

Another way to analyse diffractive DIS is the colour dipole model (CDM) approach [176] in which, unlike in the parton model, the proton is studied at rest. Due to the smallness of x, the photon can be considered as disintegrating at a coherence length $\propto 1/x$ prior to interacting with the proton. This leads to a phenomenological prescription of diffractive scattering cross sections as the convolution of dipole wave functions and a dipole–proton cross section, which is to be determined from the data.

The accuracy and scope of the diffractive measurements have improved dramatically over the past years. Much more accurate and complete data are now available based partially on the LRG identification of diffractive DIS [177,178]. The agreement of all data is approaching an acceptable level, both for the LRG method data and also including more recent results applying the so-called M_X selection to diffractive scattering [179]. Inclusive diffractive measurements have been extended to high $Q^2 \leq 2000$ GeV^2. Diffractive DIS has also been observed in charged current scattering. The fraction of hard diffraction to inclusive DIS is about 10% at low $Q^2 \sim 20$ GeV^2 and diminishes, both in NC and in CC, to a few % at high $Q^2 \sim 2000$ GeV^2, where, however, the mean x is correspondingly larger by roughly two orders of magnitude at HERA.

Both H1 and ZEUS operated forward proton spectrometers in HERA I, tagging the proton downstream, near the proton beam line with the "FPS" (H1) and "LPS" (ZEUS), at $\simeq +100$ m distance from the interaction point. In the HERA II phase, H1 installed in addition to the FPS a Very Forward Proton Spectrometer, accessing an x_{IP} range near to 0.01, while ZEUS had dismantled the LPS. The FPS and LPS detectors allow a direct comparison of the LRG based cross sections to the ones obtained

with p tagging. For a diffractive mass range $M_Y < 1.6$ GeV, H1 measured the ratio of the LRG to the FPS cross sections as 1.23 ± 0.05 and to be constant within the kinematic range of the measurement, $2 < Q^2 < 30$ GeV^2, $0.01 < \beta < 0.7$ and $0.001 < x_{I\!P} < 0.05$, where $\beta = x/x_{I\!P}$ is the momentum fraction of the diffractive exchange carried by its partons. The ZEUS result is 1.23 with a total error of 0.05 [180] for the ratio of the LRG to LPS data, in agreement with the H1 measurement and also constant in the kinematic range of the measurement, $2.5 \leq Q^2 \leq 40$ GeV^2, $0.007 \leq \beta \leq 0.816$ and $0.0002 < x_{I\!P} < 0.02$. Thus the dominant process in the gap data is indeed diffraction and further processes such as resonance or neutron production do not alter the kinematic dependencies beyond the point to point uncertainty, of typically 5%–10%, of the LRG/FPS or LRG/LPS ratio.

It is satisfying to observe that the tagged differential diffractive cross section data are consistent between H1 and ZEUS. The tagged data also allow the t dependence of the cross sections to be measured which can be parameterised as $\mathrm{d}\sigma/\mathrm{d}t \propto \mathrm{e}^{-bt}$. A slope of 7 ± 0.3 is obtained by ZEUS [180]. H1 has parameterised the slope as $b = b_{I\!P} - 2\alpha_{I\!P} \ln x_{I\!P}$ corresponding to a trajectory $\alpha_{I\!P}(t) = \alpha_{I\!P}(0) + \alpha'_{I\!P} t$. At small $x_{I\!P}$ one obtains $b_{I\!P} = 6.0$ with an error of about 2 and a small $\alpha'_{I\!P} = 0.02$ consistent with zero within the errors [177]. A large $\alpha'_{I\!P}$ would have been an indication for shrinkage of the diffractive peak.

7.2. Diffractive parton distributions

The diffractive measurements based on the LRG method, which has the widest kinematic coverage, allowed QCD analyses to be performed in order to derive the quark and gluon distributions of the diffractive exchange. Such analyses are based on the diffractive cross section $\sigma^{D(3)}$

$$\frac{\mathrm{d}^3\sigma^{ep\to eXY}}{\mathrm{d}x_{I\!P}\mathrm{d}x\mathrm{d}Q^2} = \frac{2\pi\alpha^2}{xQ^4} \cdot Y_+ \cdot \sigma_r^{D(3)}(x_{I\!P}, x, Q^2), \tag{47}$$

which is integrated over the ranges of t and M_Y. Similarly to inclusive DIS, the reduced ep cross section depends on the diffractive structure functions $F_2^{D(3)}$ and $F_L^{D(3)}$ in the one-photon exchange approximation according to

$$\sigma_r^{D(3)} = F_2^{D(3)} - \frac{y^2}{Y_+} F_L^{D(3)}. \tag{48}$$

For y not too close to unity, $\sigma_r^{D(3)} = F_2^{D(3)}$ holds to very good approximation.

Recently a detailed QCD analysis was published by H1 [177]. Since data are used for a range of $x_{I\!P}$ values, it is required to factorise the $x_{I\!P}$ dependence out which in [177] is done with an ansatz inspired by Regge theory. The QCD fit, similar to truly inclusive scattering as described above, then determines parton distributions, here a singlet quark distribution $\Sigma(x, Q^2)$, assuming $u = d = \bar{u} = \bar{d} = s = \bar{s}$, and a gluon distribution $xg(x, Q^2)$, where $x = \beta x_{I\!P}$. The data, as is shown for example in Fig. 29 (left) for a medium $x_{I\!P}$ value, are well described in their x and Q^2 dependence by this approach. In the analysis, rather stable results were obtained for both distributions, with the exception of the behaviour of the gluon distribution at large momentum fractions which is rather uncertain. This can be understood from the consideration of the $\ln Q^2$ derivative of the diffractive reduced cross section (see Fig. 29 (right)). As the two QCD fit components reveal, at large β there is not much sensitivity to gluons.[5] Thus H1 decided to publish two fits, with very similar χ^2 but different xg at large β. A distinction between these two possibilities was made possible with diffractive dijet data [181]. The diffractive dijet production leads to improved sensitivity to the gluon distribution in the diffractive exchange (see Fig. 30). Thus the gluon distribution uncertainties can be reduced significantly, similar to the influence of dijet DIS data on the determination of the gluon distribution in the proton.

There are many further similarities between diffractive and inclusive DIS: The derivatives of σ_r^D and σ_r, with respect to $\ln Q^2$, are measured to be the same for $\beta < 0.6$. Thus low β diffraction and low x inclusive scattering seem to reflect a common origin, the dynamics of the QCD vacuum. It is not surprising, then, that a number of recent observations in diffractive DIS resemble those in inclusive DIS; such observations include the rise towards low β or x of the $\ln Q^2$ derivatives and the fraction of charm of about 20%, for Q^2 away from thresholds, in both the diffractive cross section and in the inclusive cross section. Diffraction has evolved from the first surprise of its presence at HERA to a rather exact and interesting testing ground of perturbative QCD. Further data from both HERA collaborations and studies of universality in comparing DIS ep and photoproduction predictions [183], as well as of HERA data with Tevatron and later LHC data, will certainly contribute to this field in the future. Recently, diffraction is being considered as a means of studying possible SM and SUSY Higgs particle production at the LHC, in a probably rare but possibly clean double diffractive scattering process $pp \to pHp$ [184].

[5] This result is reminiscent of inclusive DIS: at large x the scaling violations are driven by α_s only and no direct sensitivity to the gluon distribution appears. This is the main reason why older fixed target DIS experiments have not determined xg well. It required a high energy ep collider to measure the gluon distribution in the proton. The same holds for polarised ep scattering, the determination of the polarised gluon distribution G cannot reliably be obtained from lower energy data as these are essentially sensitive to chromodynamic bremsstrahlung only.

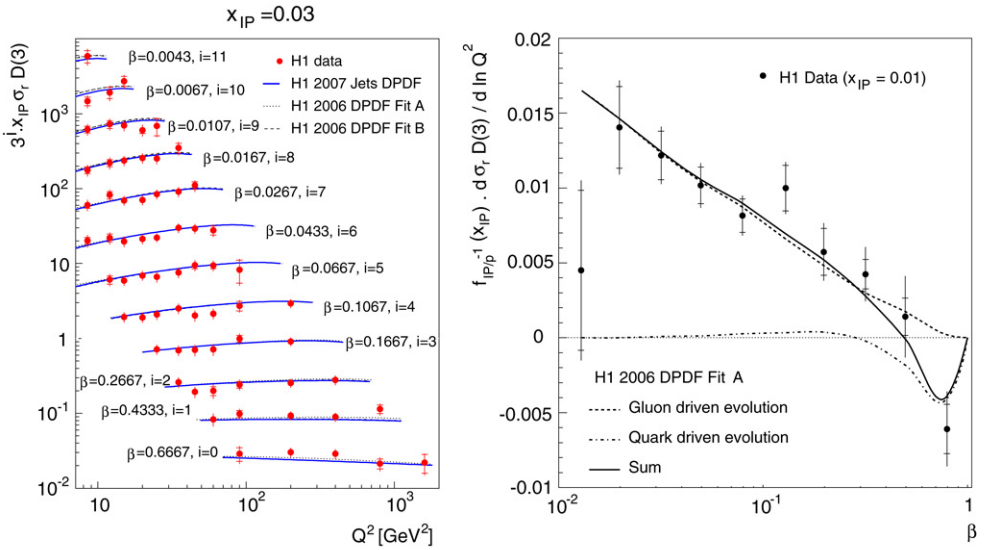

Fig. 29. Left: Diffractive reduced cross section at $x_{IP} = 0.03$ as a function of Q^2 for different $\beta = x/x_{IP}$. The data are H1 data from HERA I. The curves are different NLO QCD fits, dashed: fits A and B (see text) to the inclusive data only, solid: fit to inclusive and diffractive dijet data. Right: Derivative of the reduced diffractive cross section at $x_{IP} = 0.01$ and its decomposition into the gluon and quark parts in the H1 NLO QCD analysis.

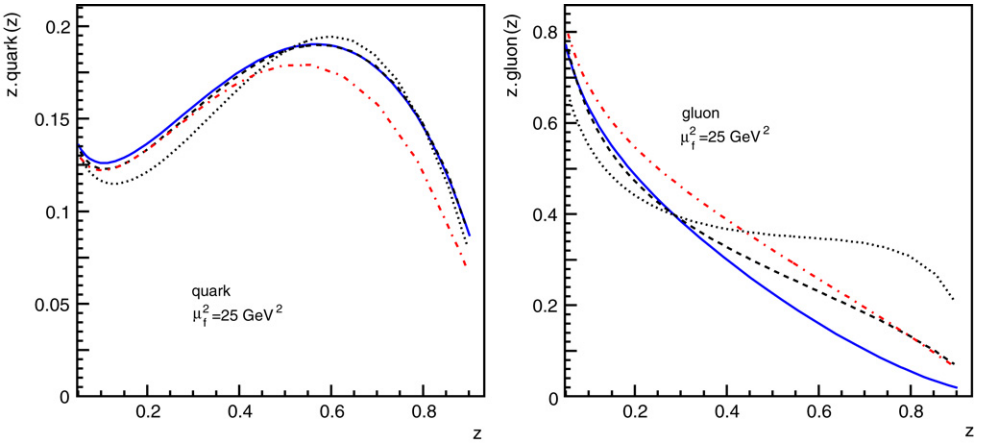

Fig. 30. Diffractive partons as determined in various NLO QCD fits: dotted: inclusive H1 fit (A); dashed: inclusive H1 fit (B); solid: H1 fit to inclusive and dijet data; dashed-dotted: from [182]. Here z is the momentum fraction of the diffractive exchange carried by the parton.

7.3. Colour dipole model description of diffraction

Diffractive parton densities lead to predictions in the same way conventional parton densities do. However, the x_{IP} dependence, which is some measure of the colour singlet formation within the proton, is factored out and remains a phenomenological assumption made prior to the subsequent QCD analysis.

An alternative way to study the phenomenon of diffractive DIS is through the application of the Colour Dipole Model (CDM). The cross-section is here given by the convolution of the quark–antiquark colour dipole wave-function and the dipole–proton cross-section. This formalism connects the inclusive low x cross-section, discussed in Section 3.4.3, to the DDIS cross-section in the same way forward elastic hadron scattering is related to the total cross-section.

The dipole–proton cross-section may be describable in terms of the DGLAP, or the BFKL formalisms in their respectively applicable kinematic regions. This has not yet been fully demonstrated. In the very low x or low Q^2 regions, gluon recombination and/or non-perturbative effects should influence the cross-section.

Fig. 31 shows an example of a fit to DDIS cross-section data [185] using a CDM-type model, BEKW [186]. The description achieved can be very good, and some models describe a number of cross-sections, DDIS, inclusive DIS, Heavy Quark production, simultaneously. While the phenomenological success is remarkable, it is fair to say that at this stage, there is no theoretical consensus in the interpretation of these models. The reader is referred to recent articles and reviews [60, 176] for further discussions.

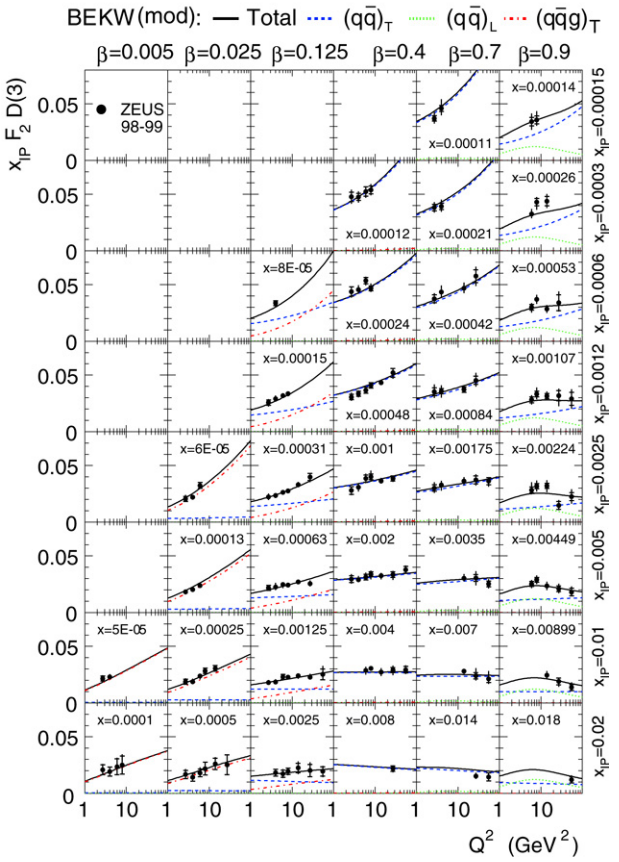

Fig. 31. DDIS measurements by ZEUS [179]. The lines are fits to a CDM-type model BEKW [186].

7.4. Elastic vector meson production

The description of exclusive electroproduction of vector mesons, $ep \to eVp$, is closely related to the CDM model described above. The virtual photon emitted from the electron fluctuates into a quark–antiquark dipole, which then scatters elastically off the proton. Long after the interaction, the $q\bar{q}$ pair forms a vector meson. At sufficiently high energies, the three steps, the $q\bar{q}$ formation, the dipole scattering and the formation of the vector meson are well separated in time. The cross-section for the process, then, is factorised into the $q\bar{q}$ coupling to the photon, the dipole–proton scattering amplitude, and the final-state formation [187,188]. The first and the last steps involve the electromagnetic coupling of the $q\bar{q}$ pair and the wave function of the vector meson, respectively. In case of light mesons, parton–hadron duality is sometimes invoked for the last step.

If there is a sufficiently large scale involved, the dipole–proton cross-section is calculable in terms of two-gluon exchange. In principle this cross-section depends on the generalised parton distribution function (GPD) [189] of the gluon. GPDs contain information on the correlation of partons within the proton. At low x, i.e. where leading $\ln 1/x$ approximation is valid (and if t is small), the generalised gluon distribution can be approximated by the usual gluon distribution. The cross-section then should rise steeply in $1/x$ (or equivalently in W, the virtual photon–proton cms energy, which at low x is given by $\sqrt{s/x}$.) for fixed Q^2 reflecting the steep rise of the gluon density at low x.

For those cases where the interaction is soft, the cross-section should rise slowly with W, similarly to the well-known Regge energy behaviour of hadron–hadron total cross-sections.

Fig. 32 (left) show the measurements of elastic VM photoproduction [191] from HERA as well as the fixed-target experiments. The data are fitted to the form W^{δ} to quantify the rate of the rise of the cross-section with energy. The δ increases as the mass of the VM increases. For the J/Ψ one finds a value of $\delta \approx 0.8$ which is consistent with a gluon density varying as $xg(x) \propto x^{-0.2}$ close to typical exponents extracted from the QCD fits to DIS inclusive data at small $Q_0^2 \sim M_{J/\Psi}^2$.

Fig. 32 (right) shows the quantity δ extracted from many different measurements [190,191] of VM production at HERA, now as a function of $Q^2 + M_V^2$, where M_V is the mass of the vector meson being produced. While the uncertainties are still large, at low values of $Q^2 + M_V^2$, $\delta \approx 0.2$ which is the expected value for Regge energy behaviour while at higher $Q^2 + M_V^2$ the exponent δ rises to around 0.8. The data are consistent with $Q^2 + M_V^2$ being the appropriate hard scale.

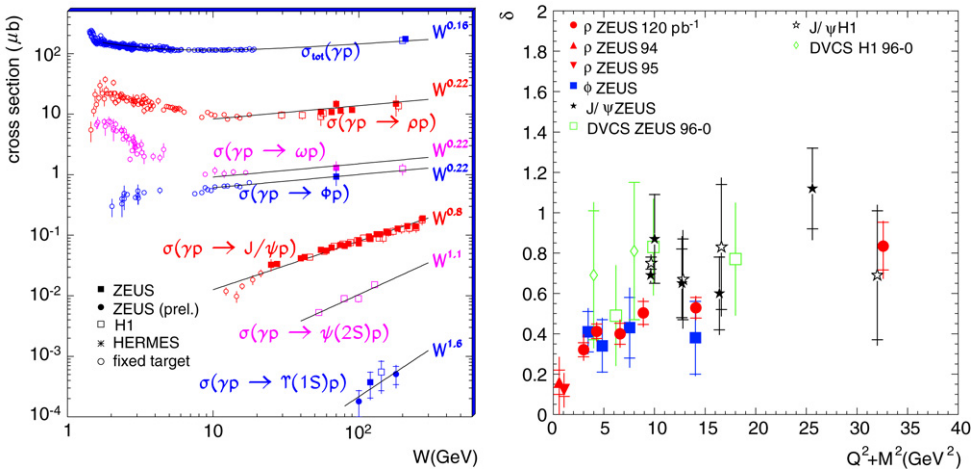

Fig. 32. (left) Elastic VM photoproduction cross-section as a function of W for a variety of species of VMs for HERA and fixed-target experiments. The data are fitted to the form W^{δ}, and the results are shown in the plot. (right) The extracted values of δ from HERA elastic VM production and DVCS data as a function of $Q^2 + M^2_{VM}$.

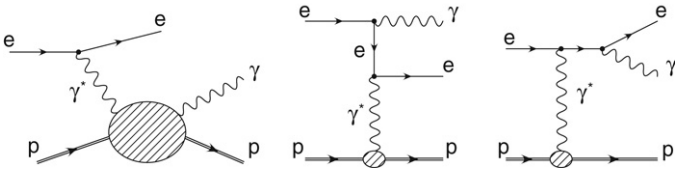

Fig. 33. Diagrams illustrating the DVCS (left) and the Bethe–Heitler (center and right) processes.

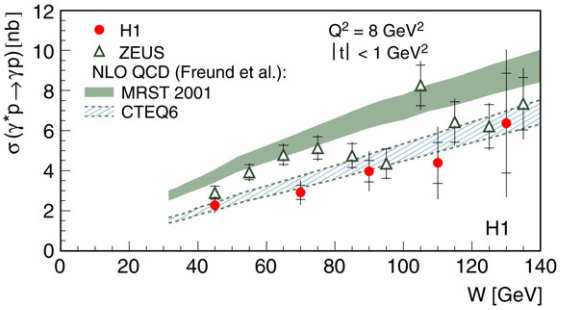

Fig. 34. The DVCS cross-section as a function of W for $Q^2 = 8$ GeV^2 and $|t| < 1$ GeV^2. The inner error bars are statistical and outer, statistical and systematic uncertainties taken in quadrature.

7.5. Deeply virtual Compton scattering

The process $ep \to e\gamma p$ at the HERA collider has contributions from both the Bethe–Heitler (BH) and the deeply virtual Compton scattering (DVCS) processes (Fig. 33). In the kinematic region of the HERA collider, the interference term between DVCS and BH processes is small, and the latter, which is precisely calculable, can be subtracted from the measured cross-section in order to obtain the DVCS cross-section.

The DVCS process is rather similar to the elastic VM production process, but has the advantage of having a simple final state with no need to rely on an understanding of meson wave functions. Fig. 34 shows the measured DVCS cross-section [192,193] as a function of W. The rise with W is relatively steep ($\delta \simeq 0.75$, see Fig. 32) demonstrating the relative "hardness" of this cross-section. The theoretical predictions of Freund and McDermott [194] use GPDs based on normal PDFs (MRST and CTEQ) [195].

In a class of CDM models called the saturation model [197], the dipole–proton cross-section is proportional to the square of the dipole separation r^2 at small $r \propto (1/Q)$. At sufficiently large r, the dipole–proton cross-section saturates (becomes constant as a function of r) to preserve unitarity. The transition of a process into the saturation regime is characterised by the saturation scale $Q_s(x) = Q_0(x_0/x)^{-\lambda/2}$, where Q_0, x_0 and λ are parameters. One prediction of such models is that certain DIS cross-sections can be expressed as a function of the single variable $\tau = Q^2/Q_s^2(x)$. Fig. 35 (left) is the total ep DIS cross-

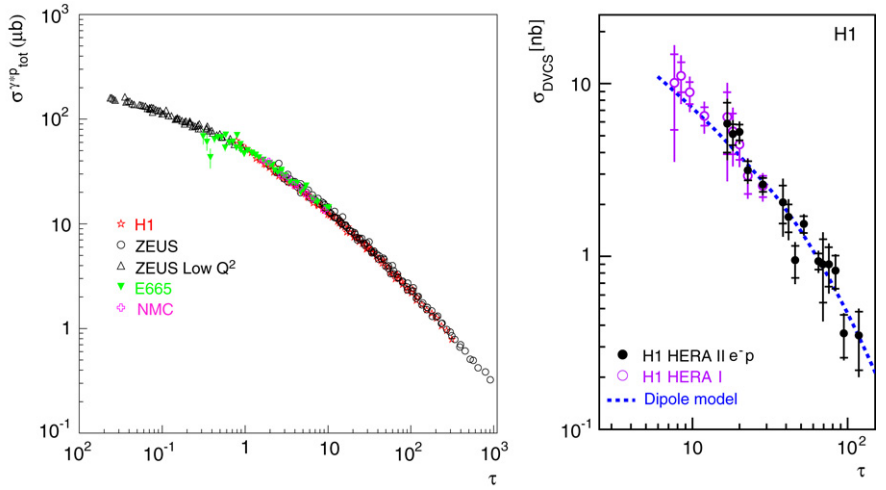

Fig. 35. (Left) Total DIS cross-section (written as the $\gamma^* p$ cross section) as a function of the saturation scaling variable τ. The figure is taken from [196]. (Right) The DVCS cross-section from the H1 collaboration as a function of τ.

section data at low-x (< 0.01) as a function of τ [196]. In this case $Q_0^2 = 1$ GeV^2, $x_0 = 3.04 \times 10^{-4}$ and $\lambda = 0.288$, as was determined in [197]. Fig. 35 (right) show the H1 DVCS data [193] using slightly different parameters, $Q_0^2 = 1$ GeV^2, $x_0 = 2.7 \times 10^{-5}$ and $\lambda = 0.25$. It has been shown that such a scaling holds relatively well also for elastic VM production and DDIS cross-sections.

8. Electroweak measurements

8.1. Charged current cross-section

Rewriting Eq. (23), the charged current DIS cross-section $\mathrm{d}^2\sigma^{CC}/\mathrm{d}x\mathrm{d}Q^2$, for the reaction $ep \to \nu(\bar{\nu})X$, can be expressed as:

$$\frac{\mathrm{d}^2\sigma^{CC}(e^{\pm})}{\mathrm{d}x\mathrm{d}Q^2} = \frac{G_F^2 Y_+}{2\pi x}\left[\frac{M_W^2}{M_W^2 + Q^2}\right]^2 \sigma^{\pm}_{r,CC}, \tag{49}$$

where $\sigma^{\pm}_{r,CC}$ contains three charged current proton structure functions depending on the lepton beam charge. If the Fermi constant G_F, is equated with that measured in muon decay, then the residual correction to the above equation from higher order electro-weak corrections amounts to only a few parts per mille [198].

If the structure functions are known, then the measurement in the region $Q^2 \ll M_W^2$ is a measurement of G_F independently of Q^2. In the region $Q^2 \approx M_W^2$, the Q^2 dependence of the cross-section is a measurement of the mass of the particle exchanged in the t channel, namely the W.

Fig. 36 shows the charged current cross-section as a function of Q^2 at HERA for all data [199] with unpolarised initial leptons. The effect of the propagator mass can be seen as Q^2 increases towards M_W^2. The difference between e^+p and e^-p charged current cross-sections arises mostly from the fact that in the former primarily the d-valence quark is probed whereas in the latter the u-valence is probed.

The neutral current cross-section [199,200] is also compared to that of the charged current, in Fig. 36. It is observed that the two cross-sections indeed become about the same at the scale of $Q^2 \approx 10^4$ GeV^2 giving an explicit demonstration of the electro-weak unification as had been anticipated.

A unique check of the standard model can be made by using the precisely measured muon decay constant (1.1639×10^{-5} GeV^{-1} [42]) and determining the propagator mass M_W that appears in Eq. (49). A fit, with M_W as a free parameter gives, for example:

$$M_W = 78.9 \pm 2.0(\text{stat.}) \pm 1.8(\text{syst.})^{+2.0}_{-1.8}(\text{PDF})\ \text{GeV}, \tag{50}$$

for the ZEUS determination using e^+p data from HERA I only. The H1 collaboration determined:

$$M_W = 80.9 \pm 3.3(\text{stat.}) \pm 1.7(\text{syst.}) \pm 3.7(\text{theo.})\ \text{GeV}, \tag{51}$$

using 35.6 pb^{-1} of e^+p data from HERA I. These uncertainties are much larger than the direct measurements of M_W and the measurements in the time-like region [42]. However, the HERA measurements demonstrate a consistency of the space-like measurements with the Standard Model.

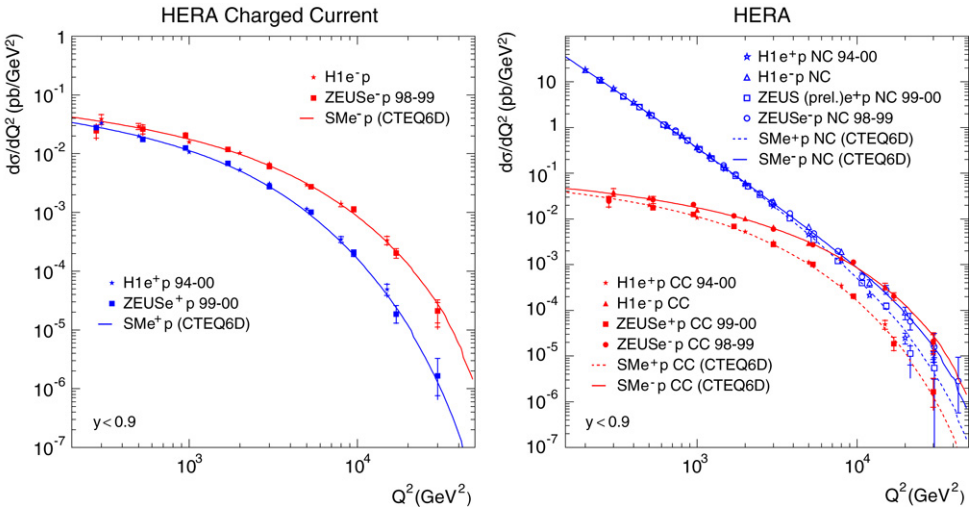

Fig. 36. Left: The charged current cross-section as a function of Q^2 measured at HERA I. Both the e^+p and e^-p cross-sections are shown. Right: the charged current cross-sections are compared with the neutral current cross-sections measured at HERA.

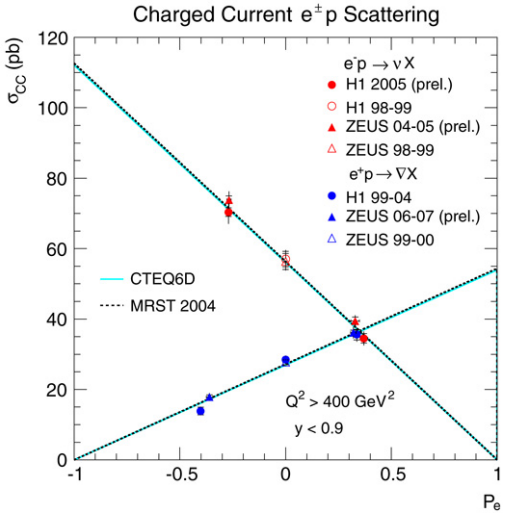

Fig. 37. The total cross-section for $e^{\pm}p$ CC DIS with $Q^2 > 400$ GeV^2 as a function of the longitudinal polarisation of the lepton beam. The lines show the prediction of the SM evaluated using CTEQ and MRST PDFs.

The purely weak nature of the charged current interaction means that the cross-section for polarised initial leptons is directly related to the unpolarised cross-sections as:

$$\frac{\mathrm{d}^2\sigma^{CC}_{\mathrm{pol}}(e^{\pm}p)}{\mathrm{d}x\mathrm{d}Q^2} = (1 \pm P)\frac{\mathrm{d}^2\sigma^{CC}_{\mathrm{unpol}}(e^{\pm}p)}{\mathrm{d}x\mathrm{d}Q^2} \tag{52}$$

where the longitudinal polarisation of the lepton beam is defined as

$$P = \frac{N_R - N_L}{N_R + N_L}, \tag{53}$$

where N_R and N_L are the numbers of right- and left-handed leptons in the beam, respectively.

With the advent of longitudinally polarised lepton beams in collider mode, in HERA II, it became possible to directly measure the polarisation dependence of charged current DIS. The result [199,201,202] is shown in Fig. 37.

Within the standard model, G_F is a function of the fine structure constant, α, the masses of the gauge bosons M_W and M_Z. Through radiative corrections, G_F also depends on the top mass, M_t, as well as on the Higgs mass, M_H, though only logarithmically. Rather than taking G_F from the muon decay constant, it is possible to take values of α, M_Z and M_t from other experiments, and determine M_W at HERA. Given the uncertainty of M_t from the Tevatron, which is at the level of 2 GeV [203], it is estimated that the uncertainty of M_W in the order of 50 MeV will be possible using the full statistics from

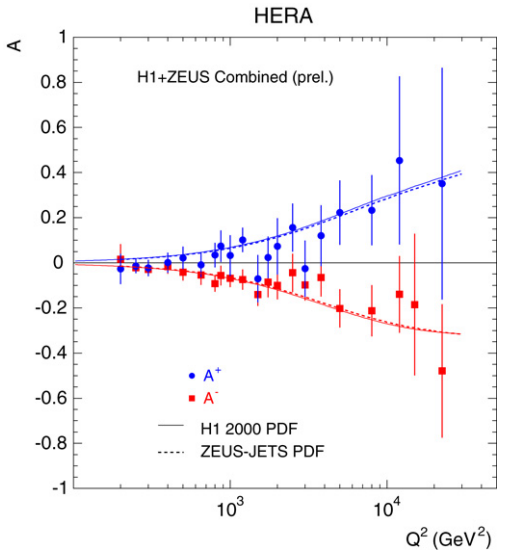

Fig. 38. Measurements of the polarisation asymmetries $A^{\pm}$ by the H1 and ZEUS collaborations. The error bars denote the total uncertainty. The curves describe the standard model predictions using the PDF sets obtained from unpolarised data.

HERA [204]. This uncertainty, which is comparable to those of current direct measurements [42], is not enough to predict the Higgs mass with any certainty; however it is interesting to see if the trend at the Tevatron for M_W and M_t measurements to predict a low mass for the standard model Higgs boson is confirmed by this result.

8.2. Neutral current cross section

A polarisation asymmetry measurement of the NC scattering, for helicities P_R and P_L, according to Eqs. (18) and (19), determines a combination of $F_2^{\gamma Z}$ and $xF_3^{\gamma Z}$

$$\frac{\sigma^{\pm}_{r,NC}(P_R) - \sigma^{\pm}_{r,NC}(P_L)}{P_R - P_L} = \kappa_Z \left[\mp a_e F_2^{\gamma Z} + \frac{Y_-}{Y_+} v_e x F_3^{\gamma Z} \right] \tag{54}$$

neglecting the pure Z exchange terms, which are small at HERA. The second term is a small correction since the vector coupling is small, as is the factor $Y_- = 1-(1-y)^2$, in most of the kinematic range at HERA. The product $a_e F_2^{\gamma Z}$ is proportional to combinations $a_e v_q$ and is thus a direct measure of parity violation at very small distances, $\sim 10^{-18}$ m, as they are probed with electroweak cross section measurements at HERA.

The polarisation NC cross-section asymmetry

$$A^{\pm} = \frac{2}{P_R - P_L} \cdot \frac{\sigma^{\pm}_{NC}(P_R) - \sigma^{\pm}_{NC}(P_L)}{\sigma^{\pm}_{NC}(P_R) + \sigma^{\pm}_{NC}(P_L)} \tag{55}$$

to a very good approximation measures the structure function ratio

$$A^{\pm} \simeq \mp \kappa_Z a_e \frac{F_2^{\gamma Z}}{F_2}. \tag{56}$$

Thus A^+ is expected to be positive and about equal to $-A^-$. At large x these asymmetries measure the d/u ratio of the valence quark distributions according to

$$A^{\pm} \simeq \pm k \frac{1 + d_v/u_v}{4 + d_v/u_v}. \tag{57}$$

The preliminary measurements of $A^{\pm}$ from HERA, Fig. 38, based on the combined data [201] from H1 and ZEUS show a significant polarisation effect and the asymmetries $A^{\pm}$ to be of opposite sign as predicted. The lines, which describe the data well, are the predictions of the standard model as obtained from the H1 and ZEUS QCD fits.

It is clear from Eqs. (18) and (21) that neutral current cross-sections at HERA are sensitive to the vector and axial-vector couplings of the quarks. The sensitivity of the cross-sections to a_q through $\mathbf{xF_3}$ is enhanced by polarisation. Unpolarised cross-sections are sensitive to v_q mainly via $\mathbf{F_2}$ whereas polarised cross-sections have further sensitivity through $\mathbf{xF_3}$. Fig. 39 shows the published measurement of a_q and v_q by the H1 collaboration compared to determinations from LEP and Tevatron.

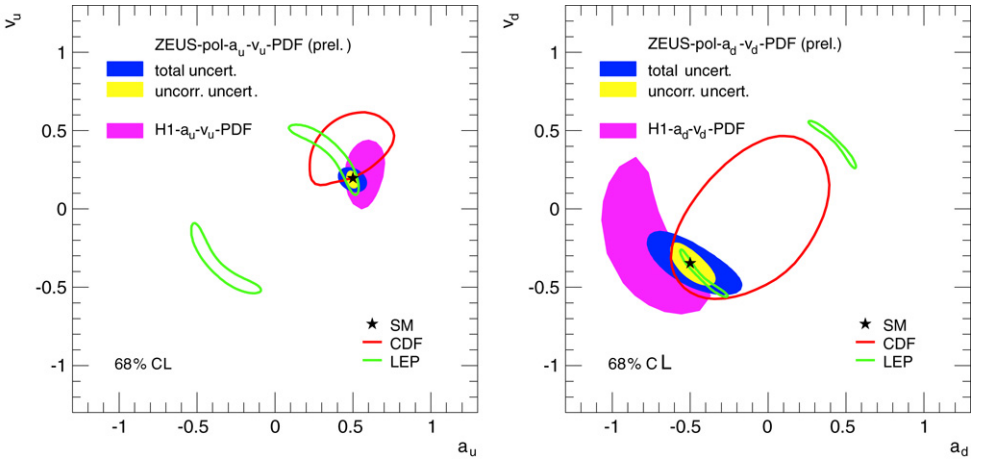

Fig. 39. The 68% confidence level contours of the electroweak parameters a_u vs v_u and a_d vs v_d from the fits to H1 (polarised only) and preliminary ZEUS (polarised and unpolarised data) compared to the results from LEP and Tevatron.

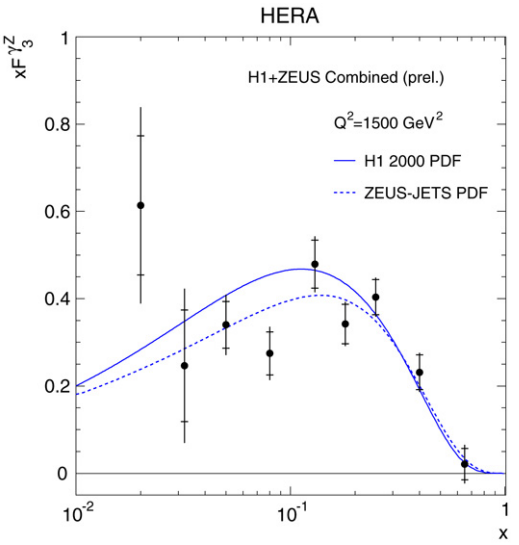

Fig. 40. The measurement of the structure function $xF_3^{\gamma Z}$ by the H1 and ZEUS collaborations. The inner error bars denote the statistical uncertainty while the full error bars comprise the statistical and systematic uncertainty added in quadrature. The data are from HERA I but include also part of the polarised HERA II data, in which, however, effectively polarisation effects average out leading to a small correction only, see [201]. The curves describe the Standard Model predictions as obtained in the H1 and ZEUS NLO QCD fits.

The figure also shows the preliminary determinations [205] of ZEUS using the polarised data which shows the expected improvement in precision.

From Eqs. (18) and (19), it can be seen that the difference between the unpolarised e^+p and e^-p cross-sections can be defined to be $\mathbf{xF_3}$. Terms proportional to v_e, which is small (0.036), can be neglected so that, to leading order in pQCD, one has

$$\mathbf{xF_3^{\pm}} \simeq \pm a_e \kappa_Z x F_3^{\gamma Z} \tag{58}$$

to a good approximation, with

$$xF_3^{\gamma Z} = 2x[e_u a_u (U - \bar{U}) + e_d a_d (D - \bar{D})] \tag{59}$$

and $U = u + c$ and $D = d + s$ for four flavours. Assuming that there are no anomalous differences between sea quark and anti-quark distributions, $xF_3^{\gamma Z}$ depends on the valence quark distributions of the proton only, and on the axial vector couplings of the u and d quarks.

The preliminary measurement [201] by the ZEUS and H1 collaborations of this quantity as a function of x at Q^2 of 1500 GeV^2 is shown in Fig. 40. The measurements are well described by the standard model predictions using PDFs as obtained from the HERA data.

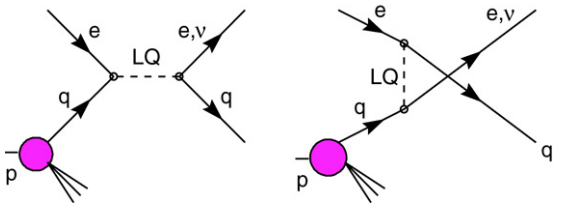

Fig. 41. Diagrams for s-channel leptoquark production and u-channel LQ exchange. Here e stands for both electron and positron, and ν for both neutrino and anti-neutrino.

Substituting the standard model values for the couplings, one finds

$$xF_3^{\gamma Z} = \frac{x}{3}(2u_v + d_v) \tag{60}$$

where u_v and d_v are the valence up and down quarks distributions. To leading order, the above equation leads to a sum rule [206]

$$\int_0^1 xF_3^{\gamma Z}\frac{\mathrm{d}x}{x} = \frac{1}{3}\int_0^1 (2u_v + d_v)\mathrm{d}x = \frac{5}{3}. \tag{61}$$

In the range of the data, the integral of $F_3^{\gamma Z}$ is measured to be

$$\int_{0.02}^{0.65} F_3^{\gamma Z}\mathrm{d}x = 1.21 \pm 0.09(\mathrm{stat}) \pm 0.08(\mathrm{syst}) \tag{62}$$

which is in agreement with predictions of the SM for this x range, using, for example, H1 and ZEUS-Jets PDFs.

9. Searches

Searches for "Beyond the Standard Model" (BSM) phenomena at HERA is a large topic, reviewed at some length in [207] relatively recently. Here only a few selected topics are covered based on updated results.

Unlike LEP and the Tevatron, HERA does not have a particle and its anti-particle in the colliding beams. Therefore, pair production cross-sections of particles are rather small but new particles may favourably be produced singly. As a result, the limits obtained at HERA are generally presented as a function of the couplings of the new particle as well as its mass.

9.1. Leptoquarks

In general, measurements for BSM searches may be interpreted, or analysed, in the context of a particular model ("model-dependent analysis"). On the other hand, the data, very often the very same data used in the model-dependent analysis, can be interpreted simply as possible deviations from the Standard Model. A first example of the former is the search for Leptoquarks.

Leptoquarks (LQs) [208], colour triplet bosons carrying both baryon and lepton numbers are postulated in many extensions of the Standard Model. An example are squarks in R-parity violating supersymmetry [209]. In ep collisions at HERA, LQ states may be produced directly though e-quark fusion, or in the s-channel, with subsequent decay into eq or νq yielding resonant peaks at the LQ mass (see Fig. 41). LQs may also be exchanged in the u-channel, in which case characteristic deviations from the SM cross-sections are expected at high Q^2.

Both H1 and ZEUS have published the results of searches [210,211] for LQs from the HERA I period using 120–130 pb^{-1} of data each. In the H1 search for LQs, the reconstructed CC and NC events are searched for deviations from the SM. In the s-channel production of LQs, an enhancement is expected at the x corresponding to the LQ mass of $M_{LQ} = \sqrt{xs_{eq}}$. In the ZEUS search, the invariant mass of the final-state e-jet and ν-jet system is reconstructed directly; in this case $M_{LQ} = M_{e(\nu)-jet}$. The two methods are rather similar in the large Q^2 region which corresponds to large LQ masses.

Neither search finds evidence for LQs and limits are set. At HERA, it is usual to set limits based on the phenomenological model proposed by Buchmüller, Rückl and Wyler (BRW) [208] which describes fourteen types of LQs. It is out of the scope of this review to give the limits for each of these. As an example, Fig. 42 shows the limits obtained by the experiments for one of the 14 BRW LQs compared to the limits set at LEP and the Tevatron. At LEP, the searches are sensitive mostly to the coupling, λ, as is the case at HERA above the kinematic limit of $M = \sqrt{s}$ since both rely on the virtual exchange of the LQs. The Tevatron searches, on the other hand, are mainly sensitive to the mass since the LQs would be pair produced via quark-anti-quark annihilation.

There are many ways to state the limits, and the reader is referred to the original papers for a fuller discussion. Also limits for LQ couplings to higher generation quarks have been set in searches for lepton-flavour violation by both ZEUS and H1 collaborations [216,217].

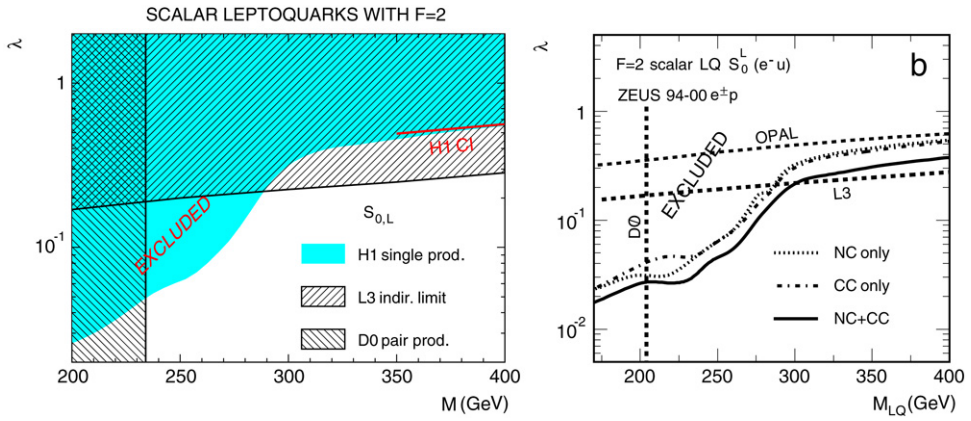

Fig. 42. Exclusion limits at 95% confidence level on the coupling λ as a function fot leptoquark mass for $S_{0,L}$ in the framework of the BRW model from H1 and ZEUS collaborations. The limits from L3, OPAL and D0 collaborations [212–214] are also shown. The D0 limit in the ZEUS plot is an older one [215] current at the time of the publication of the ZEUS result.

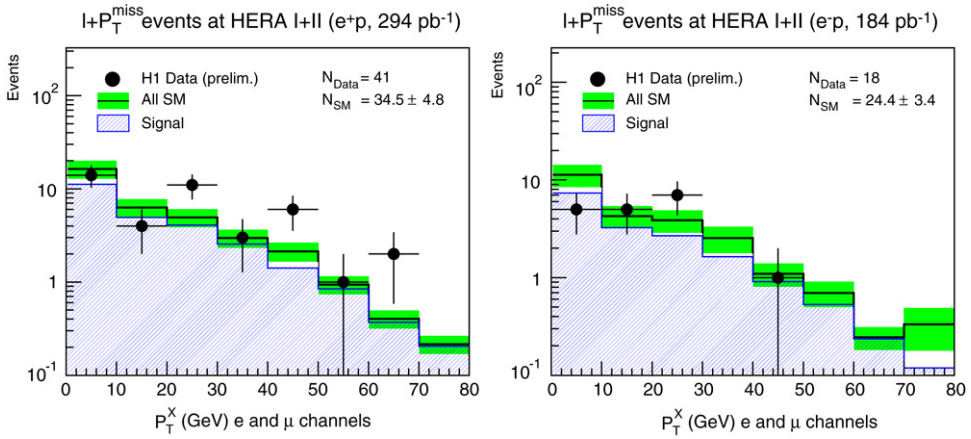

Fig. 43. The distribution of transverse hadronic energy, P_T^X, for events with isolated leptons as measured by the H1 collaboration. The e^+p (left) and e^-p (right) data are compared to the SM expectations (histogram labeled "All SM"). The component due to true SM signal, dominated by W production, is given by the histogram labeled "Signal". N_{data} is the total number of data events observed, N_{SM} is the total SM expectation. The total uncertainty of the SM expectation is given by the shaded band.

9.2. Excesses beyond the SM

Rather than doing a model-dependent search for phenomena beyond the Standard Model, one may study processes with a low cross-section in the SM in order to observe possible deviations from expectations.

In 2002, the H1 collaboration reported an excess of events with high energy isolated electrons or muon accompanied by missing transverse momentum [218]. In approximately 100 pb^{-1} of data, H1 observed 10 events with transverse energy of the hadronics system, P_T^X, greater than 25 GeV. Such events are expected in the SM from W boson production with subsequent leptonic decay. The prediction from the SM and background from misidentified CC and NC events was 2.9 ± 0.5. In a similar search, the ZEUS collaboration found no excess over the SM [219].

Both collaborations have recently made preliminary updates [220] including the data from HERA II which amounts to a five fold increase in integrated luminosity. Fig. 43 shows the distributions of these events as a function of P_T^X as reported by the H1 collaboration.

The results from both collaborations in the region of excess observed by H1 originally is summarised in Table 4. Overall, the data show a good agreement with SM expectations. In detail, there is an excess observed by H1 in the e^+p sample for both electrons and muons. The excess is at the level of 3 σ if these two H1 samples are summed. The ZEUS data in the same channel, on the other hand, is in good agreement with the SM. In a combined analysis [221], where a common phase space was defined, 29 isolated electrons and muons were observed at $P_T^X > 25$ GeV, in 0.97 fb^{-1} of data, where 25.3 ± 3.2 events are expected from SM. Both H1 and ZEUS collaborations have also looked in the τ channel, and have found no significant excess beyond the SM [222,223].

Having done a model-independent search, one can use the data to set limits on particular models. One interpretation of this type of excess would be an anomalous coupling of the u-quark to the t-quark. Such a coupling in the SM is negligibly

Table 4
The summary of HERA preliminary results for events with isolated electrons or muons and missing transverse momentum with $P_T^X > 25$ GeV

Isolated e candidates	H1 Prelim.	ZEUS Prelim.
e^-p (H1: 184 pb^{-1}, ZEUS: 204 pb^{-1})	$3/3.8 \pm 0.6(61\%)$	$5/3.8 \pm 0.6(55\%)$
e^+p (H1: 294 pb^{-1}, ZEUS: 228 pb^{-1})	$11/4.7 \pm 0.9$ (75%)	$1/3.2 \pm 0.4$ (75%)
$e^\pm p$ (H1: 478 pb^{-1}, ZEUS: 432 pb^{-1})	$14/8.5 \pm 1.5$ (68%)	$6/7.0 \pm 0.7$ (64%)
Isolated μ candidates	H1 Prelim.	ZEUS Prelim.
e^-p (H1: 184 pb^{-1}, ZEUS: 204 pb^{-1})	$0/3.1 \pm 0.5(74\%)$	$2/2.2 \pm 0.3(86\%)$
e^+p (H1: 294 pb^{-1}, ZEUS: 228 pb^{-1})	$10/4.2 \pm 0.7(85\%)$	$3/3.1 \pm 0.5(80\%)$
$e^\pm p$ (H1: 478 pb^{-1}, ZEUS: 432 pb^{-1})	$10/7.3 \pm 1.2(79\%)$	$5/5.3 \pm 0.6(82\%)$

The number of observed events is compared to the SM prediction. The signal component of the SM expectation, dominated by W production, is given as a percentage in the parenthesis. The selections for H1 and ZEUS results are similar but not identical. See [220] for details.

small. Indeed the same type of analysis has been used to set limits on a single top production at HERA, and thus on the anomalous $tu\gamma$ and tuZ couplings [216,224].

The H1 collaboration had observed events with high P_T di- or tri-electrons in excess of those expected by the SM via higher order electroweak events [225]; there were three di-electron events and three tri-electron events, with the mass of a pair of electrons in excess of 100 GeV, in a data sample corresponding to the integrated luminosity of 115 pb^{-1} where the expectations were 0.30 ± 0.04 and 0.23 ± 0.04 events respectively.

In recent updates, both H1 and ZEUS collaborations have released preliminary results on multi-electron production using over 450 pb^{-1} each [226]. Neither collaboration finds a significant excess beyond the SM in the larger data sample. H1 collaboration searched for multi-lepton events, where leptons are either electrons or muons, and found four events with a scalar sum of lepton transverse momenta greater than 100 GeV, whereas 1.9 ± 0.4 events are expected from SM. ZEUS searched for di- and tri-electrons with the mass of a pair of electrons in excess of 100 GeV, and found 6 events where 5.4 ± 1.1 events are expected from SM. In a combined analysis [227], done in a common phase space, H1 and ZEUS together observed 6 di- and tri-electron events with a scalar sum of electron transverse momenta greater than 100 GeV, in 0.94 fb^{-1} of data, where 3.0 ± 0.3 events are expected from SM.

10. Summary

HERA was the first electron–proton collider ever built. It allowed the investigation of physics of deep inelastic lepton hadron scattering to be extended by two orders of magnitude into a new kinematic domain in terms of four-momentum transfer squared, Q^2, and Bjorken x. Unlike previous fixed target experiments, which scattered either charged leptons (electron and muons) or neutrinos off nucleon targets, the very large Q^2 region at HERA, at which weak interactions become manifest, allowed the simultaneous investigation of neutral current ($ep \to eX$) and charged current ($ep \to \nu X$) interactions. Furthermore almost real photon–proton interactions – the photoproduction processes – could be investigated in which particles or jets at high masses are produced.

The accelerator, comprising separate $e^\pm$ and p sources, pre-accelerators and rings, was a new challenge for machine physics. The challenges included the problem of polarised ep collisions, which was mastered successfully and will provide a knowledge base for future ep machines such as that being considered in conjunction with the LHC p beam. The collider detectors, H1 and ZEUS, were developed independently and used very different detector techniques; for example, calorimeter techniques were based on liquid argon and uranium at H1 and ZEUS, respectively. The physics results obtained turned out to be of similar quality and coverage and in good agreement. Occasional discrepancies between the data or methods used led to constructive and sometimes challenging interactions between the two collaborations.

The intra-H1-ZEUS collaboration is currently being moved to a new level, in which H1 and ZEUS will combine their final data sets where appropriate. An example is the combination and common QCD analysis of the inclusive NC and CC cross section data. Such an analysis can be used to, in essence, cross-calibrate the results, taking advantage of the different detector techniques and different kinematic reconstruction methods. The combination is expected to lead to results of a new quality, exceeding what is to be expected in accuracy from a simple statistical average of the data. HERA will, in this way, provide a base for predictions of various processes to be studied at the LHC; and QCD will have to be used to extrapolate HERA measurements to the LHC kinematic regime. While the final results of HERA are being obtained, the first observations at the LHC are expected to be made. This will lead to a fruitful link between ep and pp physics, between HERA and the LHC.

The main results of HERA as had been presented in this overview may be summarised as follows:

- HERA opened the field of low x physics having reached values of $x = Q^2/sy$ of the order of 10^{-4} at Q^2 larger than a few GeV^2, owing to the unprecedented large energy s. In this newly accessed range, parton densities were discovered to be rising towards lower x at fixed Q^2 which is the consequence of gluon dominance at low x. This is in contrast to valence quark dominance at high x. Thus, a new phase of matter was discovered in which the densities are high but the coupling constant is small compared to unity. This discovery has immediate consequences for the understanding of quark–gluon dynamics in QCD as well as for high density states which are being investigated, for example, in nucleus–nucleus scattering or in super-high energy neutrino interactions.

- A further discovery of HERA was the observation of hard diffractive scattering comprising a significant fraction (order 10%) of the cross-section. This, attributed to the exchange of vacuum quantum numbers, is a process subject to perturbative QCD calculations due to the large momentum transfer squared involved. These colourless exchange reactions may lead to a firmer understanding of confinement, and, at the LHC, to the measurement of quantum numbers of the Higgs boson in a supersymmetric extension of the theory, in a rather clean experimental environment.
- As a machine of cleanest resolution of the structure of matter, HERA has set a new limit of 7×10^{-19} m to a possible substructure of quarks, about 10^3 times smaller than the proton radius. While one could have hoped to find a preonic substructure, this result constitutes an important milestone and signals that higher energy experiments will have to be performed in order to look even deeper into the structure of matter.
- The results of H1 and ZEUS have led to an unexpectedly rich harvest of QCD related results which are the basis of developing a further understanding of the theory of strong interactions. This refers, for example, to the findings on multi-jet production in DIS, the measurement of the strong coupling constant and the determination of a rather complete set of parton distributions, the analysis of heavy quarks as dynamically produced in boson–gluon fusion, and the first measurements on deeply virtual Compton scattering at low x which access parton correlations.
- The recent results of HERA have a precision which is becoming competitive for certain measurements of electroweak theory parameters at highest energies; an example is the determination of the light quark weak neutral current couplings.

There have been many searches performed for signals of new physics, new particles, new symmetries, *eq* resonances and QCD phenomena. At the present stage of the data analyses, a few years prior to the final results, there have been no signals observed of SUSY phenomena, R-parity violating single production of SUSY particles, leptoquarks or high density instanton states. The limits set on new particles are competitive and complementary to the limits set in the crossed amplitude reactions at similar fermion energies, as have been studied in e^+e^- reactions at LEP and in $p\bar{p}$ reactions at the Tevatron. If there is physics beyond the Standard Model, near the accelerator energy frontier, it is thus most likely to appear at TeV energies rather than at energies of a few hundred GeV, which characterise the Fermi scale as has been thoroughly studied in the last two decades of particle physics.

The operation of HERA ended in 2007. The analysis of data taken by the collider experiments ZEUS and H1, at the time of this publication, is expected to still take a few years. More precise results and also new results will still emerge. The remaining puzzles, such as that on the existence of penta-quark states, is expected to be resolved. The physics of deep inelastic ep scattering has proven to be a vital part of particle physics, and it may possibly be continued at even higher energies than HERA.

Acknowledgements

The overview presented here is a brief summary of the work of perhaps a thousand technicians, engineers and physicists for more than two decades. The authors had the great privilege to be part of a most exciting period of particle physics which in a few years will come to an end. It is our great pleasure to thank many colleagues, too numerous to be named here, for the possibility to share their wisdom and expertise and for most fruitful years of collaboration. As spokesmen of H1 and ZEUS during the times where HERA's upgrade was in some difficulty, it is particularly pleasant to acknowledge the success of the HERA crew and to thank them for their impressive efforts without which the collider experiments could not have been conducted so well. We acknowledge the strong support of the H1 and ZEUS experiments by the theoretical particle physics community. DESY had been a generous host to us and many of our collaborators from many countries. It is not forgotten, that the wisdom and dedication of Volker Soergel, Bjoern Wiik and others laid the foundations so that the following generation (to which we belong) was able to work on a most exciting machine and on some of the most fundamental problems in elementary particle physics.

We would like to thank M. Derrick, S. Magill and P. Nadolsky for careful reading of parts of this manuscript. Any remaining inconsistencies or errors are, of course, our own. We would like to thank the H1 and ZEUS collaborations for permission to show some of their results, presented so far at conferences only, also in this review.

RY's work at Argonne National Laboratory was supported by the U.S. Department of Energy, Office of Science, under contract DE-AC02-06CH11357.

References

[1] B. Wiik, C. Llewellyn Smith, Physics With Large Electron–Proton Colliding Rings, preprint DESY 77/38 (1977) (unpublished).
[2] HERA and the LHC, Workshop Proceedings, CERN-2005-014, DESY-PROC-2005-014, eds. A. DeRoeck and H. Jung, see also http://www.desy.de/~heralhc/ for further studies.
[3] H1 Collaboration, see http://www.h1-desy.de, ZEUS Collaboration, see http://www.zeus-desy.de.
[4] Deep Inelastic Scattering and QCD, DIS Workshop Series. Since 1994 this annual series of workshops provides a most complete overview on HERA physics. For recent workshops see: DIS07, Munich, Germany, April 2007, proceedings to be published, http://dx.doi.org/ ed. G. Grindhammer and K. Sachs DIS06, Tsukuba, Japan, April 2006, proceedings, eds. M. Kuze, K. Nagano and K. Tokushuku (2006).
[5] H. Abramowicz, A. Caldwell, Rev. Mod. Phys. 71 (1999) 1275.
[6] R. Devenish, A. Cooper-Sarkar, Deep Inelastic Scattering, Oxford Univ. Press, 2004.
[7] E.D. Bloom, et al., Phys. Rev. Lett. 23 (1969) 930;
M. Breidenbach, et al., Phys. Rev. Lett. 23 (1969) 935.
[8] BCDMS Collaboration, A.C. Benvenuti, et al., Phys. Lett. B 223 (1989) 485.

[9] EMC Collaboration, J.J. Aubert, et al., Phys. Lett. B 123 (1983) 275; Nuclear Phys. B 259 (1985) 189.
[10] A. Febel, H. Gerke, M. Tigner, H. Wiedemann, B.H. Wiik, IEEE Trans. Nucl. Sci. 20 (1973) 782. and DESYF35,H,S1-73/1.
[11] PEP Conceptual Design Report, LBL-4288/SLAC-189 (1976) Particle Physics with Colliding Proton–Electron–Positron Beams, LBL-750/SLAC-146 (1972) (unpublished).
[12] T. Kamae and J. Shimizu, eds., Tristan ep Working Group Report, University of Tokyo, UTPN-165 (1980) (unpublished).
[13] B. Wiik, et al. PROPER, DESY 1974 (unpublished).
[14] J.R. Ellis, B.H. Wiik, K. Hübner, CHEEP: An ep Facility in the SPS, CERN-78-02 (1978) (unpublished).
[15] W.R. Frisken, et al. "CHEER Canadian High Energy Electron Ring Feasibility Study", Fermilab Proposal 703 (1980) (unpublished).
[16] HERA Technical Proposal, DESY-HERA-81-10 (1981) (unpublished).
[17] A.A. Sokolov, I.M. Ternov, Sov. Phys. Dokl. 8 (1964) 1203.
[18] H1 Collaboration, Technical Proposal, Hamburg 1986 (unpublished).
[19] ZEUS Collaboration, Technical Proposal, Hamburg 1986 (unpublished).
[20] HERMES Collaboration, see for example the g_1 measurement: A. Airapetian, et al. Phys. Rev. D 75 (2007) 012007.
[21] HERA-B Collaboration, see for example the Υ cross section measurement: I. Abt et al. Phys. Lett. B 638 (2006) 13.
[22] V. Andreev, et al. H1 Background Working Group, Technical Report on the Beam Induced Backgrounds in the H1 Detector, H1 Note 606/10 (2002) (unpublished). Available upon request to H1.
[23] D. Bailey, et al. ZEUS Background Working Group, Study of Beam-Induced Backgrounds in the ZEUS detector from 2002 HERA running, ZEUS note 02–018, addenda 02–20 and 02–27 (2002) (unpublished). Available upon request from ZEUS.
[24] T. Alexopoulos, et al. eD Scattering with H1, A Letter of Intent, DESY 03–194;
H. Abramowicz, et al. A New Experiment for HERA, MPP-2003-62;
M. Klein, T. Greenshaw, J. Phys. G Nucl. Part. Phys. 28 (2002) 2505.
[25] A. Blondel, F. Jaquet, Proc. ep Facility for Europe, Amsterdam 1979, DESY 79/48 (1979) 391 (unpublished).
[26] J. Blümlein, M. Klein, Snowmass Workshop 1990, proceedings, ed. R. Craven, (1990) 549.
[27] U. Bassler, G. Bernardi, Nucl. Instr. Meth. A 361 (1995) 197.
[28] S. Bentvelsen, et al. HERA Workshop 1991, Proceedings, eds. W. Buchmüller and G. Ingelman, V1 (1992) 23.
[29] K. Hoeger, HERA Workshop 1991, Proceedings, eds. W. Buchmüller and G. Ingelman, V1 (1992) 43.
[30] ZEUS Collaboration, M. Derrick, et al., Z. Phys. C 72 (1996) 399.
[31] A. Glazov, DIS05 Workshop, April 2005, Madison, WI, USA, proceedings, eds. W. Smith and S.R. Dasu, (2005) 237.
[32] H1 Collaboration, I. Abt, et al., Nucl. Instr. and Meth. A 386 (1997) 310;
H1 Collaboration, I. Abt, et al., Nucl. Instr. and Meth. A 386 (1997) 348.
[33] ZEUS Collaboration, The ZEUS Detector, Status Report 1993, DESY 1993 (unpublished).
[34] I. Antoniadis, L. Baulieu, C. Kounnas, Nuclear Phys. B 168 (1980) 394.
[35] M. Klein, T. Riemann, Z. Phys. C 24 (1984) 151.
[36] E. Derman, Phys. Rev. D 7 (1973) 2755.
[37] C. Callan, D. Gross, PRL 22 (1969) 156.
[38] C.Y. Prescott, et al., Phys. Lett. B 84 (1979) 524.
[39] S.L. Glashow, Nuclear Phys. 22 (1961) 579;
A. Salam, in: N. Svartholm (Ed.), Proceedings of the 8th Nobel Colloquium, Almqvist and Wiksell, Stockholm, 1968;
S. Weinberg, PRL 19 (1967) 1264.
[40] A. Zee, F. Wilczek, S.B. Treiman, Phys. Rev. D 10 (1974) 2881;
G. Altarelli, G. Martinelli, Phys. Lett. B 76 (1978) 89.
[41] A. Arbuzov, D.Y. Bardin, J. Bluemlein, L. Kalinovskaya, T. Riemann, Comput. Phys. Commun. 94 (1996) 128.
[42] Particle Data Group, W.M. Yao, et al., J. Phys. G 33 (2006) 1.
[43] Inclusive cross section papers of the ZEUS Collaboration, M. Derrick, et al., Phys. Lett. B 303 (1993) 183;
M. Derrick, et al., Phys. Lett. B 316 (1993) 412;
M. Derrick, et al., Z. Phys. C 65 (1995) 379;
M. Derrick, et al., Phys. Rev. Lett. 75 (1995) 1006;
M. Derrick, et al., Z. Phys. C 69 (1996) 607;
M. Derrick, et al., Z. Phys. C 72 (1996) 399;
J. Breitweg, et al., Phys. Lett. B 407 (1997) 432;
J. Breitweg, et al., Eur. Phys. J. C 7 (1999) 609;
J. Breitweg, et al., Phys. Lett. B 487 (2000) 53;
J. Breitweg, et al., Eur. Phys. J. C 12 (2000) 411;
J. Breitweg, et al., Eur. Phys. J. C 27 (2003) 305 (erratum);
S. Chekanov, et al., Eur. Phys. J. C 21 (2001) 443;
S. Chekanov, et al., Phys. Lett. B 539 (2002) 197;
S. Chekanov, et al., Eur. Phys. J. C 552 (2003) 308 (erratum);
S. Chekanov, et al., Eur. Phys. J. C 32 (2003) 1;
S. Chekanov, et al., Phys. Rev. D 70 (2004) 052001;
S. Chekanov, et al., Phys. Lett. B 637 (2006) 210;
S. Chekanov, et al., Eur. Phys. J. C 49 (2007) 523.
[44] Inclusive cross section papers of the H1 Collaboration, T. Ahmed, et al., Phys. Lett. B 299 (1993) 385;
I. Abt, et al., Nuclear Phys. B 407 (1993) 515;
I. Abt, et al., Phys. Lett. B 321 (1994) 161;
T. Ahmed, et al., Phys. Lett. B 324 (1994) 241;
T. Ahmed, et al., Nuclear Phys. B 439 (1995) 471;
S. Aid, et al., Nuclear Phys. B 470 (1996) 3;
S. Aid, et al., Phys. Lett. B 379 (1996) 319;
C. Adloff, et al., Nuclear Phys. B 497 (1997) 3;
C. Adloff, et al., Eur. Phys. J. C 13 (2000) 609;
C. Adloff, et al., Eur. Phys. J. C 19 (2001) 269;
C. Adloff, et al., Eur. Phys. J. C 21 (2001) 33;
C. Adloff, et al., Eur. Phys. J. C 30 (2003) 1;
A. Aktas, et al., Phys. Lett. B 634 (2006) 173.
H1 Collaboration, Measurement of the Inclusive ep Scattering Cross Section at low Q^2 and x at HERA, Hamburg 2008 (in preparation).
[45] A. De Rújula, S.L. Glashow, H.D. Politzer, S.B. Treiman, F. Wilczek, A. Zee, Phys. Rev. D 10 (1974) 1649.
[46] A. Donnachie, P.V. Landshoff, Proceedings HERA Workshop, Hamburg 1987, ed. R. Peccei, Vol.1, p. 351 and CERN-Th. 5020/88 (1988).
[47] M. Glück, E. Reya, A. Vogt, Z. Phys. C 53 (1992) 127.
[48] Y. Watanabe, et al., PRL 35 (1975) 898.
[49] K. Prytz, Phys. Lett. B 311 (1993) 286.

[50] A. Mueller, Nuclear Phys.: Proc. Suppl. A 29 (1992) 275.
[51] A. DeRoeck, M. Klein, T. Naumann, Phys. Lett. B 385 (1996) 411.
[52] G. Altarelli, R.D. Ball, S. Forte, Nuclear Phys. B 742 (2006) 1. and references therein.
[53] D. Haidt, Eur. Phys. J. C 35 (2004) 519.
[54] E.A. Kuraev, L.N. Lipatov, V.S. Fadin, Sov. Phys. JETP 44 (1976) 443; Sov. Phys. JETP 45 (1977) 199;
Y.Y. Balitsky, L.N. Lipatov, Sov. J. Nuclear Phys. 28 (1978) 822.
[55] ZEUS Collaboration, J. Breitweg, et al., Eur. Phys. J. C 7 (1999) 609.
[56] H1 Collaboration, C. Adloff, et al., Phys. Lett. B 520 (2001) 183.
[57] A. Donnachie, P.V. Landshoff, Z. Phys. C 61 (1994) 139.
[58] ZEUS Collaboration, J. Breitweg, et al., Phys. Lett. B 487 (2000) 53.
[59] P. Newman, Int. J. Mod. Phys. A 19 (2004) 1061.
[60] C. Ewerz, O. Nachtmann, Phys. Lett. B 648 (2007) 279.
[61] C.E. Hyde-Wright, L. Frankfurt, M. Strikman, C. Weiss, DIS06 Workshop, April 2006, Tsukuba, Japan, proceedings, eds. M. Kuze, K. Nagano and K. Tokushuku, (2006) 279.
[62] P. Jacobs, X.-N. Wang, Prog. Part. Nuclear Phys. 54 (2004) 443.
[63] S. Kretzer, F.I. Olness, R.J. Scalise, R.S. Thorne, U.K. Yang, Phys. Rev. D 64 (2001) 033003;
M. Nakahata, Proceedings of LP07, Aug. 2007, Daegu, Korea (in press).
[64] L.A.T. Bauerdick, A. Glazov, M. Klein, HERA Physics Workshop, 1996/97, Proceedings, eds. G. Ingelman, A. DeRoeck and R. Klanner V1 (1996) 77;
M. Klein, DIS04, Strbske Pleto, 1994, proceedings, eds. D. Bruncko, J. Ferencei and P. Strizenec V1 (1994) 309 J. Feltesse Ringberg Workshop, October 2005, Proceedings. http://www.mppmu.mpg.de/.
[65] S. Moch, J.A.M. Vermaseren, A. Vogt, Phys. Lett. B 606 (2005) 123;
R. Thorne, Ringberg Workshop, October 2005, Proceedings. http://www.mppmu.mpg.de/.
[66] H1 Collaboration, C. Adloff, et al., Phys. Lett. B 393 (1997) 452; see also Eur. Phys. J. C 13 (2000) 609.
[67] H1 Collaboration, C. Adloff, et al., Eur. Phys. J. C 21 (2001) 33.
[68] H1 Collaboration, EPS2003, July 2003, Aachen, Germany H1 prel. 03-043,
http://www-h1.desy.de/h1/www/publications/H1preliminary.short_list.html;
T. Lastovicka, EPJC direct, Eur. Phy. J. C 33 (2004) s01,s388–s390.
[69] H1 Collaboration, Running at Low Proton Beam Energies, Expression of Interest, subm. to the DESY PRC, October 2005, PRC 11/05, H1-10/05-622 (unpublished).
[70] Yu.L. Dokshitzer, Sov. Phys. JETP 46 (1977) 641.
[71] V.N. Gribov, L.N. Lipatov, Sov. J. Nuclear Phys. 15 (1972) 438,675.
[72] G. Altarelli, G. Parisi, Nuclear Phys. B 126 (1977) 298.
[73] J.A.M. Vermaseren, A. Vogt, S. Moch, Nuclear Phys. B 691 (2004) 129; Nuclear Phys. B 724 (2005) 3.
[74] For detailed discussions and further references see: Small x Collaboration B. Andersson, et al., Eur. Phys. J. C 25 (2002) 77; Eur. Phys. J. C 35 (2004) 67;
J.R. Andersen, et al., Eur. Phys. J. C 48 (2006) 53.
[75] M. Ciafaloni, Nuclear Phys. B 296 (1988) 49;
S. Catani, F. Fiorani, G. Marchesini, Phys. Lett. B 234 (1990) 339;
S. Catani, F. Fiorani, G. Marchesini, Nuclear Phys. B 336 (1990) 18;
G. Marchesini, Nuclear Phys. B 445 (1995) 49.
[76] J.B. Dainton, M. Klein, P. Newman, E. Perez, F. Willeke, JINST 1 P10001 (2006); see also http://www.lhec.org.uk/.
[77] M. Botje, Phys. J. C 14 (2000) 285. http://www.nikhef.nl/~h24/qcdnum/.
[78] C. Pascaud, F. Zomer, preprints LAL-94-42 (1994) and 95-05 (1995) (unpublished).
[79] MRST, now MSTW Collaboration, see for example A.D. Martin, R.G. Roberts, W.J. Stirling, R.S. Thorne, Eur. Phys. J. C 4 (1998) 463;
A.D. Martin, R.G. Roberts, W.J. Stirling, R.S. Thorne, Eur. Phys. J. C 23 (2002) 73;
A.D. Martin, W.J. Stirling, R.S. Thorne, G. Watt, Phys. Lett. B 652 (2007) 292.
[80] CTEQ Collaboration, see for example H.L. Lai, et al., Eur. Phys. J. C 12 (2000) 375;
J. Pumplin, et al., JHEP 0207 (2002) 012;
H.L. Lai, et al., JHEP 0704 (2007) 089.
[81] S. Alekhin, Phys. Rev. D 68 (2003) 014002;
S. Alekhin, K. Melnikov, F. Petriello, Phys. Rev. D 74 (2006) 054033.
[82] E 866/NuSea Collaboration, R.S. Towell, et al., Phys. Rev. D 64 (2001) 052002.
[83] M. Klein, B. Reisert, HERA–LHC Workshop, March 2004 to March 2005, proceedings, ed. A. DeRoeck and H. Jung, V1 (2005) 99.
[84] See the PDF section of the HERA–LHC Workshop, March 2004 to March 2005, in: Proceedings, ed. A. DeRoeck and H. Jung, V1 (2005) 41.
[85] For a recent paper see W.K. Tung, et al., JHEP 0702 (2007) 053. and references therein.
[86] R.S. Thorne, R.G. Roberts, Phys. Rev. D 57 (1998) 6871.
[87] ZEUS Collaboration, S. Chekanov, et al., Z. Phys. C 21 (2001) 441.
[88] ZEUS Collaboration, S. Chekanov, et al., Phys. Rev. D 67 (2003) 012007.
[89] H1 Collaboration, C. Adloff, et al., Eur. Phys. J. C 30 (2003) 1.
[90] A.D. Martin, et al., Eur. Phys. J. C 23 (2002) 73.
[91] J. Pumplin, et al., JHEP 0207 (2002) 012.
[92] B. Portheault, PhD Thesis, 03/05, Univ. Paris XI Orsay (2005) (unpublished) available at H1 http://www-h1.desy.de.
[93] A. Vogt, in DIS99, Proc. Suppl. Nuclear Phys. B 79 (1999) 102, ed. J. Blümlein and T. Riemann.
[94] ZEUS Collaboration, Phys. Rev. D 67 (2003) 012007.
[95] M. Klein, Proceedings of DIS07, April 2007, Munich, Germany, http://www.sciencewisepublishing/publications/DIS07/.
[96] S. Catani, M.H. Seymour, Nuclear Phys. B 485 (1997) 291.
[97] E. Mirkes, D. Zeppenfeld, Phys. Lett. B 380 (1996) 205.
[98] D. Graudenz, arXiv:hep-ph/970244.
[99] A.D. Martin, et al., Phys. Lett. B 531 (2002) 216.
[100] J. Pumplin, et al., JHEP 0207 (2002) 012.
[101] S.V Chekanov, the 14th Topical Conference on Hadron Collider Physics, Sept. 2002, Karlsruhe, proceedings, eds. M. Erdmann and T. Mueller (2003) 478. ArXiv:hep-ph/0211298v1.
[102] G.C. Blazey, et al. Physics at RUN II: QCD and Weak Boson Physics Workshop, Nov. 1999, Batavia, in: Proceedings, eds. U. Baur, R.K. Ellis and D. Zeppenfeld (2000) 47. ArXiv:hep-ex/0005012v2.
[103] S. Catani, et al., Nuclear Phys. B 406 (1993) 187.
[104] S.D. Ellis, D.E. Soper, Phys. Rev. D 48 (1993) 3160.
[105] G. Ingelman, A. Edin, J. Rathsman, Comput. Phys. Commut 101 (1997) 108.
[106] L. Lönnblad, Comput. Phys. Commut 71 (1992) 15.
[107] L. Lönnblad, Z. Phys. C 65 (1995) 285.
[108] B. Andersson, Phys. Rep. 97 (1983) 31.

[109] S. Frixione, G. Ridolfi, Nuclear Phys. B 507 (1997) 315.
[110] G. Corcella, et al., JHEP 0101 (2001) 010;
G. Marchesini, et al., Comput. Phys. Commut. 67 (1992) 465.
[111] T. Sjöstrand, et al., Comput. Phys. Commut. 135 (2001) 238;
T. Sjöstrand, et al., Comput. Phys. Commut. 82 (1994) 74.
[112] H1 Collaboration, C. Adloff, et al., Eur. Phys. J. C 13 (2000) 397;
ZEUS Collaboration, J. Breitweg, et al., Phys. Lett. B 479 (2000) 37;
ZEUS Collaboration, S. Chekanov, et al., Eur. Phys. J. C 35 (2004) 487;
H1 Collaboration, A. Aktas, et al., Eur. Phys. J. C 37 (2004) 141.
[113] P. Aurenche, J. Guillet, M. Fontannaz, ZPC 64 (1994) 621.
[114] R. Brun, et al. Technical Report CERN-DD/EE/84-1, CERN, 1987.
[115] ZEUS Collaboration, S. Chekanov, et al., Phys. Lett. B 547 (2002) 164.
[116] H1 Collaboration, A. Aktas, et al., Phys. Lett. B 653 (2007) 134. DESY-07-073.
[117] R.P. Feynman, Photon–Hadron Interactions, Benjamin, New York, 1972;
K.H. Streng, T.F. Walsh, P.M. Zerwas, Z. Phys. C 2 (1979) 237.
[118] A.D. Martin, et al., Eur. Phys. J. C 4 (1998) 463;
A.D. Martin, et al., Eur. Phys. J. C 14 (2000) 133.
[119] ZEUS Collaboration, S. Chekanov, et al., Eur. Phys. J. C 23 (2002) 615.
[120] M. Glück, E. Reya, A. Vogt, Phys. Rev. D 45 (1992) 3986.
[121] M. Glück, E. Reya, A. Vogt, Phys. Rev. D 46 (1992) 1973.
[122] H1 Collaboration, A. Aktas, et al., Phys. Lett. B 639 (2006) 21.
[123] ZEUS Collaboration, S. Chekanov, et al., Phys. Rev. D 76 (2007) 0720011. DESY-07-092.
[124] ZEUS Collaboration, S. Chekanov, et al., Nuclear Phys. B 765 (2007) 1.
[125] H1 Collaboration, C. Adloff, et al., Phys. Lett. B 515 (2001) 17.
[126] ZEUS Collaboration, S. Chekanov, et al., Eur. Phys. J. C 44 (2005) 183.
[127] ZEUS Collaboration, S. Chekanov, et al., Phys. Lett. B 649 (2007) 12.
[128] ZEUS Collaboration, S. Chekanov, et al., Nuclear Phys. B 792 (2008) 1. DESY-07-102;
ZEUS Collaboration, S. Chekanov, et al., Eur. Phys. J. C 52 (2007) 515. DESY-07-100;
ZEUS Collaboration, S. Chekanov, et al., Nuclear Phys. B 786 (2007) 152. DESY-07-062;
ZEUS Collaboration, S. Chekanov, et al., Phys. Lett. B 649 (2007) 12;
H1 Collaboration, A. Aktas, et al., Eur. Phys. J. C 51 (2007) 271;
ZEUS Collaboration, S. Chekanov, et al., Nuclear Phys. B 729 (2007) 492;
H1 Collaboration, A. Aktas, et al., Eur. Phys. J. C 46 (2006) 27;
H1 Collaboration, A. Aktas, et al., Eur. Phys. J. C 37 (2004) 141;
H1 Collaboration, A. Aktas, et al., Eur. Phys. J. C 33 (2004) 477.
[129] ZEUS Collaboration, J. Breitweg, et al., Phys. Lett. B 507 (2001) 70;
ZEUS Collaboration, S. Chekanov, et al., Phys. Lett. B 547 (2002) 164;
H1 Collaboration, C. Adloff, et al., Eur. Phys. J. C 19 (2001) 289;
ZEUS Collaboration, S. Chekanov, et al., Phys. Rev. D 67 (2003) 012007;
ZEUS Collaboration, S. Chekanov, et al., Eur. Phys. J. C 42 (2005) 1;
H1 Collaboration, C. Adloff, et al., Eur. Phys. J. C 21 (2001) 33;
ZEUS Collaboration, S. Chekanov, et al., Phys. Lett. B 558 (2003) 41;
ZEUS Collaboration, S. Chekanov, et al., Eur. Phys. J. C 31 (2003) 149;
ZEUS Collaboration, S. Chekanov, et al., Phys. Lett. B 560 (2003) 7;
ZEUS Collaboration, S. Chekanov, et al., Eur. Phys. J. C 44 (2005) 183;
ZEUS Collaboration, S. Chekanov, et al., Nuclear Phys. B 700 (2004) 3;
ZEUS Collaboration, S. Chekanov, et al., Phys. Lett. B 207 (2006) 12.
[130] C. Glasman, arXiv:hep-ex/0506035.
[131] S. Bethke, arXiv:hep-ex/0407021.
[132] S. Bethke, arXiv:hep-ex/0606035.
[133] H1 and ZEUS Collaborations, EPS07, July 2007, Manchester, UK, H1prelim-07-007, ZEUS-prel-07-026,
http://www-h1.desy.de/h1/www/publications/H1preliminary.short_list.html.
[134] ZEUS Collaboration, S. Chekanov, et al., Eur. Phys. J. C 42 (2005) 1.
[135] A.M. Cooper-Sarkar, Ringberg Workshop, October 2005, Proceedings. http://www.mppmu.mpg.de/.
[136] B.W. Harris, J. Smith, Phys. Rev. D 57 (1998) 2306.
[137] R.S. Thorne, J. Phys. G 25 (1999) 1307.
[138] R.G. Roberts, R.S. Thorne, Eur. Phys. J. C 19 (2001) 339.
[139] M.A.G. Aivazis, et al., Phys. Rev. D 50 (1994) 3102;
M.A.G. Aivazis, F.I. Olness, W.-K. Tung, Phys. Rev. D 50 (1994) 3085.
[140] B.A. Kniehl, et al., Phys. Rev. D 71 (2005) 014018;
B.A. Kniehl, et al., Eur. Phys. J. C 41 (2005) 199.
[141] P.M. Nadolsky, et al., Phys. Rev. D 67 (2003) 074015.
[142] M.G. Bowler, Z. Phys. C 11 (1981) 169.
[143] V.G. Kartvelishvili, A.K. Likhoded, V.A. Petrov, Phys. Lett. B 78 (1978) 615.
[144] C. Peterson, et al., Phys. Rev. D 27 (1983) 105.
[145] M. Ciafaloni, Nuclear Phys. B 296 (1988) 49;
S. Catani, F. Fiorani, G. Marchesini, Phys. Lett. B 234 (1990) 339;
S. Catani, F. Fiorani, G. Marchesini, Nuclear Phys. B 336 (1990) 18;
G. Marchesini, Nuclear Phys. B 445 (1995) 49.
[146] H. Jung, G.P. Salam, Eur. Phys. J. C 19 (2001) 339.
[147] H. Jung, arXiv:hep-ph/0411287.
[148] W.K. Tung, S. Kretzer, C. Schmidt, J. Phys. G 28 (2001) 983.
[149] H1 Collaboration, A. Aktas, et al., Eur. Phys. J. C 51 (2007) 271.
[150] B.A. Kniehl, et al., Phys. Rev. Lett. 96 (2006) 012001;
B.A. Kniehl, G. Kramer, M. Maniatis, Nuclear Phys. B 711 (2005) 345;
B.A. Kniehl, G. Kramer, M. Maniatis, Nuclear Phys. B 720 (2005) 345 (erratum).
[151] ZEUS Collaboration, S. Chekanov, et al., Phys. Rev. D 69 (2004) 012004.
[152] H1 Collaboration, C. Adloff, et al., Phys. Lett. B 528 (2002) 199.
[153] H1 Collaboration, A. Atkas, et al., Eur. Phys. J. C 50 (2007) 251.

[154] S. Frixione, P. Nason, G. Ridolfi, Nuclear Phys. B 454 (1995) 3;
S. Frixione, M.L. Mangano, P. Nason, G. Ridolfi, Phys. Lett. B 348 (1995) 633.
[155] G. Heinrich, B.A. Kniehl, Phys. Rev. D 70 (2004) 094035.
[156] ZEUS Collaboration, S. Chekanov, et al., Nuclear Phys. B 729 (2005) 492.
[157] ZEUS Collaboration, S. Chekanov, et al., Phys. Rev. D 70 (2004) 012008.
[158] H1 Collaboration, A. Aktas, et al., Eur. Phys. J. C 41 (2005) 453.
[159] ZEUS Collaboration, S. Chekanov, et al., Phys. Lett. B 599 (2005) 173.
[160] H1 Collaboration, A. Aktas, et al., Phys. Lett. B 621 (2005) 56.
[161] ZEUS Collaboration, S. Chekanov, et al., Eur. Phys. J. C 50 (2007) 299.
[162] ZEUS Collaboration, EPS07, July 2007, Manchester, UK, http://www-zeus.desy.de/physics/hfla/public/abstracts07/.
[163] A.V. Lipatov, N.P. Zotov, Phys. Rev. D 75 (2007) 014028.
[164] D. Pitzl, et al., Nucl. Instr. Meth. A 454 (2000) 334.
[165] E.N. Koffeman, Nucl. Instr. Meth. A 473 (2001) 26.
[166] H1 Collaboration, A. Aktas, et al., Eur. Phys. J. C 40 (2005) 349.
[167] H1 Collaboration, A. Aktas, et al., Eur. Phys. J. C 45 (2006) 23.
[168] ZEUS Collaboration, S. Chekanov, et al., Phys. Lett. B 599 (2004) 173.
[169] ZEUS Collaboration, S. Chekanov, et al., JHEP 07 (2007) 074;
ZEUS Collaboration, S. Chekanov, et al., Eur. Phys. J. C 44 (2005) 351;
H1 Collaboration, A. Aktas, et al., Eur. Phys. J. C 38 (2005) 447;
ZEUS Collaboration, J. Breitweg, et al., Phys. Lett. B 481 (2000) 213.
[170] ZEUS Collaboration, S. Chekanov, et al., Phys. Lett. B 649 (2007) 111.
[171] H1 Collaboration, A. Aktas, et al., Eur. Phys. J. C 47 (2006) 597.
[172] ZEUS Collaboration, M. Derrick, et al., Phys. Lett. B 346 (1995) 399.
[173] H1 Collaboration, T. Ahmed, et al., Phys. Lett. B 348 (1995) 681.
[174] J. Collins, Phys. Rev. D 57 (1998) 3051;
J. Collins, Phys. Rev. D 61 (2000) 019902 (erratum).
[175] J. Blümlein, D. Robaschik, Phys. Rev. D 65 (2002) 096002.
[176] For a review see J.R. Forshaw, R. Sandapen, G. Shaw, JHEP 0611 (2006) 025.
[177] H1 Collaboration, A. Aktas, et al., Eur. Phys. J. C 48 (2006) 715;
H1 Collaboration, A. Aktas, et al., Eur. Phys. J. C 48 (2006) 749.
[178] ZEUS Collaboration, S. Chekanov, et al., Euro. Phys. J. C 52 (2007) 813.
[179] ZEUS Collaboration, S. Chekanov, et al., Nuclear Phys. B 713 (2005) 3.
[180] J. Lukasi, Proceedings of DIS07, April 2007, Munich, Germany, http://sciencewisepublishing.com/publications/DIS07/.
[181] H1 Collaboration, A. Aktas, et al., JHEP 0710 (2007) 042.
[182] A. Martin, M. Ryskin, G. Watt, Phys. Lett. B 644 (2007) 131.
[183] H1 Collaboration, A. Aktas, et al., Eur. Phys. J. C 51 (2007) 549.
[184] The LHC FP420 Project, see http://www.fp420.com/.
[185] ZEUS Collaboration, S. Chekanov, et al., Nuclear Phys. B 713 (2005) 3.
[186] J. Bartel, et al., Eur. Phys. J. C 7 (1999) 443.
[187] B.K. Kopeliovitch, et al., Phys. Lett. B 324 (1994) 469.
[188] S.J. Brodsky, et al., Phys. Rev. D 50 (1994) 3134.
[189] L.L. Frankfurt, A. Freund, M. Strikman, Phys. Rev. D 58 (1998) 114001;
L.L. Frankfurt, A. Freund, M. Strikman, Phys. Rev. D 59 (1999) 119901 (erratum);
D. Müller, et al., Fortschr. Phys. 42 (1994) 347;
X. Ji, Phys. Rev. Lett. 78 (1997) 610;
K. Golec-Biernat, A. Martin, Phys. Rev. D 59 (1999) 014029.
[190] ZEUS Collaboration, S. Chekanov, et al., Nuclear Phys. B 695 (2004) 3.
[191] ZEUS Collaboration, M. Derrick, et al., Eur. Phys. J. C 6 (1999) 603;
H1 Collaboration, A. Aktas, et al., Eur. Phys. J. C 13 (2000) 371;
H1 Collaboration, C. Adloff, et al., Phys. Lett. B 483 (2000) 360;
ZEUS Collaboration, J. Breitweg, et al., Phys. Lett. B 487 (2000) 273;
ZEUS Collaboration, S. Chekanov, et al., Nuclear Phys. B 718 (2005) 3;
H1 Collaboration, A. Aktas, et al., Eur. Phys. J. C 46 (2006) 585;
ZEUS Collaboration, S. Chekanov, et al., PMC Physics A 1 (2007) 6.
[192] ZEUS Collaboration, S. Chekanov, et al., Phys. Lett. B 573 (2003) 46.
[193] H1 Collaboration, A. Aktas, et al., Eur. Phys. J. C 44 (2005) 1.
[194] A. Freund, M.F. McDermott, Phys. Rev. D 65 (2002) 091901;
A. Freund, M.F. McDermott, Eur. Phys. J. C 23 (2002) 651.
[195] A. Freund, M.F. McDermott, M. Strikman, Phys. Rev. D 67 (2003) 036001.
[196] C. Marquet, L. Schoeffel, Phys. Lett. B 639 (2006) 471.
[197] K. Golec-Biernat, M. Wüsthoff, Phys. Rev. D 59 (1999) 014017.
[198] H. Spiesberger, et al. Physics at HERA, in: Proceedings for the Workshop, Hamburg, 1991, V2 (1991) 195.
[199] ZEUS Collaboration, S. Chekanov, et al., Eur. Phys. J. C 32 (2003) 1;
H1 Collaboration, C. Adloff, et al., Eur. Phys. J. C 30 (2003) 1;
ZEUS Collaboration, S. Chekanov, et al., Phys. Rev. Lett. 539 (2002) 197;
ZEUS Collaboration, S. Chekanov, et al., Phys. Rev. Lett. 552 (2003) 308;
H1 Collaboration, C. Adloff, et al., Eur. Phys. J. C 19 (2001) 269.
[200] ZEUS Collaboration, S. Chekanov, et al., Phys. Rev. D 70 (2004) 052001;
ZEUS Collaboration, S. Chekanov, et al., Eur. Phys. J. C 28 (2003) 2.
[201] V. Chekelian, in: A. Sissakian, G. Kozlov, E. Kolganova (Eds.), Proceedings of ICHEP06, July 2006, Moscow, p. 701.
[202] H1 Collaboration, A. Aktas, et al., Phys. Lett. B 634 (2006) 173.
[203] CDF and D0 collaborations, ArXiv:hep-ex/0703034.
[204] J. Bluemlein, M. Klein, T. Naumann, T. Riemann, Workshop on HERA Physics, 1986/7, in: Proceedings, ed. R. Peccei, V1 (1987) 67;
R. Beyer, et al. Future HERA Physics, in: R. Klanner, A. De Roeck (Eds.), Proceedings for the Workshop, Hamburg, 1995/6, V1 (1996) 140.
[205] Y.D. Ri, in: A. Sissakian, G. Kozlov, E. Kolganova (Eds.), Proceedings of ICHEP06, July 2006, Moscow, p. 725.
[206] E. Rizvi, T. Sloan, Eur. Phys. J. direct C 3 (2001) N2.
[207] M. Kuze, Y. Sirois, Prog. Part. Nuclear Phys. 50 (2003) 1;
M. Kuze, Y. Sirois, Prog. Part. Nuclear Phys. 53 (2004) 583 (erratum).
[208] W. Buchmüller, R. Rückl, D. Wyler, Phys. Lett. B 191 (1987) 442;
W. Buchmüller, R. Rückl, D. Wyler, Phys. Lett. B 448 (1999) 320 (erratum).

[209] J. Butterworth, H. Dreiner, Nuclear Phys. B 397 (1993) 3.
[210] ZEUS Collaboration, S. Chekanov, et al., Phys. Rev. D 68 (2003) 052004.
[211] H1 Collaboration, A. Aktas, et al., Phys. Lett. B 629 (2005) 9.
[212] L3 Collaboration, M. Acciarri, et al., Phys. Lett. B 486 (2000) 81.
[213] OPAL Collaboration, G. Abbiendi, et al., Eur. Phys. J. C 6 (1999) 1.
[214] D0 Collaboration, V.M. Abazov, et al., Phys. Rev. D 71 (2005) 071104.
[215] D0 Collaboration, B. Abbot, et al., Phys. Rev. Lett. 79 (1997) 4321;
D0 Collaboration, B. Abbot, et al., Phys. Rev. Lett. 80 (1998) 2051;
D0 Collaboration, V.M. Abazov, et al., Phys. Rev. D 64 (2001) 029004;
D0 Collaboration, V.M. Abazov, et al., Phys. Rev. Lett. 88 (2002) 191801.
[216] ZEUS Collaboration, S. Chekanov, et al., Eur. Phys. J. C 44 (2005) 463.
[217] H1 Collaboration, A. Aktas, et al. DESY-07-009, Eur. Phys. J. C (submitted for publication).
[218] H1 Collaboration, V. Andreev, et al., Phys. Lett. B 561 (2003) 241.
[219] ZEUS Collaboration, S. Chekanov, et al., Phys. Lett. B 559 (2003) 153.
[220] Y. De Boer, Proceedings of DIS07, April 2007, Munich, Germany, http://sciencewisepublishing.com/publications/DIS07/;
K. Korcsak-Gorzo, Proceeding of DIS07, April 2007, Munich, Germany, http://sciencewisepublishing.com/publications/DIS07/.
[221] H1 and ZEUS Collaborations, Paper submitted to LP07, August 2007, Daegu, Korea, H1prelim-07-162, ZEUS-prel-07-029.
[222] ZEUS Collaboration, S. Chekanov, et al., Phys. Lett. B 583 (2004) 41.
[223] H1 Collaboration, A. Aktas, et al., Eur. Phys. J. C 48 (2006) 699.
[224] H1 Collaboration, A. Aktas, et al., Eur. Phys. J. C 33 (2003) 9.
[225] H1 Collaboration, A. Aktas, et al., Eur. Phys. J. C 31 (2003) 17.
[226] O. Ota, Proceedings of DIS07, April 2007, Munich, Germany, http://sciencewisepublishing.com/publications/DIS07/;
G. Brandt, Proceedings of DIS07, April 2007, Munich, Germany, http://sciencewisepublishing.com/publications/DIS07/.
[227] H1 and ZEUS Collaborations, EPS07, Manchester, UK, H1prelim-07-166, ZEUS-prel-07-024,
http://www-zeus.desy.de/physics/exo/public/EPS07/H1prelim-07-166.ps.gz.